Silvana Prando

Avaliação dos métodos de quantificação do metabolismo glicolítico cerebral em ratos anestesiados utilizando microPET/CT com ^{18}F-FDG

Tese apresentada à Faculdade de Medicina da Universidade de São Paulo para obtenção do título de Doutor em Ciências

Programa de Radiologia

Orientador: Prof. Dr. Marcelo Tatit Sapienza

"(Versão corrigida. Resolução CoPGr 6018/11, de 13 de novembro de 2011. A versão original está disponível na Biblioteca da FMUSP)"

São Paulo
2019

Silvana Prando

Avaliação dos métodos de quantificação do metabolismo glicolítico cerebral em ratos anestesiados utilizando microPET/CT com ^{18}F-FDG

Tese apresentada à Faculdade de Medicina da Universidade de São Paulo para obtenção do título de Doutor em Ciências

Programa de Radiologia

Orientador: Prof. Dr. Marcelo Tatit Sapienza

São Paulo
2019

Dados Internacionais de Catalogação na Publicação (CIP)

Preparada pela Biblioteca da
Faculdade de Medicina da Universidade de São Paulo

©reprodução autorizada pelo autor

Prando, Silvana
Avaliação dos métodos de quantificação do metabolismo glicolítico cerebral em ratos anestesiados utilizando microPET/CT com 18F-FDG / Silvana Prando. -- São Paulo, 2019.
Tese(doutorado)--Faculdade de Medicina da Universidade de São Paulo.
Programa de Radiologia.
Orientador: Marcelo Tatit Sapienza.

Descritores: 1.Tomografia por emissão de pósitrons 2.Sistema nervoso 3.Quantificação 4.Glucose 5.Fluordesoxiglucose F18 6.Anestésicos 7.Isoflurano 8.Ketamina 9.Xilazina

USP/FM/DBD-359/19

Responsável: Erinalva da Conceição Batista, CRB-8 6755

AGRADECIMENTOS

Ao Marcelo Tatit Sapienza, pela orientação e mais, pela amizade, paciência e compreensão em todos os momentos da elaboração da tese.

À Cecil Chow Robilotta, pela discussões e orientações durante todo o período da tese e principalmente, pela amizade de todos esses anos.

À Camila de Godoi Carneiro, pela ajuda na aquisição dos dados e na edição das imagens e gráficos.

Aos membros da banca do exame de qualificação, Carla Rachel Ono, Fábio Duran e Ana Maria Marques pelas valiosas sugestões oferecidas.

À Carla Rachel Ono, pelas discussões no início do trabalho e pelas sugestões na elaboração do artigo de revisão.

Ao LIM 43, nas figuras do Dr. Carlos Alberto Buchpiguel e da Miriam Okamoto, que acreditaram no trabalho além de possibilitar apoio logístico e financeiro.

À todo o LIM 43, por toda a dedicação à pesquisa e atenção aos pesquisadores.

NORMALIZAÇÃO ADOTADA

Esta tese está de acordo com as seguintes normas, em vigor no momento:

Referências: adaptado de *International Committee of Medical Journals Editors* (Vancouver).

Universidade de São Paulo. Faculdade de Medicina. Divisão de Biblioteca e Documentação. *Guia de apresentação de dissertações, teses e monografias*. Elaborado por Anneliese Carneiro da Cunha, Maria Julia de A. L. Freddi, Maria F. Crestana, Marinalva de Souza Aragão, Suely Campos Cardoso, Valéria Vilhena. 3a ed. São Paulo: Divisão de Biblioteca e Documentação; 2011.

Abreviaturas dos títulos dos periódicos de acordo com *List of Journals Indexed in Index Medicus*.

SUMÁRIO

Lista de abreviaturas

Lista de figuras

Lista de gráficos

Lista de tabelas

Resumo

Abstract

1. INTRODUÇÃO..... 1

1.1 Cérebro..... 2

1.2 Métodos de imagem na avaliação do metabolismo cerebral da glicose..... 9

1.3 A tomografia por emissão de pósitrons com ^{18}F-FDG..... 11

1.4 Os métodos de quantificação do metabolismo cerebral da glicose utilizando ^{18}F-FDG e PET..... 16

1.5 Fatores que alteram a quantificação e o consumo de glicose..... 18

2. OBJETIVOS..... 24

3. TEXTO SISTEMATIZADO..... 26

3.1 Organização do texto sistematizado..... 27

3.2 Métodos de quantificação..... 28

3.3 Efeitos dos anestésicos no metabolismo cerebral da glicose..... 40

4. CONCLUSÕES..... 45

4.1 Métodos de quantificação..... 46

4.2 Efeitos dos anestésicos no metabolismo cerebral da glicose..... 47

5. PERSPECTIVAS FUTURAS..... 48

6. ANEXOS..... 50

6.1 Comissão de ética no uso de animais..... 51

6.2 Methods for quantification of cerebral glycolytic metabolism using 2-deoxy-2-[^{18}F]fluoroglucose in small animals (Publicação 1)..... 52

6.3 Comparison of different quantification methods for 18F-flurodeoxyglucose-positron emission tomography studies in rats brains (Publicação 2)..... 71

6.4 Effects of ketamine/xylazine and isoflurane on rat brain glucose metabolism measured by ^{18}F-fluorodeoxyglucose-positron emission tomography (Publicação 3)..... 78

7. REFERÊNCIAS BIBLIOGRÁFICAS..... 89

LISTA DE ABREVIATURAS

^{14}C	Carbono-14
^{18}F	Flúor-18
^{18}F-FDG	Fluorodesoxiglicose marcada com ^{18}F
^{14}C-DG	Desoxiglicose marcada com ^{14}C
^{14}C-IAP	Iodoantipirina marcada com ^{14}C
^{15}O	Oxigênio-15
2D	Bidimensional
2TCM	*Two-tissue compartimental method*
3D	Tridimensional
ABV	Análise baseada em *voxel*
CC	Coeficiente de correlação
CHT	Colina
CMR_{gl}	Taxa metabólica cerebral de glicose
CT	Tomografia computadorizada
D	Direito
DP	Desvio padrão
E	Esquerdo
fMRI	Ressonância magnética funcional
FOV	*Field of view*
FSC	Fluxo sanguíneo cerebral
FUR	*Fractional uptake rate*
FWHM	*Full Width at Half Maximum*
GLUT	Transportadores de glicose específicos
HMIT	Transportador H^+/mio-inositol
I	Isoflurano
K_1	Transporte intra celular da ^{18}F-FDG;
k_2	Transporte extra celular da ^{18}F-FDG;
k_3	Fosforilação da ^{18}F-FDG pela hexoquinase
k_4	Desfosforilação da ^{18}F-FDG pela glicose-6-fosfatase
K_i	Taxa líquida de captação
K_E	Tamanho do *cluster*
KX	Cetamina associada a xilazina
LC	*Lumped Constant*

MBq	*Megabecquerel*
mm	Milímetro
N	Número
NIS	Cotransporte com sódio/iodo
OSEM	*Ordered Subset Expectation Maximization*
PET	Tomografia por emissão de pósitrons
RMN	Ressonância magnética nuclear
ROI	*Regions of interest*
SD	*Standard Deviation*
SGLT	Cotransporte com íon sódio
SMIT	Transportador sódio/mio-inositol
SMVT	Transportador sódio/multivitaminas
SPECT	Tomografia por emissão de fóton único
SPM	*Statistical Parametric Mapping*
SUV	*Standardized uptake value*
SUV_{gl}	*Standardized uptake value* corrigido para glicemia basal
VOI	*Volume of interest*
et al.	e outros
etc.	e outras coisas.

LISTA DE SIGLAS

CEUA	Comissão de Ética no Uso de Animais
FMUSP	Faculdade de Medicina da Universidade de São Paulo
InRad	Instituto de Radiologia
HCFMUSP	Hospital das Clínicas da Faculdade de Medicina da Universidade de São Paulo

LISTA DE FIGURAS

Figura 1 -	Localização das diferentes isoformas dos transportadores de glicose no cérebro	7
Figura 2 -	Distribuição celular do GLUT1 nas membranas luminal e abluminal das células endoteliais cerebrais	8
Figura 3 -	Processo de decaimento por emissão de pósitron e aniquilação do par elétron/pósitron	12
Figura 4 -	Equipamento FLEX Triumph™ PET/SPECT/CT - LabPET4	13
Figura 5 -	Cortes coronais da imagem tomográfica da distribuição da ^{18}F-FDG em animal da espécie *Rattus norvegicus*.	14

LISTA DE TABELAS

Tabela 1.	Família dos transportadores de glicose dependentes de sódio e transporte passivo	5
Tabela 2.	Variação dos valores da LC e CMR_{gl} em roedores anestesiados com isoflurano	17
Tabela 3.	Comparação entre os efeitos dos anestésicos nos diferentes métodos de quantificação do metabolismo glicolítico	20

RESUMO

Prando S. *Avaliação dos métodos de quantificação do metabolismo glicolítico cerebral em ratos anestesiados utilizando microPET/CT com ^{18}F-FDG* [tese]. São Paulo: Faculdade de Medicina, Universidade de São Paulo; 2019.

Introdução: A quantificação do metabolismo cerebral da glicose em pequenos animais é importante para o estudo dos mecanismos fisiopatológicos e da ação de drogas no sistema nervoso central. Atualmente, na pesquisa pré-clínica, estão disponíveis métodos qualitativos (visuais) e quantitativos para avaliação do metabolismo cerebral da glicose. Um dos problemas dos estudos *in vivo* de pequenos animais é a necessidade de contenção durante a aquisição das imagens para evitar os artefatos causados pela movimentação. Por essa razão, os animais devem ser restringidos fisicamente ou mantidos sob a ação de anestésicos. Como os anestésicos causam modificações na fisiologia dos sistemas nervoso central, cardiovascular e respiratório, a medida da captação da ^{18}F-FDG no cérebro pode ser comprometida. **Objetivos:** Avaliar a concordância e correlação entre as técnicas de quantificação do metabolismo da ^{18}F-FDG no sistema nervoso central de ratos anestesiados utilizando o método de compartimentos com dois tecidos (2TCM) e os métodos simplificados: Patlak, *Fractional uptake rate* (FUR), *Standardized uptake value* (SUV) e *Standardized uptake value* corrigido para glicemia (SUV_{gl}). Avaliar os efeitos dos anestésicos isoflurano e cetamina associada à xilazina no metabolismo da ^{18}F-FDG pelo sistema nervoso central de ratos, utilizando os métodos 2TCM, Patlak, SUV e análise baseada em *voxel* (ABV). **Métodos:** CEUA n 026/14. Trinta e três ratos, machos, adultos normais com aproximadamente 6 semanas de vida, espécie *Rattus norvegicus* da linhagem Wistar, foram submetidos a exame de imagem de PET. Os animais foram divididos em dois grupos, conforme o anestésico empregado, isoflurano (I=15) ou cetamina associada à xilazina (KX=18), e foram submetidos a cirurgia para inserção de um cateter de poliestireno na artéria femoral. A PET foi iniciada simultaneamente com a injeção do traçador ^{18}F-FDG e as imagens foram adquiridas no modo dinâmico por 60 minutos, formatadas em 20 imagens (8x30, 2x60, 2x120, 2x150, 3x300, 3x600 segundos). Durante o período de aquisição das imagens foram retiradas amostras de sangue arterial da artéria femoral. As imagens foram reconstruídas com o método OSEM-2D (20 iterações; 4 subconjuntos) e analisadas através dos métodos: 2TCM, Patlak, FUR, SUV_{gl}, SUV e ABV, conforme o objetivo em estudo. Para a análise com FUR, SUV, SUV_{gl} e AVB, utilizamos os últimos 30 minutos do estudo. **Resultados e Discussão:** O K_i 2TCM apresentou forte correlação (r=0,9935) e concordância (CC=0,991) com o valor de K_i estimado pela análise de Patlak. Os resultados obtidos pelo método FUR apresentaram excelente correlação com o K_i obtido tanto pelo 2TCM (r=0,9385) quanto pelo Patlak (r=0,9472), quando comparado com SUV ou SUV_{gl}. Na análise dos efeitos dos anestésicos através dos métodos 2TCM e Patlak, verificamos que no grupo KX houve redução do K_1 (0,173 *vs* 0,283; p<0,001) e do volume de distribuição (0,505 *vs* 0,760; p<0,001). Não houve diferença significativa do K_i entre os anestésicos estudados. Os resultados obtidos utilizando a ABV indicam que existe um

padrão heterogêneo de captação para cada anestésico estudado que concorda com a quantificação relativa do K_i e SUVR (córtex/cérebro). O SUV indicou redução significativa na captação da ^{18}F-FDG para o cérebro total sob vigência da KX (1,305 *vs* 1,879; p<0,001), entretanto, devido a alterações fisiológicas causadas pelos anestésicos, essas diferenças não devem ser valorizadas. **Conclusão:** Nossos achados sugerem que existe uma concordância entre os métodos 2TCM e Patlak, permitindo a utilização do método simplificado de Patlak em estudos pré-clínicos de quantificação do metabolismo cerebral da ^{18}F-FDG em ratos. Entre os métodos simplificados estudados, o melhor correlacionado com o padrão ouro (2TCM) foi o FUR. A correção de SUV pela glicemia basal utilizando métodos de cabeceira de leito, comuns nos estudos pré-clínicos, deve ser vista com cautela, uma vez que introduz mais uma fonte de erro à quantificação. Em relação aos efeitos dos anestésicos utilizados, verificamos que ambos produzem uma heterogeneidade no metabolismo cerebral da glicose.

Descritores: Tomografia por emissão de pósitrons; Sistema nervoso; Quantificação; Glucose; Fluordesoxiglucose F18; Anestésicos; Isoflurano; Ketamina; Xilazina.

ABSTRACT

Prando S. *Evaluation of cerebral glycolytic metabolism quantification methods in anesthetized rats using 18F-FDG microPET/CT* [thesis]. São Paulo: "Faculdade de Medicina, Universidade de São Paulo"; 2019.

Introduction: Quantification of cerebral glucose metabolism in small animals is important for the study of pathophysiological mechanisms and drug action in the central nervous system. Currently, in preclinical research, qualitative (visual) and quantitative methods are available for assessing cerebral glucose metabolism. One of the problems with *in vivo* small animal studies is the need for containment during image acquisition to avoid artifacts caused by movements. For this reason, animals should be physically restricted or kept under anesthetic action. Because anesthetics cause changes in the physiology of the central nervous, cardiovascular, and respiratory systems, the measurement of ^{18}F-FDG uptake in the brain may be compromised. **Objectives:** To evaluate the agreement and correlation between ^{18}F-FDG metabolism quantification techniques in the central nervous system of anesthetized rats using the two-tissue compartment methods (2TCM) and the simplified methods: Patlak, Fractional uptake rate (FUR), Standardized uptake value (SUV) and Standardized uptake value corrected for blood glucose (SUV_{gl}). To evaluate the effects of isoflurane and xylazine-associated ketamine anesthetics on ^{18}F-FDG metabolism in rat central nervous system using 2TCM, Patlak, SUV and voxel-based analysis (ABV) methods. **Methods:** CEUA No. 026/14. Thirty-three normal male rats, approximately 6 weeks old, Wistar *Rattus norvegicus*, were submitted to PET imaging. The animals were divided into two groups according to the anesthetic used, isoflurane (I=15) or xylazine-associated ketamine (KX=18). The animals underwent surgery in order to have inserted a polystyrene catheter into the femoral artery. PET was started simultaneously with the injection of the ^{18}F-FDG tracer and the images were acquired in dynamic mode for 60 minutes, formatted into 20 images (8x30, 2x60, 2x120, 2x150, 3x300, 3x600 seconds). During the image acquisition, arterial blood samples were taken from the femoral artery. Image reconstruction was performed with OSEM-2D (20 iterations; 4 subsets) and the results analyzed using 2TCM, Patlak, FUR, SUV_{gl}, SUV and ABV methods, according to the study objective. For the analysis with FUR, SUV, SUV_{gl}, and AVB, we used the last 30 minutes of the study. **Results and Discussion:** K_i 2TCM showed a strong correlation (r=0.9935) and agreement (CC=0.991) with the K_i value estimated by Patlak analysis. The results obtained by the FUR method presented excellent correlation with the K_i obtained by both 2TCM (r=0.9385) and Patlak (r=0.9472) in relation to SUV or SUV_{gl}. In the analysis of the effects of anesthetics by the methods 2TCM and Patlak, we found that in the KX group there was a reduction in K_1 (0.173 *vs* 0.283; p<0.001) and volume of distribution (0.505 *vs* 0.760; p<0.001). There was no significant difference in brain glucose metabolism concerning the anesthetics studied. The results obtained using ABV demonstrate that there is a heterogeneous uptake pattern for each studied anesthetic that agrees with the relative quantification of K_i and SUVR (cortex/brain). SUV demonstrated a significant reduction in ^{18}F-FDG uptake by

the whole brain under KX (1.305 *vs* 1.879; $p<0.001$), however, due to physiological changes caused by anesthetics, these differences should not be considered. **Conclusion:** Our findings suggest that there is an agreement between 2TCM and Patlak methods, allowing the use of Patlak's simplified method in preclinical studies of ^{18}F-FDG brain metabolism quantification in rats. Among the simplified methods studied, the best correlated with the gold standard (2TCM) was the FUR. The correction of SUV by basal glycemia using bedside methods, common in preclinical studies, should be viewed with caution as it introduces yet another source of error in quantification. Regarding the effects of the anesthetics used, we found that both produce heterogeneity in cerebral glucose metabolism.

Descriptors: Positron-emission tomography; Nervous system; Quantification; Glucose; Fluorodeoxyglucose F18; Anesthetics; Isoflurane; Ketamine; Xylazine.

1.INTRODUÇÃO

1.1 Cérebro

O cérebro é um produto da evolução de milhões de anos após o surgimento do ancestral comum aos mamíferos. A evolução que diferenciou os seres humanos das outras espécies de mamíferos também os isolou em um intrincado quebra-cabeça sobre o funcionamento do cérebro e das características que nos tornam humanos.

Na antiguidade, o cérebro era um órgão menosprezado e relegado a segundo plano nos estudos; o coração era considerado o responsável pelas nossas emoções e pela essência da vida. Somente no século XIV, que o cérebro foi alçado a órgão central responsável pelo pensamento, sensação, consciência e pela moral.

Desde os meados do século XIX, com os primeiros estudos sobre a estrutura anatômica do tecido nervoso realizados por Jan Evangelista Purkinje e a concepção da teoria neuronal criada por Santiago Ramón y Cajal (Amaral et al., 2017), progressos ocorreram no sentido de entender os intricados processos neuronais que nos caracterizam.

Atualmente, os maiores avanços no entendimento do cérebro são oriundos do progresso da neurologia clínica associada ao desenvolvimento de métodos de imagem, como a ressonância magnética nuclear (RMN) ou a tomografia por emissão de pósitrons (PET), que permitiram o estudo do sistema nervoso em condições normais e na modificação por doenças.

Além das doenças, o cérebro pode ser alterado por diversas substâncias encontradas na natureza ou por produtos fabricados pelos humanos com objetivo recreacional ou medicinal. Na categoria de drogas medicinais, a invenção do anestésico no século XX permitiu diminuir a dor em procedimentos

invasivos. Além da analgesia, o anestésico pode levar a perda da consciência através de mecanismos de ação no cérebro que ainda não foram completamente esclarecidos.

Durante as últimas cinco décadas, um enorme progresso tem sido feito no sentido de compreender as demandas de energia locais do cérebro e as relações entre a função cerebral e os fluxos em vias metabólicas que correspondem ao desenvolvimento, metabolismo, à neuroproteção e aos requisitos de biossíntese de células do cérebro.

Essa compreensão proporciona oportunidades únicas para estudar *in vivo* a fisiologia animal e a fisiopatologia de diversos modelos de doenças. Porém, o desafio é grande, pois o cérebro é um órgão complexo, composto por muitos componentes estruturais e funcionais, com diferentes níveis independentes entre si, cujas atividades funcional e metabólica são reguladas também de modo independente.

Tanto a anatomia quanto a fisiologia fazem do cérebro um órgão único, substancialmente diferente dos outros órgãos do corpo humano (Hall, 2017; Catafau, 2001). Muitas dessas diferenças são encontradas dentro do sistema circulatório cerebral, particularmente na regulação da perfusão e no metabolismo.

O cérebro é o único órgão sem nenhuma reserva energética. No humano adulto, assim como em animais adultos, a glicose representa o principal, se não o único, substrato de energia do metabolismo cerebral. Praticamente toda a glicose extraída pelo cérebro é oxidada. Assim, a glicose é utilizada paralelamente com o consumo de oxigênio cerebral, mostrando a mesma heterogeneidade regional de 4:1 entre as regiões de substância

cinzenta e substância branca. Essa proporção se repete em todas as espécies de mamíferos, por exemplo, ratos, gatos, macacos e seres humanos (Hall, 2017; Nehlig, 1997).

As artérias intracranianas são diferentes das artérias presentes no resto do corpo (Hall, 2017; Catafau, 2001). Por causa da proteção do osso e da pressão externa, a parede vascular tem menor espessura. Nenhuma fibra elástica é encontrada neste meio, mas uma membrana elástica interna bem desenvolvida existe em artérias cerebrais. A barreira sanguínea, que consiste de células endoteliais especiais com junções firmes dentro dos capilares cerebrais, é a maior diferença em relação a capilares encontrados em outras regiões do corpo. A existência dessa barreira hematoencefálica exige o transporte transcelular de glicose do sangue para o cérebro através das membranas luminal e abluminal das células endoteliais do cérebro (Duelli; Kuschinsky, 2001).

O transporte da glicose para o cérebro é mediado por membros da família de transportadores da glicose (Duelli; Kuschinsky, 2001). O transporte da glicose pode ser dividido em duas classes: a dependente de sódio, conhecida como cotransporte, e a difusão passiva facilitada.

O processo mediado por proteínas sódio-dependentes transporta a glicose contra o gradiente de concentração da mesma. Vários desses transportadores são encontrados nos rins e em outros órgãos, e sua presença no tecido cerebral ainda é controversa (Duelli; Kuschinsky, 2001). Em contraste com o cotransporte, a difusão passiva transporta a glicose a favor do gradiente de concentração e várias isoformas já foram identificadas e caracterizadas no tecido cerebral (tabela1).

Tabela 1 - Família dos transportadores de glicose dependentes de sódio e transporte passivo

Tipo	Proteína (gene)	Sítios de Expressão	Substrato/transporte
Facilitado/Dependente de Sódio	**GLUT1** (SLC2A1)	Endotélio cerebral e barreiras cerebrais epiteliais; células gliais; barreiras tecido/sangue; olho; nervos periféricos; placenta; glândula mamária em lactação (distribuição ubíquo na maioria das células dos mamíferos)	>> Glicose; galactose; manose; glucosamina; ácido ascórbico
	GLUT2 (SLC2A2)	Rins, intestino delgado (células epiteliais), fígado, pâncreas (ilhotas), cérebro (astrócitos)	Manose; Galactose; frutose; glicose; glucosamina
	GLUT3 (SLC2A3)	Neurônios, testículos, placenta, células cerebrais endoteliais	Glicose; galactose; manose; xilose; ácido dehidroascórbico
	GLUT5 (SLC2A5)	Intestino (jejuno); rins; testículos, microglia cerebral	Frutose
	GLUT6 (SLC2A6)	Cérebro, leucócitos periféricos e do baço	Glicose
	GLUT8 (SLC2A8) Insulina-responsivo	Blastócitos, testículos, cérebro (neurônios), músculo, adipócitos, glândula mamária	Glicose
	GLUT10 (SLC2A10)	Fígado, pâncreas, coração, pulmão, cérebro, músculo esquelético, placenta	Glicose; galactose
	HMIT (SLC2A13) cotranporte	Cérebro (vesículas intracelulares dos neurônios)	H^+/mio-inositol

continua

Tabela 1 - Família dos transportadores de glicose dependentes de sódio e transporte passivo

conclusão

Tipo	Proteína (gene)	Sítios de Expressão	Substrato/transporte
Sódio-Glicose Cotransportadores/Dependente de Sódio	**SGLT1** (SLC5A1)	Intestino delgado, traqueia, rins, coração, cérebro (corticais, piramidais e células neuronais de purkinje), testículos, próstata, glândula mamária	> Glicose, ≥ galactose, água
	SGLT2 (SLC5A2)	Rins (córtex/túbulos proximais), cérebro, fígado, tireoide, músculo, coração	Glicose, galactose
	SGLT3 (SLC5A4/SAAT1) sensor de glicose	Intestino delgado, testículos, útero, rins, pulmão, cérebro, tireoide	Glicose, Na^+ (H^+)
	SGLT4 (SLC5A9)	Intestino, rins, fígado, cérebro, pulmão, traqueia, útero, pâncreas	Glicose, manose, frutose
	SGLT6 (SLCA11/KST1/SM1T2)	Cérebro (neurônios), medula espinhal, intestino delgado (íleo e jejuno), rins (córtex e medula), músculo esquelético	Mio-inositol, glicose
	SMIT (SLC5A3)	Rins (medula), tireoide, vaso sanguíneo do plexo coroide, glândula pineal, gânglio da raiz dorsal, testículos	Mio-inositol, glicose
	SMVT (SLC5A6)	Cérebro, coração, rins, pulmão, placenta	Multivitaminas (Biotina, ácido lipoico, ácido pantotenico)
	CHT (SLC5A7/CHT1)	Medula espinal e medula (vesículas intracelulares)	Colina

FONTE: Shah et al., 2012.
GLUT: Transportadores de glicose específicos; SGLT: cotransporte com íon sódio; NIS: cotransporte com sódio/iodo; CHT: colina; HMIT: transportador H^+/mio-inositol; SMIT: transportador sódio/mio-inositol; SMVT: transportador sódio/multivitaminas.

Os principais transportadores de glicose no cérebro são GLUT1 e GLUT3. O GLUT1 existe em duas isoformas de diferentes pesos moleculares. A isoforma 55-kDa está localizada nas membranas das células endoteliais cerebrais e a isoforma 45-kDa está presente nos astrócitos (figura1)

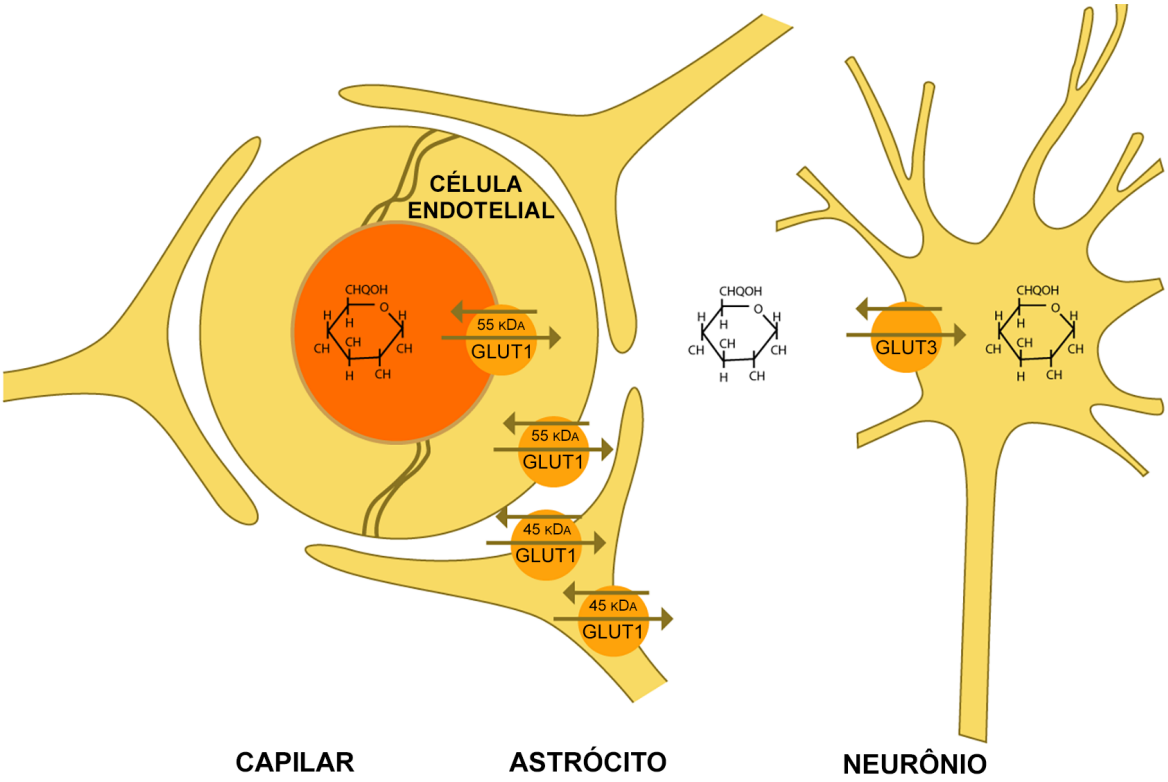

Figura 1: Localização das diferentes isoformas dos transportadores de glicose no cérebro (adaptado de Shah et al., 2012).

A glicose entra no espaço extracelular cerebral através do sangue utilizando a isoforma 55-kDa do transportador GLUT1, presente nas membranas luminal e abluminal das células endoteliais que formam a barreira hematoencefálica (Shah et al., 2012). O GLUT1 está localizado tanto na membrana luminal como na abluminal na proporção aproximada de 1:4 respectivamente (Shah et al., 2012) (figura 2). Muitos estudos também tem confirmado a presença do GLUT1 em células endoteliais microvascularizadas como os astrócitos.

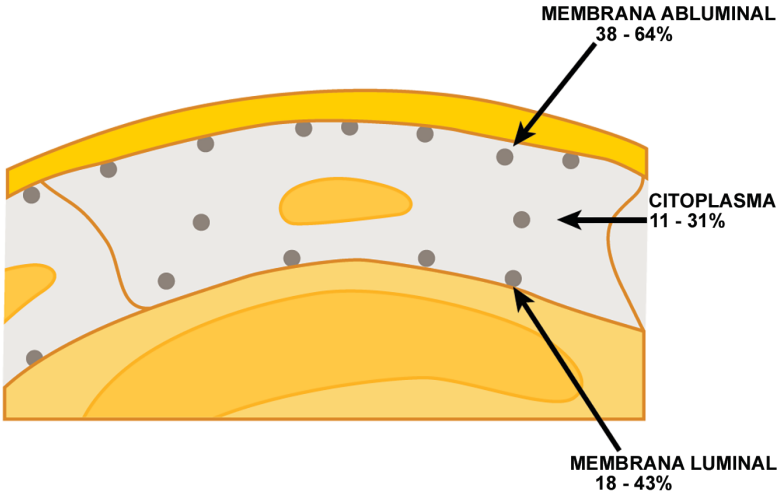

Figura 2: Distribuição celular do GLUT1 nas membranas luminal (18 - 43%) e abluminal (38 – 64%) das células endoteliais cerebrais e citoplasma (11 – 31%)(adaptado de Shah et al., 2012).

Em condições normais, a capacidade de transporte da GLUT1 é suficientemente alta para que o influxo normal de glicose seja consideravelmente superior à necessidade, e a taxa de consumo de glicose representa apenas uma fração do fluxo de glicose para dentro e para fora do cérebro através da barreira hematoencefálica. A taxa de utilização de glicose cerebral nunca é limitada pelo transporte de glicose através da barreira hematoencefálica, exceto quando esse transporte é limitado por restrições na liberação de glicose ao cérebro, seja por hipoglicemia ou isquemia cerebral, por exemplo, ou para níveis além da capacidade da circulação cerebral e dos mecanismos de transporte para se adaptar (Leybaert et al., 2007; Phelps et al., 1986).

Contrariamente ao cérebro humano, a glicose é pouco consumida pelo cérebro do rato no nascimento, alcançando o ápice na idade adulta. O consumo de glicose em cérebros de ratos imaturos são baixos e homogêneos no início do estágio de desenvolvimento pós-natal, isto é, entre 10 e 17 dias de vida, com exceção de algumas áreas posteriores e do tronco cerebral. A

maioria dos aumentos significativos no metabolismo cerebral ocorre entre 10 e 17 dias de vida e correlacionam-se com a aquisição de funções especificas, tais como a audição, visão, locomoção. Entre 17 e 21 dias de vida, um aumento de até 50% do metabolismo pode ser verificado. Entretanto, esse aumento é generalizado e inespecífico. Após o desmame, entre 21 e 22 dias de vida, ainda ocorre um aumento de até 25% no consumo da glicose alçando seu máximo em torno de 60 dias de vida (Nehlig, 1997). Podemos concluir que o aumento do consumo da glicose em filhotes de ratos acompanha as alterações comportamentais, neurofisiológicas e anatômicas que ocorrem durante o desenvolvimento do cérebro.

1.2 Métodos de imagem na avaliação do metabolismo cerebral da glicose

A primeira correlação entre metabolismo e fluxo sanguíneo cerebral (FSC) foi postulada por Roy e Sherrington (1890). O fluxo sanguíneo e o metabolismo cerebrais estão relacionados com a maioria das condições patológicas, com exceção de alguns tumores cerebrais. Em geral, o suprimento adequado de oxigênio e glicose de cada área cerebral é regulado de acordo com sua necessidade metabólica, a qual é determinada pela intensidade de atividade neuronal daquela região. Assim, esta atividade está diretamente relacionada ao fluxo sanguíneo cerebral.

Grandes avanços na compreensão do metabolismo e do fluxo sanguíneo cerebral foram impulsionados pela evolução da metodologia, que evoluiram desde técnicas micro analíticas e ensaios bioquímicos, estudos de biologia molecular, até técnicas de imagem, como a autorradiografia

quantitativa, PET, espectroscopia por ressonância magnética com [^{13}C]glicose, fMRI (ressonância magnética funcional) e microscopia de fluorescência.

Esses métodos podem ser classificados em métodos diretos e indiretos. Os métodos indiretos se valem do paralelismo entre o FSC, a atividade neuronal e o metabolismo para estimar o consumo de glicose pelo cérebro. Os métodos diretos estão fundamentados no desenvolvimento de novas moléculas que mimetizam o comportamento da glicose no cérebro, permitindo a quantificação de taxas e capacidades metabólicas globais ou regionais.

Os métodos mais frequentemente utilizados de imagem metabólica cerebral são a tomografia por emissão de pósitron com ^{18}F-FDG, a autorradiografia *ex vivo* e a fluorescência utilizando produtos derivados da 2-DG. Porém, a determinação quantitativa do consumo de glicose com os análogos fluorescentes requer uma avaliação da cinética de competição desses agentes com a glicose no processo de transporte e de fosforilação (Mergenthaler et al., 2013).

As primeiras tentativas realizadas para medir a taxa metabólica de glicose utilizaram a molécula de glicose marcada com ^{14}C, a [^{14}C]glicose, a qual é metabolizada de forma análoga a glicose e sua concentração nos tecidos pode ser medida por métodos de autorradiografia. Entretanto, a desvantagem da [^{14}C]glicose é a rapidez com que é feita sua conversão para CO_2 e água. Como o CO_2 é rapidamente removido do tecido, o acúmulo da radioatividade no tecido é pequeno e difícil de avaliar (Sokoloff et al., 1977).

Sokoloff e colaboradores (1977) publicaram o trabalho que descreve a preparação da 2-desoxi-D-[^{14}C]glicose (^{14}C-DG). Devido à sua diferença de composição química, sua participação se restringe à parte da via metabólica da

glicose, à internalização celular pelas proteínas GLUTs e à fosforilação pela hexoquinase. O produto gerado, a DG-6-fosfato, fica retido no interior das células e não sofre mais processos de metabolização, tornando mais fácil medir a quantidade de ^{14}C-DG captada pelas células, por autorradiografia.

Ido e colaboradores (1978) publicaram os resultados da preparação da 2-desoxi-2-[^{18}F]fluoro-D-glicose, uma desoxiglicose marcada com um emissor de pósitron, o flúor-18, o que permite a obtenção de imagens do consumo de glicose em tecidos, utilizando o processo de tomografia por emissão de pósitrons. Isto levou a avanços no entendimento do funcionamento do cérebro, como a relação direta entre a atividade funcional, o metabolismo e o fluxo sanguíneo (Ingvar, 1982), e na detecção de tumores com alta captação e metabolismo de glicose.

Embora a ^{18}F-FDG seja estruturalmente diferente da DG, a ^{18}F-FDG é considerada muito semelhante à DG na absorção e metabolismo *in vivo*. Phelps e colaboradores (1979) adotaram o modelo da ^{14}C-DG desenvolvido por Sokoloff (1981) para estimar a cinética da ^{18}F-FDG e demonstraram que a PET, com a modelagem para ^{18}F-FDG, pode ser utilizada de forma confiável para estimar a taxa do metabolismo da glicose (Phelps et al., 1979; Sokoloff, 1981a, 1981b).

1.3 A tomografia por emissão de pósitrons com ^{18}F-FDG

A PET é baseada na administração de fármacos marcados com radioisótopos emissores de pósitrons, onde a forma química do radiofármaco é concebida para investigar um processo de interesse, tais como as taxas de

absorção da glicose ou populações de receptores específicos.

A partir de uma modalidade de imagem baseada principalmente na análise visual, a PET evoluiu para uma ferramenta de imagem quantitativa bastante precisa, na qual os processos biológicos podem ser medidos e comparados em termos de potencial de ligação ou taxas de transferência. Fatores que contribuem para esta evolução incluem o aumento da sensibilidade e da resolução espacial dos equipamentos (Sossi;Ruth, 2005).

As imagens de PET são formadas a partir da detecção, em coincidência, dos fótons de aniquilação, figura 3. Este processo tem início quando dois fótons resultantes da aniquilação de um par elétron/pósitron depositam toda ou parte de sua energia no sistema de detecção de coincidência.

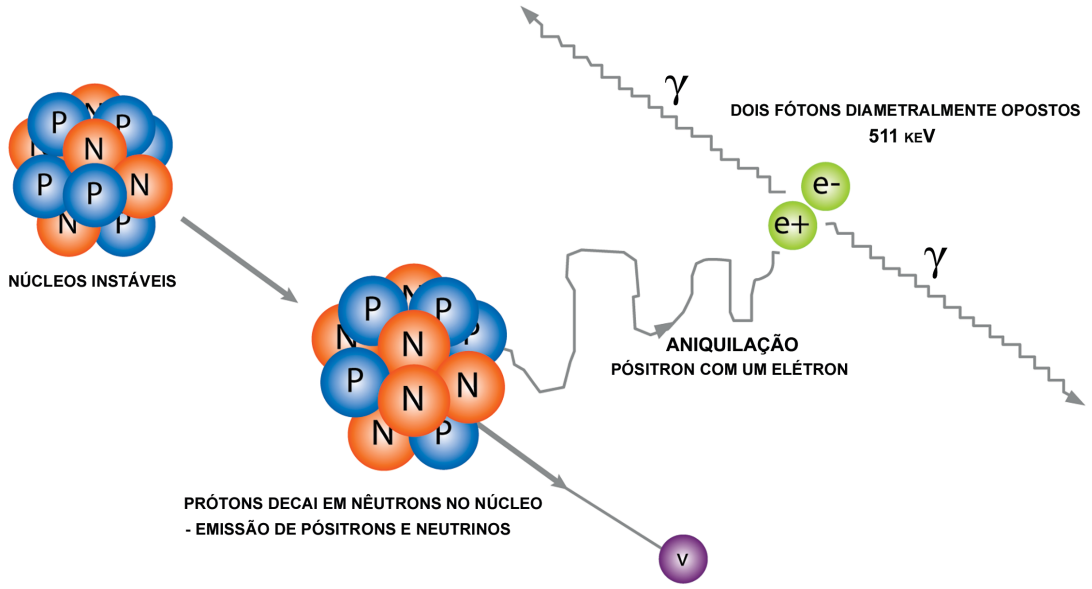

Figura 3: Processo de decaimento por emissão de pósitron e aniquilação do par elétron/pósitron

Essa energia é absorvida pelo cristal de cintilação e, como consequência, dá origem a uma cascata de fótons com frequência na faixa da luz ultravioleta, que são convertidos pelos tubos fotomultiplicadores em sinais

elétricos. A detecção de um único fóton se dá em um intervalo de tempo denominado tempo de resolução do cintilador. Se dois fótons forem contados dentro de um intervalo de tempo, que define a janela de coincidência, serão interpretados como sendo provenientes de um mesmo evento de aniquilação. Os sinais elétricos resultantes do processo de detecção são armazenados e posteriormente processados. Todo esse conjunto forma o sistema básico de detecção.

O equipamento de tomografia por emissão de pósitrons (figura 4) é constituído de conjuntos de blocos de cristais formando anéis, e pode produzir imagens em 3 dimensões que representam o objeto (figura 5). Elaborados algoritmos de reconstrução 2D ou 3D fornecem a distribuição espacial do radioisótopo através da combinação da informação proveniente de um grande número de detectores de fótons.

Figura 4: Equipamento FLEX Triumph™ PET/SPECT/CT - LabPET4

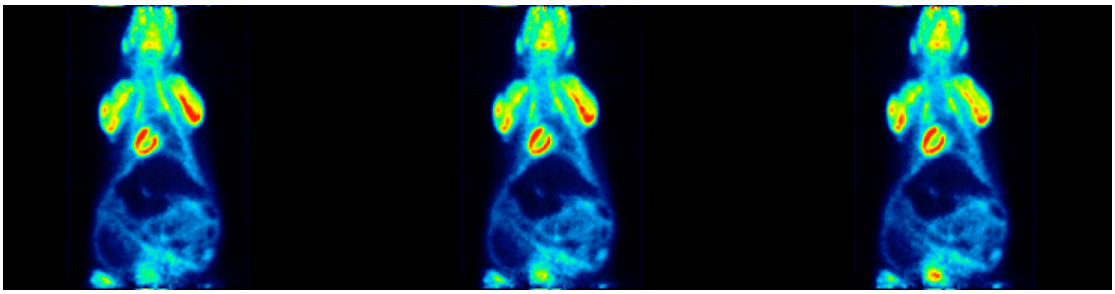

Figura 5: Cortes coronais da imagem tomográfica da distribuição da ^{18}F-FDG em animal da espécie *Rattus norvegicus*

Novos desenvolvimentos nos sistemas de PET tem melhorado o contraste e a resolução espacial das imagens, enquanto mantém a alta sensibilidade.

A resolução espacial do PET é definida como a habilidade do sistema em distinguir duas estruturas adjacentes que podem ser visualizadas separadas em uma imagem. A resolução espacial é determinada por parâmetros de *hardware*, como o tamanho do cristal e o diâmetro do anel detector, bem como por parâmetros físicos intrínsecos, como a distância de deslocamento do pósitron no tecido e a colinearidade dos fótons de aniquilação. Ambos os efeitos resultam em borramento das imagens reconstruídas e dificultam a detectabilidade e a quantificação de pequenas lesões nas imagens PET (Elsinga et al., 2012).

Em resumo, esses efeitos fornecem um limite físico da resolução espacial. Estudos demonstraram que a melhor resolução espacial possível em imagens reconstruídas adquiridas em sistemas de PET dedicados a pequenos animais está na faixa de 0,4 mm enquanto os sistemas clínicos possuem uma resolução entre 5 e 10 mm (Cherry et al., 2012; Elsinga et al., 2012). No entanto, quando cristais menores são usados, o número de linhas de respostas é diretamente aumentado e pode causar estatísticas insuficientes para a

reconstrução se o tempo de varredura for curto e a quantidade injetada de radioatividade for baixa (Elsinga et al., 2012).

O outro parâmetro importante de desempenho do sistema PET para pequenos animais é a sensibilidade de detecção para raios gama de 511 keV. A sensibilidade está relacionada com a capacidade do equipamento em detectar o máximo de coincidências verdadeiras em relação ao número de eventos reais de aniquilação, isto é, em relação à atividade da fonte compreendida no campo de visão do equipamento. A sensibilidade de um sistema de PET depende das propriedades geométricas e das características físicas do cintilador. A sensibilidade de um sistema PET clínico com aquisição 3D é de 2% a 10%, enquanto nos sistemas pré-clínicos e de 4% a 11% (Cherry et al., 2012; Elsinga et al., 2012).

Assim, projetar um equipamento de PET é sempre um compromisso entre resolução espacial e sensibilidade. A resolução espacial e a sensibilidade de detecção são de enorme importância para os estudos de pequenos animais, pois pequenas lesões e órgãos precisam ser detectados e a concentração da atividade deve ser quantificada com precisão.

Antes da quantificação das imagens é necessária a aplicação de algoritmos que realizam a correção dos efeitos da interação da radiação com a matéria, principalmente, os efeitos de atenuação e espalhamento, assim como o tempo morto e a resposta do sistema aos eventos aleatórios.

Além dos fatores técnicos, vários outros fatores afetam a quantificação das imagens de PET: o modo de aquisição, o nível de glicose no sangue, o movimento do paciente/animal, o efeito de volume parcial e os métodos escolhidos para reconstrução e quantificação da imagem.

1.4 Os métodos de quantificação do metabolismo cerebral da glicose em pequenos animais utilizando a ^{18}F-FDG e PET

A quantificação do metabolismo glicolítico cerebral em pequenos animais é importante para o estudo dos mecanismos fisiopatológicos e da ação de drogas no sistema nervoso central. Existem várias técnicas de avaliação do metabolismo disponíveis, desde métodos visuais, bem conhecidos na rotina clínica, até métodos elaborados que permitem o estudo dos mecanismos de transporte e das enzimas envolvidas no metabolismo da glicose pelo cérebro.

Atualmente, estão disponíveis para pequenos animais os métodos de análise qualitativos, semiquantitativos e quantitativos para as imagens de PET, além dos métodos *ex vivo.* Essas técnicas de quantificação fornecem diferentes resultados e sua aplicabilidade está relacionada ao objetivo do estudo e aos múltiplos fatores que interferem em todo o processo.

A falta de precisão ou reprodutibilidade da quantificação é observada em populações de animais e de humanos devido à variabilidade associada a imagens de PET e a incerteza nos parâmetros estimados, como no caso da *Lumped Constant*, nos modelos cinéticos, ou do conhecimento a priori.

Mais recentemente, Alf e colaboradores (2014), publicaram uma revisão sobre quantificação absoluta em estudos de PET com ^{18}F-FDG em pequenos roedores anestesiados com isoflurano e, encontraram variações da ordem de duas a cinco vezes para os valores da CMR_{gl} em ratos (tabela 2). No geral, a imprecisão na estimativa da *Lumped Constant* causam diferenças substanciais entre os resultados publicados que impossibilitam a comparação da CMR_{gl} entre estudos de diferentes grupos de pesquisa. Alf e colaboradores

(2014) recomendam que a *Lumped Constant* seja estimada para cada anestésico utilizado.

Tabela 2 - Variação dos valores da LC e CMR_{gl} em roedores anestesiados com isoflurano

Autor	Espécie	Região Cerebral	Traçador	LC	CMR_{gl}
Shimoji	Rato	Córtex Cérebro	^{18}F-FDG	0,48	23.9 ± 4,8 28,1 ± 4,6
Backes	Rato	Cérebro	^{18}F-FDG	Derivado da cinética	20 (sem DP)
Yu	Camundongo	Córtex	^{18}F-FDG	0,6	40,6 ± 13,3
Mizuma	Camundongo	Córtex	^{18}F-FDG	0,625	13 ± 4
Kreissl	Camundongo	Cérebro	^{18}F-FDG	1	18 (sem DP)
Alf	Camundongo	Cérebro	^{18}F-FDG	0,6	61 ± 11 75 ± 24

FONTE: Shimoji et al., 2004; Backes et al., 2011; Yu et al., 2009; Mizuma et al., 2010; Kreissl et al., 2011; Alfe t al., 2012.
LC: *Lumped Constant*; CMR_{gl}: Taxa metabólica cerebral de glicose, DP: Desvio Padrão.

Em métodos de quantificação menos refinados, como o SUV ou a ABV (Análise Baseada em *Voxel*), também existem problemas na reprodutibilidade dos resultados. Porém, essas imprecisões estão mais relacionadas a fatores que alteram a curva de atividade *vs* tempo do radiofármaco e portanto, a curva do SUV, como, por exemplo, problemas na administração da ^{18}F-FDG e na escolha do tempo entre a injeção e a imagem. De modo geral, muitos fatores podem afetar os resultados do SUV e o uso de técnicas inconsistentes para

obtenção das imagens cerebrais com ^{18}F-FDG podem contribuir com variações no SUV que excedem 50% do valor real (Byrnes et al., 2014).

Em estudos clínicos, existem correlações ótimas a moderadas entre o SUV e a quantificação absoluta para sujeitos saudáveis. Entretanto, quando pacientes com alterações metabólicas são estudados, essa correlação perde força tornando-se insatisfatória (Yamaji et al., 2000).

Em estudos com pequenos animais, as correlações realizadas são entre os métodos de quantificação absoluta e esporadicamente, correlações com o SUV. Prieto e colaboradores (2011) demonstraram que existe uma correlação entre os dados obtidos por autorradiografia e aqueles processados utilizando o *Statistical Parametric Mapping* (SPM). Nenhum estudo, além dos dados publicados por Prieto e colaboradores (2011), demonstrou que existe correlação entre os resultados fornecidos pelo SPM e os demais métodos disponíveis.

Tendo em vista os dados apresentados anteriormente a respeito da literatura existente, observamos que existe uma lacuna no estudo da correlação entre os métodos de quantificação absoluta, SUV e SPM. Portanto, pretendemos, com esse trabalho, verificar a existência da correlação entre os métodos supracitados.

A existência de correlação entre os métodos sugere a possibilidade de simplificação dos métodos de quantificação para estudos cerebrais de pequenos animais utilizando ^{18}F-FDG. Com a viabilidade de utilizar o SUV para quantificação ou o SPM para a comparação entre grupos, será possível realizar estudos longitudinais empregando uma menor quantidade de animais.

1.5 Fatores que alteram a quantificação do consumo de glicose

Além dos fatores relacionados com a evolução dos equipamentos de PET, outros fatores técnicos são importantes para a acurácia e precisão das quantificações de um estudo de PET (Frey et al., 2012). A rota de administração da ^{18}F-FDG (Vanhove et al., 2015; Schiffer et al., 2007; Fueger et al., 2006), condição dietética (Vanhove et al., 2015), idade do animal (Nehlig, 1997), manejo do animal antes e durante o período de incorporação da ^{18}F-FDG (Vanhove et al., 2015), tipo de anestesia (Alstrup; Smith, 2013), entre outros fatores, também alteram a biodistribuição do composto.

Animais mantidos em salas com temperatura ambiente muito baixa tendem a produzir calor através do metabolismo da glicose pela gordura marrom, diminuindo a captação cerebral da ^{18}F-FDG. Por esse motivo, é recomendável que o animal seja mantido sobre uma placa de aquecimento antes e durante a aquisição da imagem.

Um problema dos estudos *in vivo* de pequenos animais utilizando a técnica de PET é a necessidade de contenção dos animais durante a aquisição das imagens, para evitar os artefatos causados pela movimentação. Por essa razão, os animais devem ser restringidos fisicamente ou mantidos sob a ação de anestésicos. Como os anestésicos causam modificações significativas na fisiologia dos sistemas nervoso central, cardiovascular e respiratório (Toyama et al., 2004a), a medida da captação da ^{18}F-FDG no cérebro pode ser comprometida. O consumo cerebral da glicose é tipicamente reduzido quando o animal é mantido sob anestesia e a incorporação da ^{18}F-FDG é reduzida na maioria dos protocolos anestésicos, incluindo isoflurano, cetamina, propofol e

pentobarbital (Alstrup; Smith, 2013; Matsumura et al., 2003), como foi demonstrado pelos pesquisadores relacionados na tabela 3.

Tabela 3 - Comparação entre os efeitos dos anestésicos nos diferentes métodos de quantificação do metabolismo glicolítico

Pesquisador	Método de Anestesia	Resultados	Método de Aquisição
Hansen	Isoflurano Halotano	- FSC hemisférico igual entre grupos - FSC neocortical com halotano é maior comparado ao isoflurano	Autorradiografia (^{14}C-DG)
Lenz	Isoflurano Desflurano	- diminuição do consumo glicose e aumento do FSC com ambos os anestésicos	Autorradiografia (^{14}C-IAP ou ^{14}C-DG)
Moore	Cetamina + Xilazina após 42min da injeção de ^{18}F-FDG	- demonstra que a PET é reprodutível e sensível quando comparada a autorradiografia em animais com trauma cerebral	Autorradiografia (^{18}F-FDG) PET dedicada a pequenos animais (^{18}F-FDG)
Matsumura	Cetamina Cetamina + Xilazina Hidrato de Cloral Fenobarbital Propofol Isoflurano	- diminuição do metabolismo cerebral para todos os anestésicos - diminuição acentuada nas áreas corticais com isoflurano - cetamina isolada é o anestésico que menos reduz o metabolismo cerebral	Autorradiografia (^{18}F-FDG) PET dedicada a pequenos animais (^{18}F-FDG)

continua

Tabela 3 - Comparação entre os efeitos dos anestésicos nos diferentes métodos de quantificação do metabolismo glicolítico

continua

Pesquisador	Método de Anestesia	Resultados	Método de Aquisição
Toyama	Isoflurano Cetamina + Xilazina Controle (*uptake* acordado)	- diminuição do metabolismo cerebral em todos os anestésicos em relação ao controle - aumento do metabolismo cardiaco com isoflurano em relação ao controle - diminuição do metabolismo cardiaco com cetamina + xilazina em relação ao controle	PET dedicada a pequenos animais (^{18}F-FDG) Biodistribuição (^{18}F-FDG)
Toyama	Isoflurano Cetamina + Xilazina Controle (*uptake* acordado)	- demonstra a forte correlação entre as técnicas para camundongos normoglicêmicos - maior diminuição do metabolismo cerebral com uso do isoflurano quando comparado a cetamina + xilazina	Autorradiografia (^{14}C-DG) PET dedicada a pequenos animais com quantificação por farmacocinética (^{18}F-FDG)
Yu	Isoflurano	- demonstra que a melhor estimativa para o metabolismo cerebral da ^{18}F-FDG considera o k_4 e amostras de sangue arterial	PET dedicada a pequenos animais com quantificação por farmacocinética (^{18}F-FDG)
Mizuma	Isoflurano Controle (Animal acordado durante todo o exame)	- diminuição do metabolismo cerebral de animais anestesiadas é devido a redução do k_3	Autorradiografia (^{18}F-FDG) PET dedicada a pequenos animais com quantificação por farmacocinética (^{18}F-FDG)

continua

Tabela 3 - Comparação entre os efeitos dos anestésicos nos diferentes métodos de quantificação do metabolismo glicolítico

conclusão

Pesquisador	Método de Anestesia	Resultados	Método de Aquisição
Prieto	Isoflurano Controle (*uptake* acordado)	- comparação das técnicas de aquisição utilizando SPM demonstram superioridade da autorradiografia na região dos tálamos e decréscimo do metabolismo nos animais anestesiados	Autorradiografia (^{18}F-FDG) SPM (^{18}F-FDG)

FONTE: Hansen et al., 1989; Lenz et al., 1999; Moore et al., 2000; Matsumura et al., 2003; Toyama et al., 2004a; Toyama et al., 2004b; Yu et al., 2009; Mizuma et al., 2010; Prieto et al., 2011.
^{14}C-DG: ^{14}C- desoxiglicose; ^{14}C-IAP: ^{14}C – iodoantipyrine, PET: Tomografia por Emissão de Pósitrons, SPM: *Statistical Parametric Mapping*.

Devido à facilidade e à rapidez com que o protocolo anestésico pode ser alterado, o isoflurano tem sido o anestésico de escolha na maioria dos estudos de imagem com pequenos animais. Quando comparados a animais que foram mantidos acordados durante a incorporação da ^{18}F-FDG, animais anestesiados com isoflurano apresentam redução de 29% da captação cerebral e aumento de 91% da captação cardíaca (Toyama et al., 2004a). A cetamina, associada ao relaxante muscular xilazina reduz a captação cerebral e cardíaca em 39% e 64%, respectivamente (Toyama et al., 2004a).

O relaxante muscular xilazina estimula diretamente os receptores α_2-adenergicos das células das ilhotas pancreáticas provocando a liberação de insulina, resultando em hiperglicemia (ElMotal; Sharp, 1985). A hiperglicemia causa uma inibição competitiva da ^{18}F-FDG resultando em menor incorporação da mesma (Orzi et al., 1988).

A quantificação também é afetada por outros fatores técnicos abordados anteriormente como: as correções aplicadas à imagem, movimentação, reconstrução tomográfica e a própria técnica escolhida para quantificação (Vanhove et al., 2015).

2. OBJETIVOS

Avaliar e correlacionar as técnicas de quantificação do metabolismo da ^{18}F-FDG no sistema nervoso central de ratos anestesiados utilizando os métodos de: modelo de compartimento de dois tecidos (2TCM), Patlak, *Fractional uptake value* (FUR) e semiquantificação (SUV).

Avaliar os efeitos dos anestésicos isoflurano e cetamina associada a xilazina no metabolismo da ^{18}F-FDG no sistema nervoso central de ratos utilizando os métodos de: modelo de compartimento de dois tecidos (2TCM), Patlak, semiquantificação (SUV) e análise baseada em *voxel* (ABV).

3. TEXTO SISTEMATIZADO

3.1 Organização do texto sistematizado

O texto sistematizado se refere às seguintes publicações agrupadas de acordo com os objetivos da tese:

Avaliar e correlacionar as técnicas de quantificação do metabolismo da ^{18}F-FDG no sistema nervoso central de ratos anestesiados utilizando os métodos de: modelo de compartimento de dois tecidos (2TCM), Patlak, *Fractional uptake value* (FUR) e *Standardized uptake value* (SUV).

- Estudos: Prando et al., 2018 (Publicação 1); Prando et al., 2019 (Publicação 2);

Avaliar os efeitos dos anestésicos isoflurano e cetamina associada a xilazina no metabolismo da ^{18}F-FDG no sistema nervoso central de ratos utilizando os métodos de: modelo de compartimento de dois tecidos (2TCM), Patlak, *Standardized uptake value* (SUV) e análise baseada em *voxel* (ABV).

- Estudo: Prando et al., 2019 (Publicação 3).

3.2 Métodos de quantificação

- **Publicação 1:**

Prando S, Ono CR, Robilotta CC, Sapienza MT. Methods for quantification of cerebral glycolytic metabolism using 2-deoxy-2-[18F]fluoroglucose in small animals. Res Biomed Eng. 2018; 34(3):254-272. DOI: 10.1590/2446-4740.04517

Nos últimos 50 anos, a medicina nuclear passou por uma profunda evolução, marcada, em particular, pelo progresso tecnológico dos sistemas de varredura, equipados com detectores de cintilação mais avançados, transformados de geometrias planas em cilíndricas, de configurações bidimensionais a tridimensionais, supridas com algoritmos de reconstrução baseados em modelagens, com o objetivo de tornar o equipamento melhor em termos de resolução e sensibilidade (Polidori A et al., 2019). Um desses avanços foi o desenvolvimento da versão miniaturizada do equipamento de PET, chamada de microPET, usado em imagens de pequenos animais.

Com o avanço tecnológico, estudos de neuroimagem se tornaram bastante frequentes em animais e modelos para uma variedade de doenças humanas. Os modelos animais de doenças cerebrais abrangem algumas das principais doenças neurodegenerativas, acidente vascular cerebral e doenças psiquiátricas, como depressão e ansiedade (Blandini F; Armentero MT, 2012; Haller J; Alicki M, 2012). Além disso, a PET em pequenos animais permite um acompanhamento longitudinal, o que é importante quando se investigam intervenções neurofarmacológicas ou caracterização de doenças.

Na imagiologia cerebral, a principal vantagem da PET é a sua capacidade de fornecer informações sobre processos bioquímicos, neuroquímicos ou farmacológicos utilizando métodos de quantificação (Lancelot S; Zimmer L, 2010).

A PET ainda pode ser descrita como uma versão *in vivo* da autorradiografia, com resolução espacial inferior, mas com a vantagem de que a farmacocinética do traçador pode ser medida em um único experimento ou em estudos repetidos sobre o mesmo indivíduo através da análise quantitativa. A autorradiografia, embora possua uma resolução espacial superior a PET, não permite estudos longitudinais e é considerada uma técnica *ex vivo*.

A análise quantitativa permite estabelecer uma relação direta entre a concentração de atividade variável no tempo em órgãos/tecidos de interesse e os parâmetros funcionais que representam os processos biológicos subjacentes no nível celular. Diversas técnicas de quantificação são empregadas na literatura de imagens médicas e indicam diferentes abordagens de mensuração como: quantificação relativa, também conhecida como semiquantificação, quantificação absoluta da concentração de atividade e quantificação fisiológica, onde a concentração absoluta de atividade é convertida em parâmetros moleculares de interesse (Zaidi H; Alavi A, 2014).

Não obstante o potencial inerente da PET, a mais avançada entre as técnicas de medicina nuclear para a quantificação de variáveis fisiológicas, esse potencial nem sempre é totalmente explorado nos estudos clínicos e pré-clínicos.

Neste contexto, e com o objetivo de incentivar seu uso racional, revisamos as principais técnicas de quantificação utilizadas no âmbito pré-clínico e que são aplicadas no estudo do metabolismo da ^{18}F-FDG PET em pequenos animais. A técnica de análise baseada em *voxel* (ABV), embora não seja um método de quantificação, mas comparativo, foi incluída na revisão devido a sua extensiva aplicação no contexto clínico e recentemente, no contexto pré-clínico.

A abordagem mais apropriada para derivar parâmetros fisiológicos na tomografia por emissão de pósitrons envolve quatro etapas: (1) medição da distribuição do radiofármaco no sistema fisiológico de interesse ao longo do tempo, através da aquisição de uma série temporal de imagens conhecida como imagem dinâmica; (2) medição da quantidade de radiofármaco que foi disponibilizada para os órgãos de interesse, usando amostras de sangue arterial ao longo do tempo para obter o que é chamado de função de entrada arterial; (3) modelagem do sistema fisiológico de interesse usando um pequeno número de "compartimentos" ligados através de parâmetros fisiológicos que descrevem as trocas entre compartimentos; (4) ajustando a função de entrada arterial e as concentrações do radiofármaco medidas em diferentes regiões (compartimentos) ao modelo cinético, para estimar os parâmetros fisiológicos do modelo (Buvat, 2007).

O primeiro método de avaliação do metabolismo da glicose foi criado por Sokoloff e colaboradores (Sokoloff et al., 1977) que utilizaram a glicose marcada com ^{14}C e a autorradiografia. Diante das inúmeras dificuldades do método e da utilização do radiofármaco, Ido (1978) desenvolveu a ^{18}F-FDG que

conhecemos atualmente. Phelps e colaboradores (1979) propiciaram um avanço no entendimento do metabolismo da glicose no cérebro aplicando a técnica em seres humanos.

A autorradiografia apresenta vantagens quanto à resolução espacial, porém limitações como a quantidade de animais necessários, tempo de processamento dos dados e sua aplicação *ex vivo* fizeram com que a técnica esteja em desuso nos dias atuais.

Embora a autorradiografia tenha sido considerada o padrão ouro para quantificação do metabolismo cerebral da glicose, suas desvantagens fizeram com que, nos dias atuais, a modelagem cinética, através dos modelos compartimentais com a PET, seja considerada o padrão ouro para estimativa da taxa metabólica cerebral de glicose (CMR_{gl}).

Na quantificação através da modelagem cinética em PET, o objetivo é estimar parâmetros fisiológicos utilizando imagens dinâmicas frequentemente combinadas com a medição da função de entrada arterial e, dependendo do radiofármaco empregado, da determinação da fração intacta ao longo do tempo. Embora seja considerado o padrão ouro para quantificação, o método não está isento a críticas. Para calcular o consumo de glicose no cérebro, o modelo compartimental (CM) para ^{18}F-FDG utiliza uma constante de proporcionalidade, conhecida como *lumped constant* (LC), entre a ^{18}F-FDG e a glicose. A constante, formulada por Sokoloff (1977), reflete as diferenças nas taxas de transporte e fosforilação entre a glicose e a ^{18}F-FDG e é usada para transformar a taxa de captação de ^{18}F-FDG em taxa de captação de glicose. Acredita-se que sobre condições fisiológicas, onde o nível de glicose no

sangue permanece constante, a LC mantém-se estável. Entretanto, vários estudos demonstraram que existem diferenças para a LC e ainda não existe um consenso sobre seu valor (Orzi et al., 1988).

A taxa metabólica cerebral de glicose (CMR_{gl}) pode ser usada quando há interesse em medições comparativas, principalmente se houver mudanças metabólicas ao longo do tempo, durante o tratamento, entre um tecido doente, e outro normal, ou entre diferentes estados fisiológicos, presumindo que a LC do tecido sob investigação permaneça inalterado. A utilização de anestésicos pode levar a uma alteração da LC, impossibilitando o seu uso a menos que uma nova LC seja obtida. Nesses casos, pode-se optar pela utilização da taxa de influxo líquida (K_i) ao invés da taxa metabólica cerebral de glicose (CMR_{gl}). Adotamos esta estratégia nas publicações 2 e 3 devido à incerteza do valor da LC em razão da utilização de anestésicos para imobilização dos animais durante o período de aquisição das imagens.

Os modelos compartimentais fornecem uma quantidade importante de informações sobre a cinética do traçador. Entretanto, necessita-se de imagens dinâmicas, e portanto, tempo de equipamento, amostras de sangue arterial, e de pessoal especializado para o processamento do estudo. Uma alternativa ao modelo compartimental para substâncias irreversíveis é a utilização de métodos simplificados como o método de linearização de Patlak (Patlak et al., 1983; Patlak e Blasberg, 1985). Embora esta abordagem permita uma simplificação operacional do CM, a desvantagem do método Patlak ainda é a necessidade de amostras de sangue arterial e a incapacidade de calcular os parâmetros cinéticos separadamente (K_1, k_2, k_3); para ^{18}F-FDG, por exemplo, o

método não discrimina entre o transporte de glicose (K_1) e a atividade da hexoquinase (k_3). Em compensação, é um método mais fácil de implementar e menos sensível ao ruído inerente ao início do estudo. Porém, a aquisição de imagens dinâmicas leva tempo e a coleta de sangue arterial é invasiva. É por isso que, na maioria das aplicações, um procedimento simplificado de quantificação é usado, muitas vezes à custa da exatidão quantitativa.

Entre os métodos simplificados de quantificação mais empregados na atualidade está o *Standardized uptake value* (SUV), que é uma simplificação do método de Patlak (Weber et al., 2000). O SUV relaciona a atividade do tecido com a atividade injetada e o peso corporal ou área do indivíduo. Como o SUV é um parâmetro usado com tanta frequência em diagnóstico clínico, torna-se cada vez mais aplicado no campo pré-clínico. As limitações técnicas do SUV relacionadas à aquisição e às correções da imagem já foram exploradas em inúmeras publicações e não foram exploradas na publicação 1 pois já existe uma extensa literatura a respeito.

O ruído da imagem, baixa resolução e definição da região de interesse (ROI) afetam o SUV e podem dificultar seu uso, especialmente em ensaios multicêntricos (Boellaard et al., 2004).

Além dos problemas mencionados acima, as desvantagens do SUV incluem sua fraca reprodutibilidade, que está intimamente relacionada aos parâmetros técnicos e, principalmente, a não extravasamento no local da injeção e a definição da área/volume de interesse, que é um desafio no estudo de pequenos animais (Adams et al., 2010).

Em estudos clínicos, o SUVmax é mais amplamente utilizado que o SUVmédio porque além de ser independente do operador, representa o *voxel* com maior captação e presumivelmente a área com maior taxa metabólica no volume analisado. No entanto, em estudos com pequenos animais, o SUVmédio é mais utilizado porque é menos suscetível ao ruído do que o SUVmax.

Para utilizar o SUV não é necessário o uso de amostras de sangue, que é uma das razões para o SUV ser o método preferido. Se houver amostras de sangue, uma alternativa simples e mais quantitativa que SUV é a taxa de captação fracionária (FUR).

Antes do advento da ABV, as imagens cerebrais de PET foram analisadas através da delineação manual de regiões de interesse para investigar a existência de áreas com metabolismo alterado. Esta abordagem foi estabelecida para análises de autorradiografia de escaneamentos neurofisiológicos e metabólicos básicos de humanos (Friston, 2007). Além de consumir muito tempo, o método da ROI pode introduzir imprecisões na análise, pois é dependente do avaliador. No entanto, a dificuldade mais significativa é que as análises de ROI são geralmente guiadas por informações *a priori* da mudança em uma determinada região do cérebro; portanto, possivelmente efeitos significativos fora da ROI específica podem ser perdidos ou o tratamento/intervenção pode induzir um efeito global que é expresso em todos as ROIs. Para superar o desafio de detectar mudanças regionais quando uma mudança global está presente, o *Statistical Parametric Mapping* (SPM) foi desenvolvido.

Incluimos a técnica ABV na publicação 3, onde descrevemos as alterações regionais, apesar da mudanças globais, do metabolismo da glicose utilizando a ^{18}F-FDG-PET em animais anestesiados. Embora sua utilização seja recente e com alguns limitantes, o método se mostra útil para localização de áreas com metabolismo alterado, fornecendo um norte para a aplicação de diversas técnicas de quantificação.

- **Publicação 2:**

Prando S, Carneiro CDG,, Robilotta CC, Sapienza MT. Comparison of different quantification methods for ^{18}F-fluorodeoxyglucose-positron emission tomography studies in rat brains. Clinics. 2019;74:e1273. DOI: 10.6061/clinics/2019/e1273.

A ^{18}F-FDG PET, desde a sua introdução, mostrou-se uma das técnicas de neuroimagem mais adequadas para a investigação não invasiva da função cerebral. Uma das perspectivas mais importantes da PET é a possibilidade de quantificação de um sinal biológico através da medida de concentrações locais de radioatividade no cérebro e no sangue arterial.

A tomografia por emissão de pósitrons com ^{18}F-FDG seguida de modelagem matemática é considerada o padrão ouro para avaliação do metabolismo cerebral. Entretanto, devido aos desafios técnicos e complexidade de implementação, o método não é aplicado rotineiramente. Além disso, a quantificação de parâmetros fisiológicos requer a aquisição de imagens dinâmicas longas e, dependendo do equipamento disponível, permite apenas a avaliação de um campo de visão por estudo.

Para superar esses desafios, abordagens semiquantitativas ou relativas foram introduzidas e se tornaram padrão por sua simplicidade de aplicação. Nos dias atuais é notória a procura por métodos simplificados de quantificação para os estudos pré-clínicos e sua translação para os estudos clínicos.

Neste contexto, investigamos se um método de análise simplificado poderia ser utilizado para avaliar o metabolismo cerebral da ^{18}F-FDG em uma população heterogênea.

Como a população utilizada neste estudo é mista em relação ao anestésico utilizado, e não se sabe ao certo qual o efeito dos anestésicos sob a *lumped constant*, preferimos utilizar a taxa líquida de captação (K_i) ao invés da taxa metabólica cerebral de glicose (CMR_{gl}).

Inicialmente, analisamos a correlação e a concordância do K_i obtido da análise gráfica de Patlak com o K_i fornecido pelo método compartimental de dois tecidos (2TCM) e posteriormente, avaliamos a possibilidade da correlação do padrão ouro com um método simplificado.

O método gráfico de Patlak se baseia no modelo compartimental, para traçadores irreversíveis, e utiliza a regressão linear para identificar e analisar a farmacocinética da ^{18}F-FDG. Ele supõe que o comportamento do traçador possa ser aproximado por dois compartimentos, um compartimento central e reversível que alcança rapidamente o equilíbrio com o plasma e um compartimento periférico, onde o traçador fica retido irreversivelmente durante o estudo (Patlak et al., 1983; Patlak e Blasberg, 1985). A taxa líquida de captação (K_i) da ^{18}F-FDG é obtida pela inclinação da reta quando o sistema de

compartimentos alcança o estado estacionário, o que ocorre após um intervalo de tempo depois da introdução do traçador no sistema.

Embora o método desenvolvido por Patlak e utilizado no artigo seja considerado uma simplificação do ponto de vista metodológico e do processamento, ainda assim, necessita da aquisição da imagem dinâmica e da função de entrada. Sua menor complexidade de processamento permite que seja aplicado mais facilmente na rotina pré-clínica e que os resultados obtidos pelo método sejam menos afetados pelo ruído presente no início do estudo.

Os resultados que obtivemos no estudo demonstraram que o método de Patlak pode ser utilizado na rotina pré-clínica como uma substituição ao método compartimental.

Além do Patlak, testamos se outros métodos simplificados disponíveis na literatura poderiam ser utilizados para avaliar a taxa de consumo da ^{18}F-FDG.

Dos métodos simplificados disponíveis na literatura, avaliamos se o valor de captação padronizado (SUV), o valor de captação padronizado corrigido para glicemia (SUV_{gl}) ou se a taxa de captação fracionária (FUR) poderiam ser uma alternativa à análise da ^{18}F-FDG-PET através de modelagem matemática e à imagem dinâmica para a quantificação do metabolismo cerebral.

A abordagem mais simples utilizada no artigo foi o SUV, definido como a razão entre a concentração do radiofármaco no cérebro num dado intervalo de tempo após a injeção e a quantidade de radioatividade normalizada pelo peso corporal. Esta abordagem é tecnicamente muito simples, pois requer uma

única imagem estática e nenhum conhecimento da concentração do radiofármaco no plasma, portanto não há necessidade de amostragem arterial.

Os SUVs, médio ou máximo, produzem apenas uma estimativa da captação do radiofármaco, pois os valores normalmente variam em função do intervalo de tempo em que são calculados; o método não considera as diferenças específicas da concentração do radiofármaco do plasma circulante, o que pode diminuir a quantidade do radiofármaco disponível para captação; e não distingue entre a ligação não específica e a ligação específica do radiofármaco ao alvo pretendido.

As limitações técnicas relacionadas à aquisição e ao processamento, como é o caso do intervalo de tempo em que é calculado, pode ser facilmente superada por uma equipe treinada.

As diferenças de concentração do radiofármaco no plasma circulante ocorre devido as diferenças de metabolismo entre indivíduos e o uso de medicamentos, que modificam o consumo de glicose em diferentes órgãos e consequentemente, no plasma circulante. No nosso caso, ao utilizarmos anestésicos para imobilizar os animais durante o estudo, introduzimos uma variável a mais na análise, a variação de concentração da ^{18}F-FDG com a dose e com o tipo de anestésico utilizado. Uma tentativa de superação das diferenças de metabolismo entre os indivíduos foi realizada com a incorporação de correções ao SUV. A correção mais utilizada no contexto pré-clínico é a correção pela glicemia basal, o SUV_{gl}.

Nos estudos de ^{18}F-FDG, o SUV pode ser corrigido para o nível de glicose no plasma (Woo et al., 2008). Embora a possibilidade de correção do SUV para o nível de glicemia esteja presente para estudo clínicos no *guideline* de imagem cerebral com ^{18}F-FDG PET da Associação Europeia de Medicina Nuclear (EANM – European Association of Nuclear Medicine) (Varrone et al., 2009), a própria EANM no *guideline* de ^{18}F-FDG-PET para oncologia desencoraja sua aplicação, a menos que sejam utilizados métodos validados e calibrados para verificação da glicemia. Métodos conhecidos como beira de leito são explicitamente desaconselhados e introduzem mais um fator de erro a análise (Boellaard et al., 2015).

Um método simplificado e pouco utilizado tanto na prática clínica como pré-clínica é a taxa de captação fracionária (FUR). A simplificação do método reside na necessidade de adquirir uma imagem estática ao invés da imagem dinâmica utilizada nos métodos compartimentais e gráficos. Porém, ainda é necessária a aquisição de amostras de sangue arterial para construção da função de entrada. A grande vantagem dos métodos que utilizam a função de entrada é conhecer a concentração do radiofármaco oferecida ao órgão/região em estudo já corrigida para as diferenças de metabolismo causadas, no nosso caso, pelos anestésicos utilizados. Na publicação 3, exploramos melhor as alterações no metabolismo resultante do uso dos anestésicos isoflurano e cetamina associada a xilazina. Entretanto, os resultados da publicação 2 refletem que a comparação entre indivíduos cujo metabolismo da ^{18}F-FDG, e consequentemente da glicose, é influenciado por diferentes tipos de medicamentos é melhor avaliado por métodos que utilizam a função de entrada.

No artigo demonstramos que o FUR (r=0,9385) é melhor correlacionado com o padrão ouro 2TCM do que o SUV (r=0,7336) e o SUV_{gl} (r=0,5419). Portanto, como resultado verificamos que o método simplificado mais adequado é o FUR. O FUR é um quantificador simplificado de PET, que pode ser calculado a partir de uma única imagem de PET tardio, como o SUV, porém a função de entrada é necessária para todo o tempo de metabolização do radiofármaco e reflete as alterações metabólicas causadas pelos anestésicos utilizados no estudo.

3.3 Efeitos dos anestésicos no metabolismo cerebral da glicose

- **Publicação 3:**

Prando S, Carneiro CDG, Otsuki DA, Sapienza MT. Effects of ketamine/xylazine and isoflurane on rat brain glucose metabolism measured by 18F-fluorodeoxyglucose-positron emission tomography. Eur J Neurosci. 2019;49:51–61. DOI: 10.1111/EJN.14252

A ^{18}F-Fluorodeoxyglucose (^{18}F-FDG) é um radiofármaco análogo de glicose marcado com fluor-18 usado para avaliar o metabolismo glicolítico de diferentes regiões do corpo, entre eles, o cérebro. Nos modelos animais, o aumento ou diminuição no metabolismo cerebral regional são indicativos de atividade neuronal, que pode ser alterada por doenças ou pelo uso de drogas.

Para investigar as anormalidades do metabolismo glicolítico em pequenos animais utilizando tomografia por emissão de pósitrons com fluordeoxiglicose (^{18}F-FDG-PET), devemos restringi-los fisicamente. O modo mais comum de contenção é através do uso de anestésicos, entretanto, a própria anestesia induz mudanças significativas na metabolismo do sistema

nervoso central. Os efeitos dos anestésicos sobre cinética da droga ou doença alvo nem sempre são conhecidos e podem confundir os resultados de um estudo. Além de seus efeitos diretos no metabolismo, o uso de diferentes anestésicos pode inviabilizar as comparações de resultados e a reprodução de estudos em diferentes laboratórios.

Estudos anteriores demonstraram alterações no fluxo sanguíneo e no metabolismo da glicose no cérebro em associação com diferentes classes de anestésicos (Långsjö et al., 2004; Matsumura et al., 2003; Mizuma et al., 2010; Sokoloff et al., 1977; Toyama et al., 2004a,b). Enquanto os mecanismos moleculares subjacentes às ações dos anestésicos no cérebro não são totalmente compreendidos, acredita-se que o estado anestésico é resultado de múltiplos alvos moleculares nas diferentes regiões do cérebro e do sistema nervoso central. Anatomicamente, cada ação anestésica ocorre em diferentes regiões, resultando em assinaturas distintas de eletroencefalograma (Hemmings et al., 2005; Purdon, Sampson, Pavone, & Brown, 2015) e de metabolismo.

Os anestésicos mais utilizados em nosso laboratório, na época do estudo, eram isoflurano (I) e cetamina associada a xilazina (KX). A combinação de cetamina e xilazina era utilizada quando o estudo não poderia ser realizado com o fornecimento de oxigênio para o animal, em estudos de hipóxia, por exemplo.

O isoflurano já foi extensamente estudado no contexto do metabolismo da glicose no cérebro de pequenos animais, principalmente porque a grande maioria dos laboratórios utiliza isoflurano para imobilização dos animais. A cetamina associada com xilazina é um anestésico mais antigo que o isoflurano,

entretanto, nenhum estudo de análise cinética da ^{18}F-FDG na vigência do anestésico foi localizado na literatura antes do início desse estudo.

Nesse contexto, estudamos as alterações do metabolismo da glicose no cérebro de animais anestesiados com isoflurano e com cetamina associada a xilazina.

Os métodos de quantificação do metabolismo da glicose escolhidos foram o SUV e a análise cinética e completamos o estudo com a comparação dos grupos *voxel* a *voxel* através da análise baseada em *voxel* (ABV). Os resultados da quantificação foram abordados no contexto regional e global.

No contexto global, a análise cinética pelos métodos 2TCM e Patlak não demonstraram diferença significativa entre os dois grupos de anestésicos, enquanto a análise através do SUV demonstrou que o grupo KX tem menor metabolismo cerebral que o grupo I. Considerando que existam diferenças metabólicas entre os grupos devido à ação dos anestésicos, avaliamos que a diferença registrada pelo SUV é superestimada quando comparada à análise cinética.

As principais diferenças metabólicas verificadas pela análise cinética são a redução do volume de distribuição e da taxa de transporte da glicose K_1 no grupo dos animais anestesiados com cetamina associada a xilazina. Essas alterações indicam que o SUV não é o melhor método de quantificação no caso de estudos envolvendo diferentes anestésicos.

As reduções do volume de distribuição e no transporte ocorreram principalmente por mecanismos indiretos da KX no metabolismo cerebral da glicose. Pode-se citar como principais mecanismos a influência da KX no

sistema nervoso simpático, na receptação da norepinefrina e no aumento agudo da glicemia.

Embora no contexto global se verifique a diminuição do metabolismo da glicose na vigência de anestésicos, sabe-se que os efeitos dos anestésicos no metabolismo relativo diferem em função da droga usada. Os anestésicos, de modo geral, atuam em múltiplos alvos no cérebro e no sistema nervoso central, aumentando e/ou bloqueando diferentes receptores e canais, resultando em diferentes padrões de metabolismo da glicose no cérebro.

No contexto regional, verificamos que existem diferentes padrões de metabolismo nas regiões cerebrais de acordo com o anestésico aplicado. Quando utilizamos o SUVR ou a relação córtex/cérebro do K_i para avaliação do metabolismo cerebral regional verificamos que animais anestesiados com cetamina associada com xilazina apresentam o metabolismo cortical mais preservado quando comparado ao metabolismo do cérebro global e aos animais anestesiados com isoflurano. O padrão de heterogeneidade de metabolismo da glicose se repetiu em todos os animais do grupo KX e gerou uma assinatura do anestésico no metabolismo cerebral da glicose, como pode ser verificado nos resultados obtidos através da análise baseada em *voxel*.

Esse padrão de heterogeneidade se deve principalmente às custas da perda de regulação dos interneurônios inibitórios, resultando em uma atividade excitatória em neurônios piramidais. O controle prejudicado dos neurônios piramidais é a principal causa do aumento do metabolismo cerebral cortical (Brown, Solt, Purdon & Johnson-Akeju, 2015).

Além das alterações globais e regionais do padrão metabólico verificadas pelos métodos de quantificação utilizados neste estudo,

empregamos a técnica de análise baseada em *voxel* para comparação dos grupos. Neste ponto devemos fazer uma observação a respeito da normalização das contagens. Pode-se escolher entre diversos tipos de normalização utilizando, por exemplo, a média de contagens do estudo ou de uma região especifica do cérebro que não seja afetada pela intervenção/doença. Neste caso, estaremos analisando as alterações regionais em relação a região escolhida para normalização. Neste estudo escolhemos a média de informação do estudo completo, pois não existe uma área do cérebro não afetada pelos anestésicos utilizados. A comparação realizada com a aplicação da normalização proporcional revela resultado similar ao obtido pela relação do K_i (córtex/cérebro) e do SUVR (córtex/cérebro), na qual o grupo KX têm o metabolismo cortical mais preservado em relação ao metabolismo cerebral quando comparado ao grupo I. No caso da comparação sem a normalização de contagens, obteve-se um mapa revelando a diminuição do metabolismo global do grupo KX em relação ao I.

Esta publicação lançou ainda as bases para uma linha de pesquisa, em cooperação com o departamento de Anestesiologia através do Lim 08, que tem grande tradição no estudo de alterações fisiológicas dos anestésicos em animais.

Outro mérito deste estudo é o fato de que o artigo foi o pioneiro na obtenção dos dados de análise cinética da ^{18}F-FDG em animais anestesiados com cetamina associada a xilazina.

4. CONCLUSÕES

4.1 Método de Quantificação

1. Através da comparação dos métodos utilizados neste estudo (publicação 1 e 2), verificamos que os de linearização de Patlak e o FUR apresentam os melhores resultados quando comparados ao padrão ouro e podem ser adotados sem prejuízo da quantificação do metabolismo cerebral da glicose.
2. A aquisição de imagens dinâmicas não é o fator mais importante para se obter a quantificação do metabolismo cerebral da glicose. Os métodos melhor correlacionados são aqueles que utilizam a função de entrada como estimativa do metabolismo do indivíduo.
3. A comparação do metabolismo cerebral da glicose entre indivíduos, grupos ou entre ambos utilizando o SUV deve ser realizada com extrema cautela devido às limitações do método. Enquanto as limitações referentes à aquisição e ao processamento podem ser superadas facilmente por uma equipe adequadamente treinada, aquelas relacionadas à normalização e portanto, a estimativa em relação ao metabolismo individual não são facilmente suplantadas e devem ser estudas antes da aplicação do método.
4. A correção do SUV utilizando a glicemia basal do individuo não deve ser adotada como prática rotineira a menos que a estimativa da glicemia seja realizada com um método enzimático, métodos conhecidos como de cabeceira de leito introduzem mais um fator de erro ao SUV.

4.2 Efeitos dos anestésicos no metabolismo cerebral da glicose

1. Ambos os anestésicos utilizados neste estudo (publicação 3) reduzem o metabolismo cerebral da glicose produzindo assinaturas metabólicas características. O isoflurano diminui o metabolismo em córtex cerebral enquanto a redução causada pela cetamina associada a xilazina é menos acentuada.
2. Em relação à farmacocinética, ocorreram reduções do volume de distribuição e no transporte principalmente por mecanismos indiretos da cetamina associada a xilazina no metabolismo cerebral da glicose em relação ao grupo I. Pode-se citar como principais mecanismos a influência da cetamina associada a xilazina no sistema nervoso simpático, na recaptação da norepinefrina e no aumento agudo da glicemia.
3. A análise baseada em *voxel* realizada pelo SPM com a aplicação da normalização proporcional revela resultado similar ao alcançado pela relação córtex/cérebro obtida através do K_i e do SUVR. O resultado nos permite afirmar que a técnica pode ser aplicada para comparação entre grupos para verificação de alterações do metabolismo cerebral regional da glicose

5. PERSPECTIVAS FUTURAS

A maior limitação dos estudos de pequenos animais e principalmente de sua translação para a clínica é a obtenção da função de entrada arterial.

Para obter a quantificação até o ponto de derivar as constantes regionais de taxa de troca compartimental e, portanto, parâmetros biológicos específicos, é necessária uma função de entrada de sangue arterial. Em pequenos animais é usual a obtenção da função de entrada a partir da coleta amostras de grandes artérias. Entretanto, para seres humanos a técnica é invasiva e não isenta de complicações. Por outro lado, se funções de entrada arterial de alta qualidade pudessem ser obtidas a partir de imagens de artérias, poderíamos promover a PET como uma ferramenta quantitativa de rotina no diagnóstico clínico.

6. ANEXOS

6.1 Comissão de Ética no Uso de Animais.

MEDICINA
USP

COMISSÃO DE ÉTICA NO USO DE ANIMAIS

A CEUA do Comitê de Ética em Pesquisa da Faculdade de Medicina da Universidade de São Paulo, em sessão de 08/05/2014, **APROVOU** o Protocolo de Pesquisa nº 026/14 intitulado: "**Avaliação dos métodos de quantificação do metabolismo glicolítico cerebral em ratos anestesiados utilizando microPET/CT com 18FFDG**" que utilizará **45** animais da espécie **ratos wistar**, apresentado pelo **Departamento de Clínica Médica**.

Cabe ao pesquisador elaborar e apresentar ao CEP-FMUSP, o relatório final sobre a pesquisa, (Lei Procedimentos para o Uso Científico de Animais - Lei Nº 11.794 -8 de outubro de 2008).

Pesquisador (a) Responsável: Marcelo Tatit Sapienza
Pesquisador (a) Executante: Silvana Prando

CEUA-FMUSP, 08 de Maio de 2014.

Dr. Eduardo Pompeu
Coordenador
Comissão de Ética no Uso de Animais

Prof. Dr. Roger Chammas
Coordenador
Comitê de Ética em Pesquisa

Comissão de Ética no Uso de Animais da FMUSP
e-mail: ceua.fm@usp.br

6.2 Methods for quantification of cerebral glycolytic metabolism using 2-deoxy-2-[^{18}F]fluoroglucose in small animals (Publicação 1).

RESEARCH ON BIOMEDICAL ENGINEERING
rbejournal.org
ISSN 2446-4740 (Online)
Volume , Number , p. ,
DOI: https://doi.org/10.1590/2446-4740.04517

Methods for quantification of cerebral glycolytic metabolism using 2-deoxy-2-[^{18}F]fluoroglucose in small animals

Silvana Prando[1]*, Carla Rachel Ono[1], Cecil Chow Robilotta[2], Marcelo Tatit Sapienza[1]

[1] *Nuclear Medicine Center, School of Medicine, University of São Paulo, São Paulo, SP, Brazil.*
[2] *Institute of Physics, University of São Paulo, São Paulo, SP, Brazil.*

Abstract **Introduction:** The use of the same imaging and quantification techniques in small animals and clinical studies presents the opportunity for direct translational research in drug discovery and development, in neuropharmacological basis of neurological and psychiatric diseases, and in optimization of drug therapy. Thus, positron emission tomography (PET) studies in rodents can bridge the gap between pre-clinical and clinical research. The aim should be to find a method with capability to measure, without compromising accuracy, glucose distribution in the structures of the brain, which can also be used in pathological situations and with applicability for other substances than glucose analogue. **Methods:** This is a systematic review of several assessment techniques available, including visual and quantitative methods that enable the investigation of the transport mechanisms and enzymes involved in glucose metabolism in the brain. In addition to the ex vivo methods, PET with glucose analogues allows in vivo analyses using qualitative, semiquantitative and quantitative methods. **Results:** These techniques provide different results, and the applicability of a specific method is related to the purpose of the study and the multiple factors that may interfere in the process. **Conclusion:** This review provides a solid background of tools and quantification methods for medical physicists and other professionals interested in cerebral glycolytic metabolism quantification in experimental animals. It also addresses the main factors related to animals, equipment and techniques that are used, as well as how these factors should be understood to better interpret the results obtained from experiments.

Keywords Nuclear medicine, Quantification, Positron emission tomography, Metabolism, FDG, Brain.

Introduction

The brain is an organ with high metabolism but without an energy reserve (Catafau, 2001). Neuronal activity therefore depends on a continuous supply of oxygen and energy substrate, which is guaranteed by cerebral blood flow (CBF). The energy substrate is basically represented by glucose because fatty acids do not cross the blood-brain barrier, and energy generation from ketone bodies is only substantial during the first month of life of an animal (Nehlig, 1997). The intensity of cerebral activity is regionalized due to the organization of neuronal groups and the oxygen and glucose regulatory and consumption mechanisms; thus, consumption is four times greater in the grey matter than in the white matter (Nehlig, 1997). The direct relationship between metabolism and CBF was initially postulated by Roy and Sherrington (1890) and is observed not only under physiological conditions but also in most diseases. Imaging techniques are applied for detecting cerebral blood flow or metabolism in a wide variety of clinical situations. Positron emission tomography (PET) and single-photon emission computed tomography (SPECT) are the main nuclear imaging modalities adopted, both of which provide functional information that is used in the diagnosis and prognosis of conditions such as epilepsy, dementia, brain neoplasms, and stroke (Blake et al., 2003; Silverman, 2004).

The first attempts to measure the metabolic rate of glucose used a ^{14}C-labelled glucose molecule, [^{14}C] glucose, which is metabolized via the same glycolytic pathway and the tissue concentration of which can be measured by autoradiography (Sokoloff et al., 1977). However, the disadvantage of [^{14}C] glucose is the rapid rate at which it is converted to CO_2 and water. Because CO_2 is rapidly removed from tissues, the accumulation of radioactivity in the tissue is small and difficult to assess. Sokoloff and colleagues described the preparation

This is an Open Access article distributed under the terms of the Creative Commons Attribution License, which permits unrestricted use, distribution, and reproduction in any medium, provided the original work is properly cited.

How to cite this article: Prando S, Ono CR, Robilotta CC, Sapienza MT. Methods for quantification of cerebral glycolytic metabolism using 2-deoxy-2-[^{18}F]fluoroglucose in small animals. Res Biomed Eng. ; :. DOI: 10.1590/2446-4740.04517

**Corresponding author:* Hospital das Clinicas, Departamento de Radiologia, Serviço de Medicina Nuclear, Faculdade de Medicina, Universidade de São Paulo, Rua Dr. Ovídio Pires de Campos, 872, Cerqueira César, CEP 05403-911, São Paulo, SP, Brasil. E-mail: prando@usp.br

Received: 11 August 2017 / *Accepted:* 21 June 2018

of 2-deoxy-D-[^{14}C] glucose (^{14}C-DG), a molecule that shares the metabolic pathway of glucose only at the steps of cellular internalization by the GLUT protein and phosphorylation by hexokinase. The generated product, 2-deoxyglucose-6-phosphate, does not undergo further metabolization and is retained inside cells, facilitating the measurement by autoradiography of the amount of glucose captured by the cells (Sokoloff et al., 1977).

Ido et al. (1978) published the results of the preparation of 2-deoxy-2-[^{18}F]fluoroglucose (FDG), a DG molecule labelled with a positron emitter, fluorine-18, which allows obtaining images of glucose consumption using PET. This technique led to advances in the understanding of brain functioning and in the direct relationship between functional activity, metabolism and blood flow (Ingvar, 1982), as well as in the detection of tumours with high glucose uptake and metabolism. Although structurally different from DG, FDG is considered to be very similar to DG regarding its absorption and metabolism *in vivo* (Phelps et al., 1979; Sokoloff, 1981a; 1981b). Phelps et al. (1979) adopted the ^{14}C-DG model developed by Sokoloff (1977) to estimate the FDG kinetics and demonstrated that PET, with modelling for FDG, can be reliably used to estimate the rate of glucose metabolism.

Positron emission tomography is a well-accepted method for the quantitative and non-invasive imaging of biological functions; this technique enables physicians to monitor the presence of tracers labelled with positron emitters. The delivery, distribution, and kinetic patterns of a labelled compound in relation to the specific biomolecule in the target tissue are assumed to reflect specific biological functions in the living body.

The use of the same imaging techniques in pre-clinical studies of small animals (primarily rodents such as rats and mice) and clinical studies of humans presents the opportunity for direct translational research in drug discovery and development, the neuropharmacological basis of psychiatric disease, and the optimization of drug therapy (Hargreaves and Rabiner, 2014; Tsukada, 2012). Thus, PET studies in rodents can bridge the gap between pre-clinical and clinical research. However, the ideal pre-clinical animal model does not exist because enzyme systems and metabolism may differ between humans and other animals.

This work reviews the quantification methods of cerebral glycolytic metabolism most often applied in studies in small animals (i.e., rats and mice) using FDG as a radiotracer.

Ex vivo quantification methods: Autoradiography

Histology and autoradiography are widely available techniques for anatomical and functional neuroimaging of small animals. Histological analysis is the gold standard for an accurate description of neuroanatomy and the characterization of brain tissue. Autoradiography is a technique that allows visualization of molecules or fragments of molecules that have been radioactively labelled using X-ray film, phosphor imaging plates (IP), beta imaging systems, or photonuclear emulsion. Furthermore, this technique has been used for decades to quantify and localize drugs in tissues and cells (Solon, 2015).

Autoradiography is subdivided into two broad modalities commonly referred to as quantitative whole-body autoradiography (QWBA), or autoradioluminography, and microautoradiography (MARG). QWBA provides full-body, high-resolution images of the spatial distribution of radiolabelled compounds used in laboratory animals. The major advantages of QWBA include the possibility of determining compound concentrations in regions with thicknesses between 50 and 100 µm and minimal sample manipulation, thereby reducing the chance of cross-contamination and exsanguination effects that occur during tissue extraction. However, QWBA cannot provide data at the cellular level because the procedures necessary to freeze the sample alter the cellular morphology, which does not occur with MARG (Solon, 2015). MARG provides the possibility to visually localize radiolabelled compounds at the cellular level in a histological preparation, and it has been widely used to provide important information about cellular mechanisms.

Both techniques require that the animal be euthanized at a given time after the administration of the tracer. The carcass and the tissue (in the cases of QWBA and MARG, respectively) are frozen and cryosectioned to obtain representative samples of the tissue to be studied. The sections are dehydrated and exposed to IP along with radioactivity calibration standards. The resulting images are analysed to determine the concentrations and spatial distribution of the tracer in the tissue (Figure 1). Tissue tracer concentration versus time profiles can then be constructed to provide data for organ- or tissue-specific pharmacokinetic compartmental analyses, enabling the construction and examination of complete kinetic models of the entire body, specific tissues, or both.

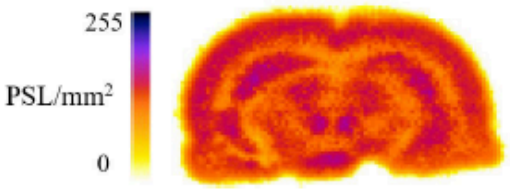

Figure 1. Coronal section of *ex vivo* autoradiography of the rat brain 1 h after intravenous injection of 37 MBq 2-deoxy-2-[^{18}F]fluoroglucose; image plate resolution: 150 µm. PSL: photostimulated luminescence.

A multimodal approach for assessing the distribution of the radiocompound is often useful because QWBA can complement *in vivo* imaging strategies such as PET and SPECT, thereby providing images of the distribution of radioactivity in tissue with enhanced resolution. When the technique is performed with FDG and immediately after PET, certain considerations must be made. Generally, autoradiography experiments use C-14 or H-3, which have physical half-lives of years and require three or more days for the preparation of samples for sectioning and subsequent exposure. For these isotopes, thawing and dehydration steps are performed prior to IP exposure. In the case of FDG, the sectioned samples should be immediately positioned on the IP, and the cassette should be kept in a refrigerated environment to avoid resolution loss due to melting. Condensation should also be kept as low as possible to avoid water formation between the samples and the IP, which degrades image quality. Much of the signal that forms the image in the IP comes from the positrons, which have a short range. The IPs are relatively insensitive to high-energy gamma rays such asF-18; therefore, the sections should be positioned with the biological material facing the IP and with a minimum amount of material between them (Stout and Pastuskovas, 2011). To avoid contaminating the IP with the tracer, a thin plastic film can be used between them.

Both QWBA and MARG are based on exposing tissue samples containing radioactive material to radiographic films or stimulated phosphor plates (i.e., IPs). Radiological films have higher spatial resolution than IPs, while the latter are more sensitive. This characteristic allows for the reduction of the exposure time to 1/10 of that required for radiological film, a significant advantage when working with short half-life radionuclides. For quantification purposes, the use of IPs is also more advantageous because there is greater linearity between the radionuclide concentration and the image density information than that observed with radiographic film. The exposure time of the IPs depends on the radionuclide used, its physical half-life, decay mode and the expected amount of radioactivity present in the sample. Detailed information on IP calibration curves and resolution measures can be found in Knol et al. (2008) and Schmidt and Smith (2005).

To establish the relationship between the degree of uptake measured with the detection system and the metabolic rate, it is necessary to construct a calibration curve between known activity levels and the photosensitized luminescence per area resulting from the exposure. A calibration curve should be constructed for each experiment at the same time the IP is exposed to the radiation derived from the tissue studied. In addition, the user must estimate the transfer constants to obtain the total metabolic rate. After obtaining the preliminary data, it is possible to calculate the absolute glucose consumption in different regions of the brain using specific software such as PMOD (www.pmod.com).

Although autoradiography is the gold standard for glucose metabolism quantification, it is important to note that autoradiography is for *ex vivo* use and, therefore, has little application in longitudinal studies. However, quantitative autoradiography data may be useful for making preliminary assessments or for determining whether PET studies are likely to have sufficient power for detecting specific regional changes in small animal images. In addition, high-resolution autoradiography is frequently used to validate the *in vivo* functional results obtained with equipment designed for small animals, and it remains a technical reference in research on functional brain images.

In vivo quantification methods: PET

PET is based on the administration of molecules labelled with positron-emitting radionuclides, and the chemical form of the molecule is designed to investigate a process of interest, such as glucose uptake rates in the case of FDG. PET has evolved from an imaging mode based primarily on visual analysis into a fairly accurate quantitative imaging tool in which biological processes can be quantitated and compared in terms of binding potential or transfer rates. Factors that contributed to this evolution include the increased sensitivity and spatial resolution of the imaging systems (Sossi and Ruth, 2005).

New developments in PET equipment have improved the contrast and spatial resolution while maintaining a high sensitivity, but the spatial resolution is still a challenging problem, especially in relation to the intrinsic limit of the positron range before the particle is annihilated. The spatial resolution of PET in clinical studies is approximately 5-10 mm, while the resolution of a system for small animals with fluorine-18-labelled radiopharmaceuticals is 1-2 mm. Despite the lower absolute value compared to clinical studies, the spatial resolution of PET with FDG remains an important limiting factor in the evaluation of glucose metabolism in the brains of small animals because there is a worse ratio between the spatial resolution and the volumes of interest within anatomical structures (Byrnes et al., 2014).

Compared with humans, the activities of radionuclide injected into small animals are proportionally larger to maintain a signal-to-noise ratio close to that obtained in clinical images (Kung and Kung, 2005; Jagoda et al., 2004; van den Hoff, 2011). However, it is necessary to ensure that the tracer principle is not violated, i.e., that the mass of injected FDG stays at a concentration that does not interfere with the glucose metabolism and that no pharmacological effects occur.

A typical 37-MBq dose of FDG corresponds to a fraction of a nanogram of radioactive material. The specific activity is given as the ratio of the activity to the number of grams of material. In the case of FDG, this number is 349 MBq/ng, assuming that all of the FDG is radioactive. If stable FDG is present, there will be more grams of chemical FDG for the same amount of radioactive FDG. However, the total chemical quantity of FDG is insignificant from a pre-clinical point of view (Jadvar and Parker, 2005; Jagoda et al., 2004).

In addition to the resolution, the accuracy and precision of the quantifications in a PET study depend on time scales and, in some cases, the arterial input function.

The input function is the time function of the tracer concentration in the arterial blood or plasma that directly affects the rate of tracer transport in local tissue (Carson et al., 1993; Huang and Phelps, 1985). Several methods exist to obtain the input function; however, the manual collection of arterial blood is considered the gold standard in small animal research. Unfortunately, the manual collection has many drawbacks, including the need of a large number of blood samples, which may alter the circulation dynamics and lead to death due to blood loss or complicate longitudinal studies (Sijbesma et al., 2016). Moreover, sample manipulation increases the researcher exposure to radiation. In addition, the activity concentration of the samples should be measured with gamma counters calibrated for the radioisotope used with the PET device and corrected for radioisotope decay from the time of injection.

An alternative to manual arterial blood sampling is the use of automatic collection devices that measure the radioactivity of the β^+ concentration in the venous blood (Convert et al., 2007; Boellaard et al., 2001; Weber et al., 2002). However, additional corrections, such as for delay and signal dispersion, might be necessary to obtain an accurate input function (Munk et al., 2008; Senda et al., 1988). Moreover, a major drawback is the impossibility of analysing blood samples for radiometabolite-producing tracers to correct the input function. Fortunately, in FDG images, this is not required when the difference between the plasma and whole blood concentration is minimal, and the relationship between the two remains relatively constant over time (Zanotti-Fregonara et al., 2012).

Currently, much effort has been made to develop non-invasive techniques to obtain the input function. Image-derived input function (IDIF) is the most common approach. In this approach, a time-activity curve from the time of injection is drawn directly from the PET image using the amount of radioactivity emitted by large blood vessels or the left ventricle. Challenges, such as the temporal and spatial resolution of the device, intra-frame movement, and noise, as well as partial volume and spillover effects, make the application of this technique a challenge for the brain imaging of small animals. In addition, the input function validated for a given device using certain acquisition and processing parameters cannot be used for another device without previous validation (Zanotti-Fregonara et al., 2011; Zanotti-Fregonara et al., 2009; Kim et al., 2006; Green et al., 1998).

Currently, another much exploited technique is the standardized arterial input function (SAIF). This technique assumes that the shape of the input function curve is constant among animals and that only the amplitude differs. Thus, the individual input function is obtained by averaging several arterial input functions purposely scaled to the individual characteristics of the animal using one or two blood samples. This technique has already been validated for humans and mice in FDG-PET images (Takikawa et al., 1993; Meyer et al., 2006). The main advantage is the absence of artefacts related to noise and partial volume because the technique does not require images to estimate the input function. However, two important restrictions exist: first, the tracer injection should be standardized for all animals; second, all animals should be metabolically similar (Zanotti-Fregonara et al., 2013; Meyer et al., 2017).

The choice of the best input function sampling method depends on the tracer kinetics and on the quantification method used. Quantification via compartmental model (CM) is primarily affected by the shape and occurrence time of the peak plasma concentration of the tracer, and small variations can lead to biased estimates of the micro- and macroparameters. Moreover, the application of non-invasive methods can lead to an increase in the uncertainty of the CM parameter estimates, which becomes a problem when groups of individuals are compared. Non-invasive input function sampling techniques have wide applicability using graphical methods because they are affected by neither the peak time nor the shape of the input function. Moreover, they primarily depend on the area under the curve, which is much easier to estimate than the input function (Zanotti-Fregonara et al., 2011, 2012).

Beyond the input function, the adequate standardization of image acquisition and processing, including factors such as the corrections applied to the acquired images and the chosen tomographic reconstruction and quantification techniques, is also important to improve the accuracy and precision of quantification (Frey et al., 2012; Vanhove et al., 2015).

In addition to these aforementioned technical factors, biological factors, such as the route of FDG administration (Vanhove et al., 2015; Schiffer et al., 2007; Fueger et al., 2006), dietary condition (Vanhove et al., 2015; Fueger et al., 2006), age of the animal (Nehlig, 1997), handling of the animal before and during the

FDG incorporation period (Vanhove et al., 2015), type of anaesthesia (Alstrup and Smith, 2013; Fueger et al., 2006), and glucose levels (Orzi et al., 1988; Viglianti et al., 2017) might alter the biodistribution of the compound. Intravenous administration is preferred due to the greater reproducibility, although intraperitoneal administration of the radiopharmaceutical is also possible (Schiffer et al., 2007). For PET imaging with the glucose analogue FDG, food is often withdrawn for hours before the experiment to reduce the plasma level of glucose, which competes with FDG for the uptake carrier (Vanhove et al., 2015). In rats, feeding is usually restricted for at least 12 h before the study (Deleye et al., 2014). As mice feed frequently and can reach a state of torpor after 7 h of food withdrawal, the fasting period should be kept at a minimum duration (Jensen et al., 2013). Animals kept in environments with very low room temperatures tend to produce heat through the metabolism of brown fat, which decreases the brain uptake of FDG. For this reason, it is recommended that the animal be kept on a heating plate throughout the entire preparation procedure and image acquisition.

There are several ways to acquire PET images. Acquisition can be performed in static, dynamic, or gated modes. For the quantification of cerebral physiological parameters such as blood flow, metabolism, or receptor concentration, static or dynamic images are used. Static acquisition refers specifically to the recording of the radiation emitted by the tracer present in the brain during a certain time interval within the study. The result is a single image that represents the average amount of radioactivity during the examination period. Only semiquantitative information can be derived from static acquisitions, the most well-known being the standardized uptake value (SUV; Huang and Wong, 2017). Dynamic images are composed of multiple sequential images so that the long-term behaviour of the tracer in the tissue can be observed. Dynamic acquisitions differ from a series of static images because they begin immediately after tracer injection, and the radioactivity from the tracer is monitored throughout the examination time and made available in the form of time-activity curves (TACs).

In dynamic images, the acquisition parameters such as the total examination time and the number and duration of the images acquired must be defined by the researcher. The total examination time primarily depends on two factors: the physical and biological half-lives of the tracer in the tissue of interest. Exams lasting a long period of time relative to the physical half-life do not improve the signal-to-noise ratio of the study. At the same time, the kinetics of the tracer, or its biological half-life, is also a determining factor of the total examination time. Tracers with faster kinetics provide biological information in a briefer period of time, reducing the total examination time (Huang and Wong, 2017).

Dynamic data are usually acquired when it is necessary to know the behaviour of the tracer in the system of interest, and it is the only way to obtain truly quantitative measures. Although the acquisition of dynamic images is slower, and the number of exams performed per day is reduced, its major advantage is the flexibility in formatting the data obtained, which produces dynamic images with different time intervals and even static images over a period of time determined by the researcher.

One problem in using the PET technique for *in vivo* studies of small animals is the need to contain the animals during image acquisition to avoid artefacts caused by movement. For this reason, animals should be physically restricted or anaesthetized. Because anaesthetics may cause significant changes in the physiology of the central nervous, cardiovascular and respiratory systems (Toyama et al., 2004), the measurement of FDG uptake in the brain can be compromised. Cerebral glucose consumption is typically reduced when the animal is anaesthetized, and FDG incorporation is reduced with most anaesthetic protocols, including inhalant anaesthetics (e.g., isoflurane or sevoflurane), ketamine, propofol, and pentobarbital (Alstrup and Smith, 2013; Matsumura et al., 2003). Because of the ease and speed with which the anaesthetic protocol can be changed, inhalant anaesthesia has been used in most small-animal imaging studies. Toyama et al. (2004) noted that, compared with animals that were kept awake during FDG incorporation, animals anaesthetized with isoflurane displayed a 29% decrease in brain uptake and a 91% increase in cardiac uptake. Ketamine, combined with the muscle relaxant xylazine, reduces brain and cardiac uptake by 39% and 64%, respectively. Xylazine directly stimulates the α_2-adrenergic receptors of pancreatic islet cells causing the decrease in insulin release, thus, resulting in hyperglycaemia (Abdel el Motal and Sharp, 1985).

Because anaesthesia can cause respiratory depression and, in some cases, cardiovascular depression, these vital signs should be monitored. The animal should always be carefully monitored during the PET scanning because metabolic and physiologic changes, such as hypercapnia, hypoxia, hypothermia and acidosis, can influence the results. An alternative to reduce the effects of anaesthesia on brain metabolism is to keep the animal awake during the tracer incorporation phase and anaesthetise it only during image acquisition. Although this procedure is common in studies not intended to evaluate the effect of the anaesthesia on glucose metabolism, acquisition is limited to static images, and quantification techniques will be restricted to semiquantitative methods. Several research groups have developed methods that enable

the acquisition of dynamic images while the animal is conscious. Mizuma et al. (2010) developed a device that restricts animal movement during experiments to obtain time-activity curves throughout the tracer incorporation time. Although the animals receive training for acclimatization, stress cannot be excluded as a confounding factor in the results (Sung et al., 2009; McLaughlin et al., 2007).

Currently, several devices have been proposed that enable the acquisition of dynamic images without restricting the animal's mobility. The RatCAP is a miniaturized PET scanner surgically mounted directly on the animal's head (in the case of rats) that moves simultaneously with the animal to avoid movement artefacts (Vaska et al., 2004; Schulz et al., 2011). Although it is an interesting system that enables researchers to study the brain during periods of activation, the scanner has less sensitivity than commercial devices, and can inhibit animal movement and cause stress. The most modern system used currently is motion compensation (Spangler-Bickell et al., 2016; Kyme et al., 2011; Weisenberger et al., 2005). In this method, the awakened animal is confined to a small space during image acquisition, and its head movement is measured and subsequently corrected so that the image can be reconstructed without movement artefacts. Of all of the methods in use, this is the one that causes less stress during examination.

Crone (1965) showed that glucose transport in the brain is affected by the plasma glucose concentration and that transport was performed by two mechanisms: passive and facilitated diffusion. Several studies have reported that FDG absorption by the cerebral cortex keeps an inverse relationship with blood glucose levels (Viglianti et al., 2017; Alf et al., 2013; Claeys et al., 2010). Orzi et al. (1988) reported that hyperglycaemia causes a competitive inhibition of FDG incorporation. However, the nonlinear response to increased glucose and the change in the cerebral FDG uptake pattern of patients with moderate hyperglycaemia observed by Viglianti et al. (2017) and Kawasaki et al. (2008) suggest that the FDG uptake mechanism is more complicated than as proposed by Crone (1965), and that it cannot be explained only on the basis of substrate competition. Under normal conditions, GLUT1 functions at less than its maximum capacity, thus, it is not a rate-limiting factor for brain function (Leybaert et al., 2007). In contrast to glucose transport, glucose phosphorylation via hexokinase is the rate-limiting step for brain energy metabolism in a hyperglycaemic state (Cunnane et al., 2011). In a clinical study, Viglianti et al. (2017) suggested that the lumped constant, which represents the correction factor for the differences in glucose and DG transport and phosphorylation rates, is not uniform over the physiological range under which imaging generally occurs, given the nonlinear relationship between plasma glucose and whole brain SUV. The change in lumped constant with plasma glucose has been observed in previous studies of small animals (Schuier et al., 1990; Suda et al., 1990), and this variation is likely caused by a change in the distribution volume due to the changes in transport and metabolism under hyperglycaemic conditions (Crane et al., 1983).

FDG-PET-based methods for analysing glucose uptake by cells can be divided into qualitative, semiquantitative and quantitative methods. Qualitative methods are purely visual and exhibit greater variability among investigators with different degrees of training, and are not the object of this review. Semiquantitative and quantitative methods, such as SUV and compartmental models, are presented below. Other methods, such as spectral analysis (Veronese et al., 2016; Cunningham and Jones, 1993) and kinetic modelling in the projection space (Germino et al., 2017; Wang and Qi, 2013), are also used in preclinical studies. However, they will not be covered in this article. Although the voxel-based analysis is not a quantification method, but can be used only for comparison, it will be addressed in this review because of its relevance in clinical and preclinical research.

Semiquantitative Methods

Standardized uptake value (SUV)

Among semiquantitative methods, the most well-known is SUV, which relates tissue activity to the injected activity and the individual´s body weight or area. The SUV or, alternatively, the maximum SUV in a volume of interest (SUVmax), has been used in many studies and been found to be useful as a benchmark in clinical studies.

The SUV is a parameter that characterizes the relative concentration of the radiotracer in the volume of interest, and is often used as a piece of data complementary to the visual evaluation of an image. To obtain SUV, careful standardization of the method and recording of the injected radioactivity levels, animal weight and injection time are necessary, as reproducibility is limited when different acquisition and processing protocols or equipment are used (Sapienza and Buchpiguel, 2017). The calculation is simple and can be expressed in equation 1:

$$SUV = \frac{C_{PET}(t)}{(Injected\ activity\ /\ Patient\ weight)} \qquad (1)$$

where $C_{PET}(t)$ represents the concentration of FDG in the region of interest (ROI) in a specific time.

Therefore, a SUV of 1 indicates that the counts obtained in the volume of interest are equal to the value expected if the activity were homogeneously distributed in the animal. However, the SUV may be affected by

multiple factors, from physiological changes between or within individuals to technical factors related to acquisition, processing or quantification (Köroğlu et al., 2017). Among the technical issues, image noise and the ROI segmentation method affect the SUV, and may produce biased results (Boellaard et al., 2004; Krak et al., 2005; Tylski et al., 2010; Silva-Rodríguez et al., 2015). Many segmentation techniques have been described with the objective of reducing intra- and inter-observer inconsistencies (White et al., 1999). Image segmentation methods can be divided into three groups based on the degree of human involvement: manual segmentation, semi-automatic segmentation, and fully automatic segmentation (Karsch et al., 2009; Fasihi and Mikhael, 2016). The technique most used currently in PET for segmentation is the manual technique followed by the semiautomatic one. Silva-Rodríguez et al. (2015) conducted a study based on simulated PET images with FDG to compare the effects of the activity and ROI used to calculate the SUV. The SUV_{50}, obtained by applying a threshold of 50% of the maximum value, and the SUVmean showed the best performance in regard to accuracy and repeatability, respectively. Another important factor to note is the variation in SUV with the FDG activity used. The SUVmean and SUV_{50} were less affected than the SUVmax by the reduction in injected activity, i.e., by increase in noise (Silva-Rodrígues et al., 2015).

In clinical studies, the SUVmax is used more widely than the SUVmean because it represents the voxel with the highest uptake and presumably the area with the highest metabolic rate in the analysed volume. However, in studies with small animals, the SUVmean (Figure 2) is more commonly used because this parameter is less susceptible than the SUVmax to statistical fluctuations in counts.

The SUV is often used as a substitute for the glucose uptake rate (K_i) or absolute glucose uptake

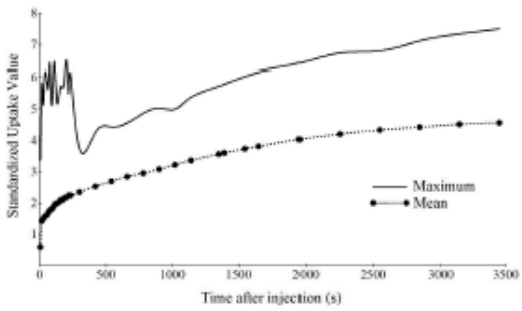

Figure 2. Mean and maximum standardized uptake values curves of rat brain, measured for approximately 1 h after intravenous injection of 37 MBq 2-deoxy-2-[^{18}F]fluoroglucose. Activities were measured within a region of interest over the whole brain. The positron emission tomography list-mode data were separated into 36 frames (1x5, 11x10, 1x12.5, 7x15, 1x67.5, 7x120, 1 x 210, 7x300 sec).

(MRGlu) (Durand and Besson, 2015). However, its accuracy depends on two factors: the amount of unmetabolized FDG present in the ROI used in the quantification and the condition that the activity normalized by weight, lean mass, or body surface area is proportional to the integral of the FDG concentration during the study time (Kotasidis et al., 2014).

In quantification via SUV estimation, the selected ROI contains information on the metabolized and unmetabolized FDG concentrations present both in the vascular and extravascular compartments. When the ROI has FDG metabolism rate close to that of the surrounding tissues, its assessment using the SUV is particularly hampered by the presence of free FDG in the vascular and/or intracellular compartment (Allen-Auerbach and Weber, 2009). In such cases, the SUV contrast between the ROI and the background is diminished by the inclusion of unmetabolized FDG, which can be treated as a "biological noise", which is a problem, especially in cases of post-therapeutic assessment, where the FDG concentrations in the tissues surrounding the lesion may be substantially larger, causing problems in the interpretation of results (Sugawara et al., 1999). Efforts have been made to estimate the amount of metabolized FDG in tissues, such as the liver and spleen (Keramida et al., 2017). In FDG studies, SUV also can be corrected for plasma glucose level, because glucose transporters may be saturated by glucose. SUV is multiplied by plasma glucose concentration and normalized by normal blood glucose level of 5.55 mmol/L (100 mg/dL). The normalisation of glucose level may decrease variability and increase the degree of concordance between studies in cases of high plasma glucose variability and the presence of extreme blood glucose values in the population studied (Paquet et al., 2004).

In addition to the amount of unmetabolized FDG, the SUV method considers that the metabolism is related to the total body weight (BW), lean body mass (LBM), or body surface area (BSA) of the animal. The BW has been used most commonly in normalization for the calculation of the SUV, regardless of whether the study is conducted with small animals or humans. However, changes in body weight or composition, which often occur in cancer patients resulting from the disease or treatments, can change the FDG distribution and dynamics in plasma, moving away from the value of the integral of activity normalized by BW, LBM or BSA (Huang, 2000). The differences between these values make unreliable the substitution of the kinetic parameters (K_i and MRGlu) by the SUV (Durand and Besson, 2015; Weber et al., 1999). To minimize the problem of correlation between the plasma FDG dynamics and the normalization applied to the SUV, more robust quantification methods using blood samples obtained during the exam time, also

known as input functions, should be used (Ishizu et al., 1994; Thie, 1995).

In addition to the problems mentioned above, disadvantages of this method include its poor reproducibility, which is closely related to maintaining the acquisition and processing parameters of study constant, the non-extravasation at the injection site, and the definition of the area/volume of interest, which is a challenge in small animal imaging (Adams et al., 2010).

Quantitative Methods

More detailed information on glucose metabolism can be obtained through quantitative methods, as described in Strauss et al. (2011). Of these, the most best accepted are compartmental analysis and graphical analysis, according to Patlak et al. (1983) and Patlak and Blasberg (1985).

Absolute quantification using the compartmental model (CM)

CM, also known as the kinetic model, is the most accurate method of PET data analysis. Gunn et al. (2001) have provided an overview and comprehensive analysis of the mathematics underlying the CM in PET. In the CM applied to PET (Figure 3), we assume that FDG is exchanged between compartments, with each compartment representing a homogeneous physiological or biochemical entity, and the rates at which the radiotracer is transferred between the compartments are described by first order differential equations.

In the CM, FDG is transported from plasma into tissue as free FDG and is subsequently metabolized into FDG-6-PO_4. The concentrations of FDG in the compartments are those of free FDG in plasma (C^*_P) and in tissue (C^*_T), and the concentration of metabolized FDG (C^*_m). The microconstants for the transfer of FDG, K^*_1 (μmol/min/100g) and k^*_2 (min^{-1}), represent the transport, mediated by the transporters of glucose across the cell membrane. The constants k^*_3 (min^{-1}) and k^*_4 (min^{-1}) represent the phosphorylation of FDG by hexokinase and dephosphorylation by glucose-6-phosphatase, respectively.

The CM requires dynamic imaging from the moment of injection and, in general, arterial blood samples to measure the plasma radiotracer concentration as a function of time, defined as the input function. Because the CM estimates kinetic parameters, we can determine glucose transport and hexokinase activity for each ROI in the image.

We can estimate the microconstants for glucose using the equations 2 and 3 (Fang and Muzic, 2008):

$$\frac{dC_p(t)}{dt} = K_1 C_p(t) - (k_2 + k_3) C_T(t) + k_4 C_m(t) \quad (2)$$

$$\frac{dC_m(t)}{dt} = k_3 C_T(t) - k_4 C_m(t) \quad (3)$$

Solving the differential equations above allows expressing the free glucose concentration in the tissue (C_T) in terms of the plasma concentration (C_p), and the rate of glucose metabolism (MRGlu) in terms of C_p is thus obtained by the equation 4:

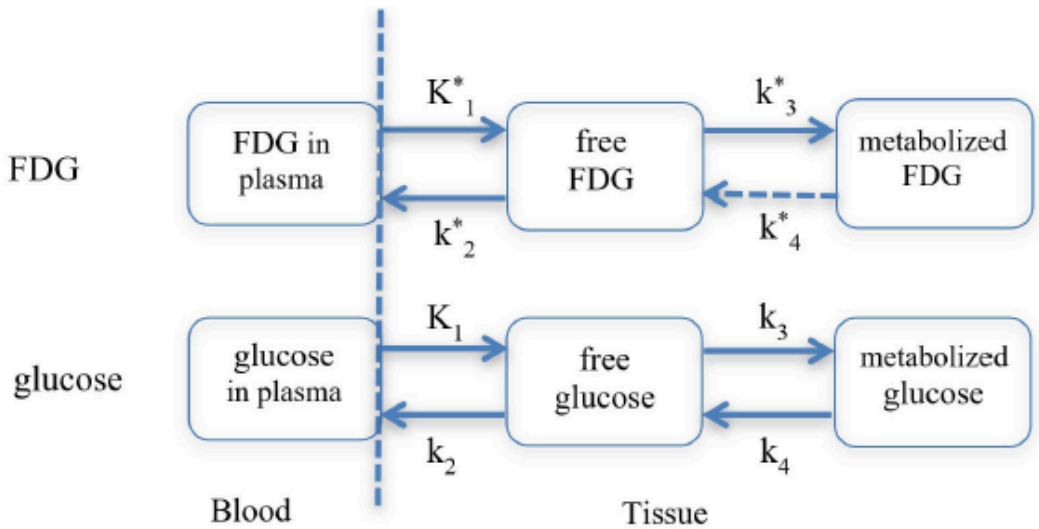

Figure 3. Two-compartment model depicting the transport of glucose and 2-deoxy-2-[^{18}F]fluoroglucose (FDG) to and from plasma to tissue, showing the rates of transport of the tracer/glucose into (K^*_1, K_1) and out of the cells (k^*_2,k_2), as well as the rates at which these molecules are converted to a form that is unable to leave the cell (k^*_3, k_3) and conversion from the trapped form back into the membrane-permeant form (k^*_4, k_4). In brain studies with FDG, it is often assumed that the dephosphorylation rate of FDG-6-phosphate in the brain tissue is small enough to be ignored (k^*_4= 0).

$$MRGlu = \phi k_3 C_T = \frac{K_1 k_3 \phi}{k_2 + \phi k_3} C_P \quad (4)$$

The difficulty in using the equation above is that the values of the transfer rates for glucose (K_1, k_2 and k_3) must be determined. The direct measurement of these transfer rates is too complicated; therefore, measurements of the PET TAC are used to estimate these values for FDG. The constant Φ represents the fraction of the phosphorylated glucose that is further metabolized in the glycolytic pathway. Sokoloff (1981a) demonstrated that in brain tissue Φ is very close to 1, indicating that only a small portion of the phosphorylated glucose will be dephosphorylated. For this reason, k^*_4 can be considered negligible.

Through the use of the lumped constant (LC) adjustment term (Sokoloff et al. 1977; Moore et al., 2000; Krohn et al., 2007), which represents the correction factor for the differences in glucose and DG transport and phosphorylation rates, and allows converting the results obtained using DG to glucose. In the brain, DG is transported 1.4 times faster than glucose, while glucose is metabolized 2.5-4.5 times faster than DG (Dienel, 2012), thereby the rate of glucose metabolism can be expressed as in equation 5:

$$MRGlu = \frac{K^*_1 k^*_3}{k^*_2 + k^*_3} \frac{C_P}{LC} = K^*_i \frac{C_P}{LC} \quad (5)$$

Thus, MRGlu can be estimated with a simple equation from only the constant rates of FDG (K^*_1, k^*_2 and k^*_3), the steady state C_P and LC.

In the LC, the distribution volume is the component sensitive to the glucose concentration due to the higher metabolism/transport rate of glucose in relation to DG. Under physiological conditions, where blood glucose remains constant, LC remains relatively stable. However, under conditions that include factors that alter plasma glucose concentration and consequently result in changes of greater or lesser magnitude in LC, LC should be determined for the specific conditions of the study. Several studies have shown changes in LC in hyperglycaemic (Orzi et al., 1988; Schuier et al., 1990), hypoglycaemic (Suda et al., 1990) and anaesthetized (Alf et al., 2014) animals, or in animals with tumours (Spence et al., 1998).

The model provides detailed information regarding glucose transport and metabolism as shown in Figure 4.

The advantages of this method are its reliability and its independence from examination or plasma clearance time, in contrast to the SUV. An important technical difficulty is the need for arterial cannulation to draw blood for the input function. It is also necessary to ensure injection without extravasation, which can be standardized using intravenous cannulation and an infusion pump. Another critical factor for the execution of this technique is the synchronization between the sampling times of arterial blood and PET imaging, since these data will be used in the differential equations shown above.

Patlak graphical analysis

Graphical methods allow the appropriate estimation of certain combinations of microparameters by transforming the estimation equations on which the CMs are based. The best-known graphical method for irreversible substances is the Patlak method (Patlak et al., 1983; Patlak and Blasberg, 1985). This method is a linearization of the compartmental equations for irreversible tracers (Figure 5). It can be shown that at a certain time t^* after the beginning of the tracer injection, all reversible compartments must be in steady state, i.e., the tracer concentrations in the plasma and in reversible tissue compartments should remain stable. This time depends on the tracer, the subject and the ROI. The relationship between the TAC of the tissue $C^*_T(t)$ and the TAC of the plasma $C^*_P(t)$ (y-axis) and the

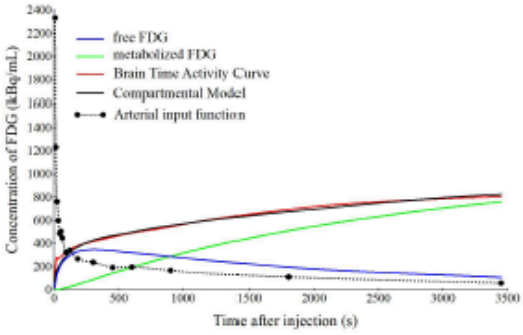

Figure 4. Compartmental model of 2-deoxy-2-[^{18}F] fluoroglucose metabolism based on the radiotracer concentration curves as a function of time in the arterial input function (plasma) and volume studied (brain), illustrating the concentration of free and metabolized FDG estimated for approximately 1 h after the intravenous injection of 37 MBq FDG.

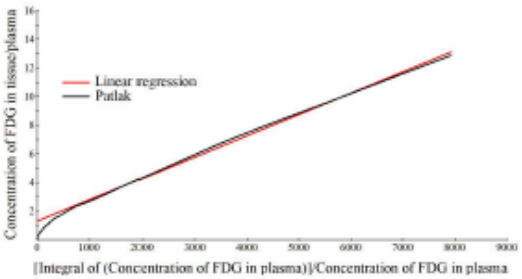

Figure 5. Patlak plot generated from the input function (plasma) and time activity curve from the brain in a representative animal after the intravenous injection of 37 MBq of 2-deoxy-2-[^{18}F]fluoroglucose. The Patlak plot becomes linear after the tracer concentrations in reversible compartments and in plasma are in steady state. The slope of the linear phase of the plot is the net uptake (influx) rate constant K_i.

ratio between the integral and the instantaneous value of $C^*_p(t)$ (x-axis) becomes linear at time t^*; that is, the system reaches a steady state, expressed by equation 6:

$$\frac{C^*_T(t)}{C^*_P(t)} = K^*_i \frac{\int_0^t C^*_P(u)\,du}{C^*_P(t)} + V \quad (6)$$

K^*_i indicates the rate at which the tracer is irreversibly retained and can be calculated from the equation 6 using a simple linear estimation procedure.

This method requires the acquisition of dynamic images, beginning 15 to 30 min after the tracer injection, as well as arterial blood samples. Due to the linearity of the above equation 6, this method is much faster and less sensitive to noise, and therefore suitable for voxel-level applications. For FDG, we can calculate the MRGlu (μmol/min/100g) from K^*_i using the equation 7:

$$MRGlu = K^*_i \frac{C_p}{LC} \quad (7)$$

Although this approach enables an operational simplification of the CM, the disadvantage of the Patlak method is the inability to calculate the kinetic parameters separately; for FDG, for example, the method does not discriminate between glucose transport and hexokinase activity.

To determine the best quantitative method, one can examine whether there is need to estimate glucose transfer constants or only the amount of glucose metabolized is sufficient to characterize the change studied. Several criteria exist for kinetic model preference identification for brain PET studies. The most commonly used models are Akaike Information Criterion (AIC), AIC unbiased, model selection criterion (MSC), Schwartz Criterion (SC) and F-test. However, all model selection criteria resulted in similar conclusions for PET FDG (Golla et al., 2017).

Voxel-Based Analysis (VBA)

Prior to the advent of VBA, PET brain images were manually analysed via manual delineation of ROIs to investigate the existence of areas with altered metabolism. This approach was established for autoradiograph analyses of basic neurophysiological and metabolic scans of humans (Friston, 2007). In addition to being time consuming, the ROI method might introduce inaccuracies into the analysis because it is an evaluator-dependent. However, the most significant difficulty is that ROI analyses are usually guided by *a priori* information of the change in a certain brain region; therefore, possibly significant effects outside the specific ROI can be lost or the treatment/intervention can induce a global effect that is expressed in all ROIs. To overcome the challenge of detecting regional changes when a global change is present, the Statistical Parametric Mapping (SPM) software was developed (Wellcome Department of Cognitive Neurology, Institute of Neurology, London, UK; Friston et al., 1994). SPM is the best-known VBA method that can be applied on a large scale in brain studies of humans and animal models of different neurological diseases or behaviours (Litaudon et al., 2017; Park et al., 2017; Cui et al., 2015; Casteels et al., 2010; Frumberg et al., 2007). SPM uses statistics to identify regions with different perfusion or metabolic rates or different volumes present in images obtained by SPECT, PET, or magnetic resonance imaging (MRI).

The SPM analysis method is based on the spatial representation of the parameters obtained (e.g., perfusion, metabolism, or volumes) via a VBA comparison of an animal (or group of animals) with a reference group of animals of the same species subjected to the same image modality. Before performing an SPM analysis, the images must be processed. This processing step is composed of three parts: spatial realignment, spatial normalization, and filtering. After this step, statistical analysis, intensity normalization and inference are performed. The most significant differences between groups are presented as a table of coordinates to represent three outline views of the brain (i.e., the glass brain) or as patches of colour on an MRI brain "slice", with the colours that represent the location of the voxels that have shown significant differences (Figure 6).

Spatial realignment, also known as the rigid registration method, involves correcting the difference in the position between the different acquired images due to differences in the positioning of the animals, through an inelastic transformation of the images.

Spatial normalization is performed to eliminate individual differences and ensure the positioning of the image voxels, so that the same structure occupies the same coordinates in all of the images. This normalization involves a stereotactic transformation of the brain images to fit an external anatomical model, the template, which corresponds to an atlas of standard anatomical space. The established and most commonly used atlases of the mouse and rat brain (Paxinos and Watson, 2017; Swanson, 2004) provide a series of sections, cut at specified angles, with external surfaces and internal boundaries of areas and nuclei indicated, as well as names assigned to the delineated structures. Atlases with 3-D representations of major brain structures have also been developed for the mouse (Chan et al., 2007; Gustafson et al., 2004; Lein et al., 2007; MacKenzie-Graham et al., 2004). This procedure allows direct intra- and inter-subject comparisons and the application of standard reference maps and masks.

Because of the relatively large differences in the spatial resolution between MRI and FDG-PET images of small animals, the automated image realignment of FDG-PET

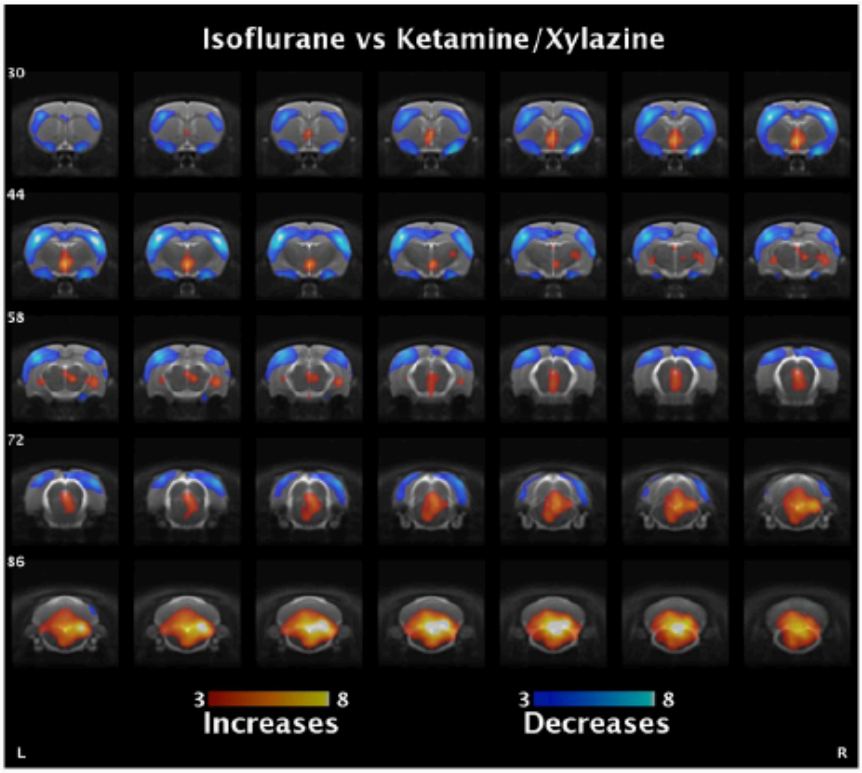

Figure 6. Representative rat brain images obtained by statistical parametric mapping of the standardized uptake values to compare rats kept under isoflurane and ketamine/xylazine anaesthesia during the 2-deoxy-2-[^{18}F]fluoroglucose uptake period. T-map data (visualization cut-off point: $p<0.05$; uncorrected) are depicted using Mango as a multi-slice coronal of magnetic resonance imaging template overlay (Schwarz et al., 2006). The colour bar was set to a minimum of 3 and a maximum of 8 for both increases and decreases in glucose uptake for isoflurane anaesthetised subjects (n=15) compared with ketamine/xylazine anaesthetised subjects (n=18).

data with MRI templates is difficult primarily because of differences in the biodistribution of the tracer and the number of anatomical landmarks (Nie et al., 2014). Therefore, the availability of specific tracer templates aligned in a standard reference space enables the use of the automatic normalization of functional images, which minimizes user-dependent variability and provides direct access to the corresponding anatomical atlases and reference coordinates. Several standard anatomical and functional space models have been developed and tested for the spatial normalisation of small rodent brains (Poussier et al., 2017; Vállez Garcia et al., 2015; Nie et al., 2014, 2013; Coelho et al., 2011; Casteels et al., 2006; Schweinhardt et al., 2003).

After the normalization step, the images are smoothed by applying a spatial filter. The main objective of spatial filtering is to eliminate residual noise and allow the application of the random Gaussian field (RGF) theory. In practice, the intensity value of a voxel is replaced by the weighted average density of the neighbouring voxels, which increases the signal-to-noise ratio and adjusts the anatomical and functional variations between subjects (Friston, 2002). According to matched filter theorem, the optimum smoothing kernel corresponds to the size of the anticipated effect. Thus, the optimum smoothing level is related to the size of the signal to be detected (Reimold et al., 2006). Unfortunately, the effect size is unknown most of the time and may undergo variations across brain studies. Welch (2013) tested various smoothing levels (0-1.5 mm) in mouse brain FDG-PET images. Although the sensitivity of the test was not significantly altered by different smoothing levels, the T-score increased between 5 and 15%. In addition to increasing the signal-to-noise ratio, spatial filtering causes the errors to approach the normal distribution, which ensures the validity of the inferences based on parametric tests.

Importantly, spatial smoothing has disadvantages in small animal brain studies. Spatial smoothing always decreases spatial resolution; therefore, the detection of small structures can be attenuated below the cut-off value attributed in the study. Therefore, it is critical to assess whether the objective of the study is accurate spatial localization because the technique might not

identify small structures with low uptake. In this case, autoradiography can be used to perform a preliminary evaluation of the structures and regional metabolic changes involved in the study.

The mean level of brain metabolism varies among different subjects and, to a lesser degree, in the same subject over time. To perform longitudinal or transverse comparisons of metabolism between subjects, it is necessary to adjust the intensity data. There are several techniques to adjust the average metabolic differences between subjects. However, the easiest way to correct these fluctuations is the count normalization to the cerebral global mean, so-called global normalization. The cerebral global mean is determined automatically by SPM as the mean voxel value of those exceeding a threshold (Buchert et al., 2005), and is implemented as default in the count-scaling algorithm, thus enabling to adjust for interindividual variability without the need of additional analyses. For this reason, global normalization by means of proportional scaling or analysis of covariance (ANCOVA) has found a wide utilization in SPM analyses of FDG brain PET data. In proportional scaling, it is considered that the subjects have an identical metabolic level, and to reach it is scale each scan by its estimated global activity (Gispert et al., 2003). This approach is based on the assumption that the measurement process introduces a global scaling of image intensities at each voxel, a gain factor. Another approach, ANCOVA, is to include the mean corrected global activity as an additional regressor in the model. Data with lower variance may be normalised by ANCOVA, while those with higher variance and number of subjects are better normalised by proportional scaling (Gispert et al., 2003).

The main problem with these intensity normalisation techniques is that they do not contemplate the possibility that the studied effects could modify the mean values of metabolism. As a consequence, the impact of regional influences on the general metabolism is lost, or areas with apparent hypermetabolism are created, as in SPM analysis of Alzheimer disease (Yakushev et al., 2009). To avoid this type of problem, we can normalise the images by ROI or cluster-based normalization, which includes only areas not affected by the pathology/intervention. In these cases, it is possible to use the average or maximum value. In the case of the mean value, it is necessary to choose an area in which the mean value is similar in all individuals. Of course, one of the precepts of the technique is to know which regions are not affected. Instead of using the mean value of the parameter of interest (SUV, MRGlu, Ki, among others) in these regions, one may use the maximum value because there is a significant probability that regions with higher metabolic rate are not affected by the pathology/intervention that decreases the consumption of glucose (Gispert et al., 2003).

Several of these techniques have been applied in studies of neurological diseases (Dukart et al., 2013, 2010; Yakushev et al., 2009). The choice of the best normalisation method for a given study can be based on the coefficient of variation of noise analysis (Gispert et al., 2003).

The disadvantage of VBA is the need to acquire multiple images from the same animal or from different animals to perform the comparison. Several possible comparisons are used in VBA and depend on the experimental design employed. In longitudinal studies, it is possible, for example, to compare the same animal at different times using a paired t-test. In transversal studies, it is possible to compare an individual against a group or to compare different groups submitted to different interventions. In many research projects, a bank of images from healthy animals must be built for comparison. However, for the interpretation of changes between groups, only the clusters should be compared as to avoid false positive results due to noise present in the voxels (Vállez Garcia et al., 2015). The size of the cluster must be defined according to the data acquisition and processing conditions (spatial resolution, voxel size).

Numerous parameters obtained with quantitative methods can be compared between groups using the VBA method, such as absolute glucose uptake, transfer rate constants, SUV and blood.

Discussion and Conclusions

The major practical differences between the application of the quantification methods for humans and those used for small animals are related to spatial resolution, time scale, and arterial input function (van den Hoff, 2011). Many target structures of small animal PET are not much larger than the spatial resolution limit, and the limited recovery of true signal intensity frequently plays a much larger role in these conditions compared with human PET. In the case of small animals, the incomplete recovery of the signal directly translates into a corresponding reduction of the absorption parameters obtained, as K_1 and, indirectly, the SUV. Regarding the structures with dimensions close to the spatial resolution limit of the tomograph, the incomplete recovery of the signal must be corrected, which in turn requires a precise knowledge of the size and shape of the object.

Although not mandatory for all quantification methods, the arterial input function is limited by practical considerations. The most important factor to consider is the blood volume of rats and (especially) mice, which are frequently used in FDG studies. The removal of a relatively small volume of blood may result in physiological changes, which can cause significant changes in the quantification results. Other factors related to the

Table 1. Advantages and disadvantages of methods to analyse cerebral glucose metabolism with 2-deoxy-2-[^{18}F]fluoroglucose.

Method	Advantages	Disadvantages
Qualitative (visual)	- Non-invasive. - Relatively fast.	- Depends on the interval between injection and image acquisition. - Subjective.
Standardized uptake value	- Semi quantitative. - Good reproducibility if acquisition and processing are standardized. - Can be applied to static or dynamic images.	- Depends on the interval between injection and image acquisition. - Does not provide constants rate or free and metabolized FDG concentrations.
Voxel-based analysis	- Comparative. - Good reproducibility. - Allows evaluating the whole brain. - Can be applied to static or dynamic images.	- Requires a reference group/bank of normal subjects. - Not adequate for small clusters.
Patlak	- Quantitative. - Possibility of obtaining parametric image of K^*_i. - Start of image acquisition after 20 min of injection.	- Acquisition of dynamic image and input function. - Does not provide rate constants (K^*_1, k^*_2 and k^*_3). - Quantification based on predefined ROIs.
Compartmental model	- Quantitative. - Allows evaluating rate constants. - Possibility to obtain parametric images of K^*_i, K^*_1, k^*_2, k^*_3.	- Acquisition of dynamic image and input function. - Noise in the initial images. - Necessity of synchronization between the start of image acquisition, injection and input function.
Autoradiography	- Quantitative. - High spatial resolution. - Can be performed with the same dose and immediately after PET-FDG.	- *Ex vivo*. - Provides a planar image. - Not possible to perform longitudinal studies in the same animal.

PET: positron emission tomography; ROI: region of interest.

animal, the acquisition and processing technique should be standardised and controlled during the experiment.

Some advantages and disadvantages of the available quantification methods (Table 1) should be weighed according to the objective of the study. In the context of preclinical research, semiquantitative and quantitative methods are preferred because these approaches provide objective analysis parameters that are not dependent on expertise in visual analysis of images. VBA has a significant advantage over the SUV, since it allows analysis of the whole brain without the *a priori* formulation of a hypothesis. In addition, statistical methods, such as SPM, reveal regional differences in metabolism that are not always visually detectable.

Quantitative methods, while providing more reliable results, however, there are several technical challenges associated with these methods. Besides that, professionals with specific skills also are required to perform image acquisition and processing. Many factors can influence the results obtained; fortunately, these influences can be studied and minimized via the appropriate standardization of the acquisition, processing, and data analysis steps.

Although autoradiography is the gold standard for quantification, this method is not widely used in research protocols because it is an *ex vivo* method and does not allow longitudinal studies. However, autoradiography can be used to verify the changes visualized by other quantification methods.

In conclusion, analysis and interpretation of PET data are not always simple, and the results will depend on many details in the study. Several approaches are available for the quantification of PET data, and the integration of data from multiple methods can strengthen the validity of the results obtained and enable the researcher to understand the problem from different perspectives.

References

Abdel el Motal SM, Sharp GW. Inhibition of glucose-induced insulin release by xylazine. Endocrinology. 1985; 116(6):2337-40. http://dx.doi.org/10.1210/endo-116-6-2337. PMid:2986946.

Adams MC, Turkington TG, Wilson JM, Wong TZ. A systematic review of the factors affecting accuracy of measurements. AJR Am J Roentgenol. 2010; 195(2):310-20. http://dx.doi.org/10.2214/AJR.10.4923. PMid:20651185.

Alf MF, Duarte J, Lei H, Krämer S, Mlynarik V, Schibli R, Gruetter R. MRS glucose mapping and PET joining forces: re-evaluation of the lumped constant in the rat brain under isoflurane anaesthesia. J Neurochem. 2014; 129(4):672-82. http://dx.doi.org/10.1111/jnc.12667. PMid:24471521.

Alf MF, Duarte J, Schibli R, Gruetter R, Krämer S. Brain glucose transport and phosphorylation under acute insulin-induced hypoglycemia in mice: an 18F-FDG PET study. J Nucl Med. 2013; 54(12):2153-60. http://dx.doi.org/10.2967/jnumed.113.122812. PMid:24159048.

Allen-Auerbach M, Weber WA. Measuring response with FDG-PET: methodological aspects. Oncologist. 2009; 14(4):369-77. http://dx.doi.org/10.1634/theoncologist.2008-0119. PMid:19357228.

Alstrup AK, Smith D. Anaesthesia for positron emission tomography scanning of animals brains. Lab Anim. 2013; 47(1):12-8. http://dx.doi.org/10.1258/la.2012.011173. PMid:23349451.

Blake P, Johnson B, VanMeter J. Positron emission tomography (PET) and single photon emission computed tomography (SPECT): clinical applications. J Neuroophthalmol. 2003; 23(1):34-41. http://dx.doi.org/10.1097/00041327-200303000-00009. PMid:12616088.

Boellaard R, Krak N, Hoekstra O, Lammertsma A. Effects of noise, image resolution, and ROI definition on the accuracy of standard uptake value: a simulation study. J Nucl Med. 2004; 45(9):1519-27. PMid:15347719.

Boellaard R, van Lingen A, van Balen SC, Hoving BG, Lammertsma AA. Characteristics of a new fully programmable blood-sampling device for monitoring blood radioactivity during PET. Eur J Nucl Med. 2001; 28(1):81-9. http://dx.doi.org/10.1007/s002590000405. PMid:11202456.

Buchert R, Wilke F, Chakrabarti B, Martin B, Brenner W, Mester J, Clausen M. Adjusted scaling of FDG positron emission tomography images for statistical evaluation in patients with suspected Alzheimer's disease. J Neuroimaging. 2005; 15(4):348-55. http://dx.doi.org/10.1111/j.1552-6569.2005.tb00335.x. PMid:16254400.

Byrnes KR, Wilson C, Brabazon F, von Leden R, Jurgens J, Oakes T, Selwyn RG. FDG-PET imaging in mild traumatic brain injury: a critical review. Front Neuroenergetics. 2014; 5:13-24. http://dx.doi.org/10.3389/fnene.2013.00013. PMid:24409143.

Carson RE, Channing MA, Blasberg RG, Dunn BB, Cohen RM, Rice KC, Herscovitch P. Comparison of bolus and infusion methods for receptor quantitation: Application to [18F] cyclofoxy and positron emission tomography. J Cereb Blood Flow Metab. 1993; 13(1):24-42. http://dx.doi.org/10.1038/jcbfm.1993.6. PMid:8380178.

Casteels C, Martinez E, Bormans G, Camon L, Vera N, Baekelandt V, Planas AM, van Laere K. Type 1 cannabinoid receptor mapping with [18F]MK-9470 PET in the rat brain after quinolinic acid lesion: a comparison to dopamine receptors and glucose metabolism. Eur J Nucl Med Mol Imaging. 2010; 37(12):2354-63. http://dx.doi.org/10.1007/s00259-010-1574-2. PMid:20680268.

Casteels C, Vermaelen P, Nuyts J, van der Linden A, Baekelandt V, Mortelmans L, Bormans G, van Laere K. Construction and evaluation of multitracer small-animal PET probabilistic atlases for voxel-based functional mapping of the rat brain. J Nucl Med. 2006; 47(11):1858-66. PMid:17079820.

Catafau AM. Brain SPECT in clinical practice. Part I: perfusion. J Nucl Med. 2001; 42(2):259-71. PMid:11216525.

Chan E, Kovacevic N, Ho SKY, Henkelman RM, Henderson JT. Development of a high resolution three-dimensional surgical atlas of the murine head for strains 129S1/SvImJ and C57Bl/6J using magnetic resonance imaging and micro-computed tomography. Neuroscience. 2007; 144(2):604-15. http://dx.doi.org/10.1016/j.neuroscience.2006.08.080. PMid:17101233.

Claeys J, Mertens K, D'Asseler Y, Goethals I. Normoglycemic plasma glucose levels affects F-18 FDG uptake in the brain. Ann Nucl Med. 2010; 24(6):501-5. http://dx.doi.org/10.1007/s12149-010-0359-9. PMid:20237872.

Coelho C, Hjornevik T, Courivaud F, Willoch F. Anatomical standardization of small animal brain FDG-PET images using synthetic functional template: experimental comparison with anatomical template. J Neurosci Methods. 2011; 199(1):166-72. http://dx.doi.org/10.1016/j.jneumeth.2011.04.026. PMid:21550366.

Convert L, Morin-Brassard G, Cadorette J, Archambault M, Bentourkia M, Lecomte R. A new tool for molecular imaging: the microvolumetric {beta} blood counter. J Nucl Med. 2007; 48(7):1197-1206. http://dx.doi.org/10.2967/jnumed.107.042606. PMid:17574990.

Crane PD, Pardridge WM, Braun LD, Oldendorf WH. Kinetics of transport and phosphorylation of 2-fluoro-2-deoxy-D-glucose in rat brain. J Neurochem. 1983; 40(1):160-7. http://dx.doi.org/10.1111/j.1471-4159.1983.tb12666.x. PMid:6848656.

Crone C. Facilitated transfer of glucose from blood into brain tissue. J Physiol. 1965; 181(1):103-13. http://dx.doi.org/10.1113/jphysiol.1965.sp007748. PMid:5866278.

Cui Y, Toyoda H, Sako T, Onoe K, Hayashinaka E, Wada Y, Yokoyama C, Onoe H, Kataoka Y, Watanabe Y. A voxel-based analysis of brain activity in high-order trigeminal pathway in the rat induced by cortical spreading depression. Neuroimage. 2015; 108:17-22. http://dx.doi.org/10.1016/j.neuroimage.2014.12.047. PMid:25536498.

Cunnane S, Nugent S, Roy M, Courchesne-Loyer A, Croteau E, Tremblay S, Castellano A, Pifferi F, Bocti C, Paquet N, Begdouri H, Bentourkia M, Turcotte E, Allard M, Barberger-Gateau P, Fulop T, Rapoport SI. Brain fuel metabolism, aging, and Alzheimer's disease. Nutrition. 2011; 27(1):3-20. http://dx.doi.org/10.1016/j.nut.2010.07.021. PMid:21035308.

Cunningham VJ, Jones T. Spectral analysis of dynamic PET studies. J Cereb Blood Flow Metab. 1993; 13(1):15-23. http://dx.doi.org/10.1038/jcbfm.1993.5. PMid:8417003.

Deleye S, Verhaeghe J, Wyffels L, Dedeurwaerdere S, Stroobants S, Staelens S. Towards a reproducible protocol for repetitive and semi-quantitative rat brain imaging with 18F-FDG: exemplified in a memantine pharmacological challenge. Neuroimage. 2014; 96:276-87. http://dx.doi.org/10.1016/j.neuroimage.2014.04.004. PMid:24736171.

Dienel GA. Fueling and imaging brain activation. ASN Neuro. 2012; 4(5):267-321. http://dx.doi.org/10.1042/AN20120021. PMid:22612861.

Dukart J, Mueller K, Horstmann A, Vogt B, Frisch S, Barthel H, Becker G, Möller HE, Villringer A, Sabri O, Schroeter ML. Differential effects of global and cerebellar normalization on detection and differentiation of dementia in FDG-PET studies. Neuroimage. 2010; 49(2):1490-5. http://dx.doi.org/10.1016/j.neuroimage.2009.09.017. PMid:19770055.

Dukart J, Perneczky R, Förster S, Barthel H, Diehl-Schmid J, Draganski B, Obrig H, Santarnecchi E, Drzezga A, Fellgiebel A, Frackowiak R, Kurz A, Müller K, Sabri O, Schroeter ML,

Yakushev I. Reference cluster normalization improves detection of frontotemporal lobar degeneration by means of FDG-PET. PLoS One. 2013; 8(2):e55415. http://dx.doi.org/10.1371/journal.pone.0055415. PMid:23451025.

Durand E, Besson F. How is the standard uptake value (SUV) linked to the influx constant in Sokoloff's model for 18F-FDG? Med Nucl (Paris). 2015; 39(1):11-7. http://dx.doi.org/10.1016/j.mednuc.2015.01.002.

Fang YH, Muzic R Jr. Spillover and partial-volume correction for image-derived input functions for small-animal 18F-FDG PET studies. J Nucl Med. 2008; 49(4):606-14. http://dx.doi.org/10.2967/jnumed.107.047613. PMid:18344438.

Fasihi M, Mikhael W. Overview of current biomedical image segmentation methods. In: International Conference on Computational Science and Computational Intelligence (CSCI); Dec 2016 15-16; Las Vegas. Las Vegas: IEEE; 2016, p. 803-8. doi: http://dx.doi.org/10.1109/CSCI.2016.0156.

Frey EC, Humm J, Ljungberg M. Accuracy and precision of radioactivity quantification in nuclear medicine images. Semin Nucl Med. 2012; 42(3):208-18. http://dx.doi.org/10.1053/j.semnuclmed.2011.11.003. PMid:22475429.

Friston K. Introduction. In: Friston K, Ashburner J, Kiebel S, Nichols T, Penny W. Statistical parametric mapping: the analysis of functional brain imaging. San Diego: Academic Press; 2007. p. 3-9. http://dx.doi.org/10.1016/B978-012372560-8/50001-2.

Friston K. Statistics I: Experimental design and statistical parametric mapping. In: Toga A, Mazziotta J, editors. Brain Mapping: The Methods. 2nd ed. San Diego: Academic Press; 2002. p. 605-10. http://dx.doi.org/10.1016/B978-012693019-1/50024-1.

Friston KJ, Holmes AP, Worsley KJ, Poline J-P, Frith CD, Frackowiak RSJ. Statistical parametric maps in functional imaging: a general linear approach. Hum Brain Mapp. 1994; 2(4):189-210. http://dx.doi.org/10.1002/hbm.460020402.

Frumberg DB, Fernando M, Lee D, Biegon A, Schiffer W. Metabolic and behavioral deficits following a routine surgical procedure in rats. Brain Res. 2007; 1144:209-18. http://dx.doi.org/10.1016/j.brainres.2007.01.134. PMid:17346680.

Fueger BJ, Czernin J, Hildebrandt I, Tran C, Halpern BS, Stout D, Phelps ME, Weber WA. Impact of animal handling on the results of 18F-FDG PET studies in mice. J Nucl Med. 2006; 47(6):999-1006. PMid:16741310.

Germino M, Gallezot JD, Yan J, Carson RE. Direct reconstruction of parametric images for brain PET with event-by-event motion correction: evaluation in two tracers across count levels. Phys Med Biol. 2017; 62(13):5344-64. http://dx.doi.org/10.1088/1361-6560/aa731f. PMid:28504644.

Gispert JD, Pascau J, Reig S, Garcia-Barreno P, Desco M. Mapas de estadísticos paramétricos (SPM) en medicina nuclear. Rev Esp Med Nucl. 2003; 22(1):43-53. http://dx.doi.org/10.1016/S0212-6982(03)72141-7. PMid:12550034.

Golla SSV, Adriaanse SM, Yaqub M, Windhorst AD, Lammertsma AA, van Berckel BNM, Boellaard R. Model selection criteria for dynamic brain PET studies. EJNMMI Phys. 2017; 4(1):30. http://dx.doi.org/10.1186/s40658-017-0197-0. PMid:29209862.

Green LA, Gambhir SS, Srinivasan A, Banerjee PK, Hoh CK, Cherry SR, Sharfstein S, Barrio JR, Herschman HR, Phelps ME. Noninvasive methods for quantitating blood time-activity curves from mouse PET images obtained with fluorine-18-fluorodeoxyglucose. J Nucl Med. 1998; 39(4):729-34. PMid:9544690.

Gunn RN, Gunn S, Cunningham V. Positron emission tomography compartmental models. J Cereb Blood Flow Metab. 2001; 21(6):635-52. http://dx.doi.org/10.1097/00004647-200106000-00002. PMid:11488533.

Gustafson C, Tretiak O, Bertrand L, Nissanov J. Design and implementation of software for assembly and browsing of 3D brain atlases. Comput Methods Programs Biomed. 2004; 74(1):53-61. http://dx.doi.org/10.1016/S0169-2607(03)00075-0. PMid:14992826.

Hargreaves RJ, Rabiner E. Translational PET imaging research. Neurobiol Dis. 2014; 61:32-8. http://dx.doi.org/10.1016/j.nbd.2013.08.017. PMid:24055214.

Huang S, Phelps M. Principles of tracer kinetic modeling in positron emission tomography and autoradiography. In: Mazziota J, Phelps M, Schelbert H editors. Positron Emission Tomography and Autoradiography. Philadelphia: Raven Press; 1985. p. 287-346.

Huang S-C, Wong K-P. Dynamic PET imaging. In: M Dahlbom, editor. Physics of PET and SPECT imaging: Imaging in medical diagnosis and therapy. Boca Raton: CRC Press, Taylor & Francis Group; 2017. p. 321-36. http://dx.doi.org/10.1201/9781315374383-16.

Huang SC. Anatomy of SUV: Standardized Uptake Value. Nucl Med Biol. 2000; 27(7):643-6. http://dx.doi.org/10.1016/S0969-8051(00)00155-4. PMid:11091106.

Ido T, Wan CN, Casella V, Fowler J, Wolf A, Reivich M, Kuhl DE. Labeled 2-deoxy-D-glucose analogs. 18F-labeled 2-deoxy-2-fluoro-D-glucose, 2-deoxy-2-fluoro-D-mannose and 14C-2-deoxy-2-fluoro-D-glucose. J Labelled Comp Radiopharm. 1978; 14(2):175-83. http://dx.doi.org/10.1002/jlcr.2580140204.

Ingvar D. Mental-illness and regional brain metabolism. Trends Neurosci. 1982; 5:199-203. http://dx.doi.org/10.1016/0166-2236(82)90114-X.

Ishizu K, Nishizawa S, Yonekura Y, Sadato N, Magata Y, Tamaki N, Tsuchida T, Okazawa H, Miyatake S, Ishikawa M, et al. Effects of hyperglycemia on FDG uptake in human brain and glioma. J Nucl Med. 1994; 35(7):1104-9. PMid:8014665.

Jadvar H, Parker J. PET radiotracers. In Jadvar H, Parker J editors. Clinical PET and PET/CT. London: Springer; 2005. p. 45-67.

Jagoda EM, Vaquero J, Seidel J, Green M, Eckelman W. Experiment assessment of mass effects in the rat: implications for small animal PET imaging. Nucl Med Biol. 2004; 31(6):771-9. http://dx.doi.org/10.1016/j.nucmedbio.2004.04.003. PMid:15246368.

Jensen TL, Kiersgaard MK, Sorensen DB, Mikkelsen LF. Fasting of mice: a review. Lab Anim. 2013; 47(4):225-40. http://dx.doi.org/10.1177/0023677213501659. PMid:24025567.

Karsch K, He Q, Duan Y. A fast, semiautomatic brain structure segmentation algorithm for magnetic resonance imaging.

In: IEEE International Conference on Bioinformatics and Biomedicine; 2009 Nov 1-4; Washington, DC. Washington: IEEE Computer Society; 2009. p. 297-302. DOI: 10.1109/BIBM.2009.40.

Kawasaki K, Ishii K, Saito Y, Oda K, Kimura Y, Ishiwata K. Influence of mild hyperglycemia on cerebral FDG distribution patterns calculated by statistical parametric mapping. Ann Nucl Med. 2008; 22(3):191-200. http://dx.doi.org/10.1007/s12149-007-0099-7. PMid:18498034.

Keramida G, Anagnostopoulos C, Peters M. The extent to which standardized uptake values reflect FDG phosphorylation in the liver and spleen as functions of time after injection of 18F-fluorodeoxyglucose. EJNMMI Res. 2017; 7(1):13. http://dx.doi.org/10.1186/s13550-017-0254-7. PMid:28176243.

Kim J, Herrero P, Sharp T, Laforest R, Rowland DJ, Tai Y-C, Lewis JS, Welch MJ. Minimally invasive method of determining blood input function from PET images in rodents. J Nucl Med. 2006; 47(2):330-6. PMid:16455640.

Knol RJ, de Bruin K, de Jong J, van Eck-Smit B, Booij J. *In vitro* and *ex vivo* storage phosphor imaging of short-living radioisotopes. J Neurosci Methods. 2008; 168(2):341-57. http://dx.doi.org/10.1016/j.jneumeth.2007.10.028. PMid:18164072.

Köroğlu R, Köksal İ, Şimşek FS, Gezer F, Kekilli E, Ünal B. Considering the relationship between quantitative parameters and prognostic factors in breast cancer: can mean standardized uptake value be an alternative to maximum standardized uptake value? World J Nucl Med. 2017; 16(4):275-80. http://dx.doi.org/10.4103/1450-1147.215485. PMid:29033675.

Kotasidis F, Tsoumpas C, Rahmim A. Advanced kinetic modeling strategies: towards adoption in clinical PET imaging. Clin Transl Imaging. 2014; 2(3):219-37. http://dx.doi.org/10.1007/s40336-014-0069-8.

Krak NC, Boellaard R, Hoekstra O, Twisk J, Hoekstra C, Lammertsma A. Effects of ROI definition and reconstruction method on quantitative outcome and applicability in a response monitoring trial. Eur J Nucl Med Mol Imaging. 2005; 32(3):294-301. http://dx.doi.org/10.1007/s00259-004-1566-1. PMid:15791438.

Krohn KA, Muzi MSA, Spence AM. What is in a number? The FDG lumped constant in the rat brain. J Nucl Med. 2007; 48(1):5-7. PMid:17204692.

Kung M-P, Kung H. Mass effect of injection dose in small rodent imaging by SPECT and PET. Nucl Med Biol. 2005; 32(7):673-8. http://dx.doi.org/10.1016/j.nucmedbio.2005.04.002. PMid:16243641.

Kyme AZ, Zhou VW, Meikle SR, Baldock C, Fulton RR. Optimized motion tracking for positron emission tomography studies of brain function in awake rats. PLoS One. 2011; 6(7):e21727. http://dx.doi.org/10.1371/journal.pone.0021727. PMid:21747951.

Lein ES, Hawrylycz MJ, Ao N, Ayres M, Bensinger A, Bernard A, Boe AF, Boguski MS, Brockway KS, Byrnes EJ, Chen L, Chen L, Chen T-M, Chi Chin M, Chong J, Crook BE, Czaplinska A, Dang CN, Datta S, Dee NR, Desaki AL, Desta T, Diep E, Dolbeare TA, Donelan MJ, Dong H-W, Dougherty JG, Duncan BJ, Ebbert AJ, Eichele G, Estin LK, Faber C, Facer BA, Fields R, Fischer SR, Fliss TP, Frensley C, Gates SN, Glattfelder KJ, Halverson KR, Hart MR, Hohmann JG, Howell MP, Jeung DP, Johnson RA, Karr PT, Kawal R, Kidney JM, Knapik RH, Kuan CL, Lake JH, Laramee AR, Larsen KD, Lau C, Lemon TA, Liang AJ, Liu Y, Luong LT, Michaels J, Morgan JJ, Morgan RJ, Mortrud MT, Mosqueda NF, Ng LL, Ng R, Orta GJ, Overly CC, Pak TH, Parry SE, Pathak SD, Pearson OC, Puchalski RB, Riley ZL, Rockett HR, Rowland SA, Royall JJ, Ruiz MJ, Sarno NR, Schaffnit K, Shapovalova NV, Sivisay T, Slaughterbeck CR, Smith SC, Smith KA, Smith BI, Sodt AJ, Stewart NN, Stumpf K-R, Sunkin SM, Sutram M, Tam A, Teemer CD, Thaller C, Thompson CL, Varnam LR, Visel A, Whitlock RM, Wohnoutka PE, Wolkey CK, Wong VY, Wood M, Yaylaoglu MB, Young RC, Youngstrom BL, Feng Yuan X, Zhang B, Zwingman TA, Jones AR. Genome-wide atlas of gene expression in the adult mouse brain. Nature. 2007; 445(7124):168-76. http://dx.doi.org/10.1038/nature05453. PMid:17151600.

Leybaert L, De Bock M, van Moorhem M, Decrock E, de Vuyst E. Neurobarrier coupling in the brain: adjusting glucose entry with demand. J Neurosci Res. 2007; 85(15):3213-20. http://dx.doi.org/10.1002/jnr.21189. PMid:17265466.

Litaudon P, Bouillot C, Zimmer L, Costes N, Ravel N. Activity in the rat olfactory cortex is correlated with behavioral response to odor: a microPET study. Brain Struct Funct. 2017; 222(1):577-86. http://dx.doi.org/10.1007/s00429-016-1235-8. PMid:27194619.

MacKenzie-Graham A, Lee EF, Dinov ID, Bota M, Shattuck DW, Ruffins S, Yuan H, Konstantinidis F, Pitiot A, Ding Y, Hu G, Jacobs RE, Toga AW. A multimodal, multidimensional atlas of the C57BL/6J mouse brain. J Anat. 2004; 204(2):93-102. http://dx.doi.org/10.1111/j.1469-7580.2004.00264.x. PMid:15032916.

Matsumura A, Mizokawa S, Tanaka M, Wada Y, Nozaki S, Nakamura F, Shiomi S, Ochi H, Watanabe Y. Assessment of microPET performance in analyzing the rat brain under different types of anesthesia: comparison between quantitative data obtained with microPET and *ex vivo* autoradiography. Neuroimage. 2003; 20(4):2040-50. http://dx.doi.org/10.1016/j.neuroimage.2003.08.020. PMid:14683708.

McLaughlin KJ, Gomez JL, Baran SE, Conrad CD. The effects of chronic stress on hippocampal morphology and function: an evaluation of chronic restraint paradigms. Brain Res. 2007; 1161(1):56-64. http://dx.doi.org/10.1016/j.brainres.2007.05.042. PMid:17603026.

Meyer M, Le-Bras L, Fernandez P, Zanotti-Fregonara P. Standardized input function for 18F-FDG PET studies in mice: a cautionary study. PLoS One. 2017; 12(1):e0168667. http://dx.doi.org/10.1371/journal.pone.0168667. PMid:28125579.

Meyer PT, Circiumaru V, Cardi CA, Thomas DH, Bal H, Acton PD. Simplified quantification of small animal [18F]FDG PET studies using a standard arterial input function. Eur J Nucl Med Mol Imaging. 2006; 33(8):948-54. http://dx.doi.org/10.1007/s00259-006-0121-7. PMid:16699768.

Mizuma H, Shukuri M, Hayashi T, Watanabe Y, Onoe H. Establishment of *in vivo* brain imaging method in conscious mice. J Nucl Med. 2010; 51(7):1068-75. http://dx.doi.org/10.2967/jnumed.110.075184. PMid:20554730.

Moore AH, Osteen C, Chatziioannou A, Hovda D, Cherry S. Quantitative assessment of longitudinal metabolic changes *in vivo* after traumatic brain injury in the adult rat using FDG-microPET. J Cereb Blood Flow Metab. 2000; 20(10):1492-501. http://dx.doi.org/10.1097/00004647-200010000-00011. PMid:11043912.

Munk OL, Keiding S, Bass L. A method to estimate dispersion in sampling catheters and to calculate dispersion-free blood time-activity curves. Med Phys. 2008; 35(8):3471-81. http://dx.doi.org/10.1118/1.2948391. PMid:18777907.

Nehlig A. Cerebral energy metabolism, glucose transport and blood flow: changes with maturation and adaptation to hypoglycaemia. Diabetes Metab. 1997; 23(1):18-29. PMid:9059763.

Nie B, Chen K, Zhao S, Liu J, Gu X, Yao Q, Hui J, Zhang Z, Teng G, Zhao C, Shan B. A rat brain MRI template with digital stereotaxic atlas of fine anatomical delineations in paxinos space and its automated application in voxel-wise analysis. Hum Brain Mapp. 2013; 34(6):1306-18. http://dx.doi.org/10.1002/hbm.21511. PMid:22287270.

Nie B, Liu H, Chen K, Jiang X, Shan B. A statistical parametric mapping toolbox used for voxel-wise analysis of FDG-PET images of rat brain. PLoS One. 2014; 9(9):e108295. http://dx.doi.org/10.1371/journal.pone.0108295. PMid:25259529.

Orzi F, Lucignani G, Dow-Edwards D, Namba H, Nehlig A, Patlak CS, Pettigrew K, Schuier F, Sokoloff L. Local cerebral glucose utilization in controlled graded levels of hyperglycemia in the conscious rat. J Cereb Blood Flow Metab. 1988; 8(3):346-56. http://dx.doi.org/10.1038/jcbfm.1988.70. PMid:3366796.

Paquet N, Albert A, Foidart J, Hustinx R. Within-patient variability of ^{18}F-FDG: standardized uptake values in normal tissues. J Nucl Med. 2004; 45(5):784-8. PMid:15136627.

Park TY, Nishida KS, Wilson CM, Jaiswal S, Scott J, Hoy AR, Selwyn RG, Dardzinski BJ, Choi KH. Effects of isoflurane anesthesia and intravenous morphine self-administration on regional glucose metabolism ([18F]FDG-PET) of male Sprague-Dawley rats. Eur J Neurosci. 2017; 45(7):922-31. http://dx.doi.org/10.1111/ejn.13542. PMid:28196306.

Patlak CS, Blasberg R, Fenstermacher J. Graphical evaluation of blood-to-brain transfer constants from multiple-time uptake data. J Cereb Blood Flow Metab. 1983; 3(1):1-7. http://dx.doi.org/10.1038/jcbfm.1983.1. PMid:6822610.

Patlak CS, Blasberg R. Graphical evaluation of blood-to-brain transfer constants from multiple-time uptake data. Generalizations. J Cereb Blood Flow Metab. 1985; 5(4):584-90. http://dx.doi.org/10.1038/jcbfm.1985.87. PMid:4055928.

Paxinos G, Watson C. The rat brain in stereotaxic coordinates: compact. 7th ed. San Diego: Elsevier Academic Press; 2017.

Phelps ME, Huang SC, Hoffman EJ, Selin C, Sokoloff L, Kuhl DE. Tomographic measurement of local cerebral glucose metabolic rate in man with (18F) fluorodeoxyglucose: Validation of method. Ann Neurol. 1979; 6(5):371-88. http://dx.doi.org/10.1002/ana.410060502. PMid:117743.

Poussier S, Maskali F, Vexiau G, Verger A, Boutley H, Karcher G, Raffo E, Marie PY. Quantitative SPM analysis involving an adaptive template may be applied to [18F]FDG PET images of the rat brain. Mol Imaging Biol. 2017; 19(5):731-5. http://dx.doi.org/10.1007/s11307-016-1043-9. PMid:28108871.

Reimold M, Slifstein M, Heinz A, Mueller-Schauenburg W, Bares R. Effect of spatial smoothing on t-maps: arguments for going back from t-maps to masked contrast images. J Cereb Blood Flow Metab. 2006; 26(6):751-9. http://dx.doi.org/10.1038/sj.jcbfm.9600231. PMid:16208316.

Roy CS, Sherrington C. On the Regulation of the blood-supply of the brain. J Physiol. 1890; 11(1-2):85-158, 17. http://dx.doi.org/10.1113/jphysiol.1890.sp000321. PMid:16991945.

Sapienza M, Buchpiguel CA. Bases da tomografia por emissão de pósitrons (PET). In Hironaka F, Sapienza M, Ono C, Lima M, Buchpiguel C, editors. Medicina nuclear: princípios e aplicações. 2nd ed. Rio de Janeiro: Atheneu; 2017. p. 372-7.

Schiffer WK, Mirrione M, Dewey S. Optimizing experimental protocols for quantitative behavioral imaging with 18F-FDG in rodents. J Nucl Med. 2007; 48(2):277-87. PMid:17268026.

Schmidt KC, Smith C. Resolution, sensitivity and precision with autoradiography and small animal positron emission tomography: implications for functional brain imaging in animal research. Nucl Med Biol. 2005; 32(7):719-25. http://dx.doi.org/10.1016/j.nucmedbio.2005.04.020. PMid:16243647.

Schuier F, Orzi F, Suda S, Lucignani G, Kennedy C, Sokoloff L. Influence of plasma glucose concentration on lumped constant of the deoxyglucose method: effects of hyperglycemia in the rat. J Cereb Blood Flow Metab. 1990; 10(6):765-73. http://dx.doi.org/10.1038/jcbfm.1990.134. PMid:2211874.

Schulz D, Southekal S, Junnarkar SS, Pratte JF, Purschke ML, Stoll SP, Ravindranath B, Maramraju SH, Krishnamoorthy S, Henn FA, O'Connor P, Woody CL, Schlyer DJ, Vaska P. Simultaneous assessment of rodent behavior and neurochemistry using a miniature positron emission tomograph. Nat Methods. 2011; 8(4):347-52. http://dx.doi.org/10.1038/nmeth.1582. PMid:21399637.

Schwarz AJ, Danckaert A, Reese T, Gozzi A, Paxinos G, Watson C, Merlo-Pich EV, Bifone A. A stereotaxic MRI template set for rat brain with tissue class distribution maps and co-registered anatomical atlas: application to pharmacological MRI. Neuroimage. 2006; 32(2):538-50. http://dx.doi.org/10.1016/j.neuroimage.2006.04.214. PMid:16784876.

Schweinhardt P, Fransson P, Olson L, Spenger C, Andersson J. A template for spatial normalisation of MR images of the rat brain. J Neurosci Methods. 2003; 129(2):105-13. http://dx.doi.org/10.1016/S0165-0270(03)00192-4. PMid:14511814.

Senda M, Nishizawa S, Yonekura Y, Mukai T, Saji H, Konishi J, Torizuka K. Measurement of arterial time-activity curve by monitoring continuously drawn arterial blood with an external detector: errors and corrections. Ann Nucl Med. 1988; 2(1):7-12. http://dx.doi.org/10.1007/BF03164580. PMid:3275106.

Sijbesma JW, Zhou X, Vállez García D, Houwertjes MC, Doorduin J, Kwizera C, Maas B, Meerlo P, Dierckx RA, Slart RH, Elsinga PH, van Waarde A. Novel approach to repeated arterial blood sampling in small animal PET: application in a test-retest study with the adenosine A1 receptor ligand [11C] MPDX. Mol Imaging Biol. 2016; 18(5):715-23. http://dx.doi.org/10.1007/s11307-016-0954-9. PMid:27091332.

Silva-Rodríguez J, Aguiar P, Domínguez-Prado I, Fierro P, Ruibal Á. Simulated FDG-PET studies for the assessment of SUV quantification methods. Rev Esp Med Nucl Imagen Mol. 2015; 34(1):13-8. http://dx.doi.org/10.1016/j.remn.2014.07.006. PMid:25107595.

Silverman DH. Brain 18F-FDG PET in the diagnosis of neurodegenerative dementias: comparison with perfusion SPECT and with clinical evaluations lacking nuclear imaging. J Nucl Med. 2004; 45(4):594-607. PMid:15073255.

Sokoloff L, Reivich M, Kennedy C, Rosiers MHD, Patlak CS, Pettigrew KD, Sakurada O, Shinohara M. The [14C] deoxyglucose method for the measurement of local cerebral glucose utilization: theory, procedure, and normal values in the conscious and anesthetized albino rat. J Neurochem. 1977; 28(5):897-16. http://dx.doi.org/10.1111/j.1471-4159.1977.tb10649.x. PMid:864466.

Sokoloff L. Localization of functional activity in the central nervous system by measurement of glucose utilization with radioactive deoxyglucose. J Cereb Blood Flow Metab. 1981b; 1(1):7-36. http://dx.doi.org/10.1038/jcbfm.1981.4. PMid:7035471.

Sokoloff L. The deoxyglucose method: theory and practice. Eur Neurol. 1981a; 20(3):137-45. http://dx.doi.org/10.1159/000115222. PMid:7262108.

Solon EG. Autoradiography techniques and quantification of drug distribution. Cell Tissue Res. 2015; 360(1):87-107. http://dx.doi.org/10.1007/s00441-014-2093-4. PMid:25604842.

Sossi V, Ruth T. MicroPET imaging: *in vivo* biochemistry in small animals. J Neural Transm. 2005; 112(3):319-30. http://dx.doi.org/10.1007/s00702-004-0272-2. PMid:15723157.

Spangler-Bickell MG, de Laat B, Fulton R, Bormans G, Nuyts J. The effect of isoflurane on 18F-FDG uptake in the rat brain: a fully conscious dynamic PET study using motion compensation. EJNMMI Res. 2016; 6(1):86. http://dx.doi.org/10.1186/s13550-016-0242-3. PMid:27888500.

Spence A, Muzi M, Graham M, O'Sullivan F, Krohn K, Link J, Lewellen TK, Lewellen B, Freeman SD, Berger MS, Ojemann GA. Glucose metabolism in human malignant gliomas measured quantitatively with PET, 1-[C-11]glucose and FDG: analysis of the FDG lumped constant. J Nucl Med. 1998; 39(3):440-8. PMid:9529289.

Stout D, Pastuskovas C. *In vitro* methods for *in vivo* quantitation of PET and SPECT imaging probes: autoradiography and gamma counting. In: Kiessling F, Pichler BJ, editors. Small animal imaging: basics and practical guide. 2nd ed. Heidelberg: Springer; 2011. p. 511-25. http://dx.doi.org/10.1007/978-3-642-12945-2_24.

Strauss LG, Pan L, Cheng C, Haberkorn U, Dimitrakopoulou-Strauss A. Shortened acquisition protocols for the quantitative assessment of the 2-tissue-compartment model using dynamic PET/CT 18F-FDG studies. J Nucl Med. 2011; 52(3):379-85. http://dx.doi.org/10.2967/jnumed.110.079798. PMid:21321263.

Suda S, Shinohara M, Miyaoka M, Lucignani G, Kennedy C, Sokoloff L. The lumped constant of the deoxyglucose method in hypoglycemia: effects of moderate hypoglycemia on local cerebral glucose utilization in the rat. J Cereb Blood Flow Metab. 1990; 10(4):499-509. http://dx.doi.org/10.1038/jcbfm.1990.92. PMid:2347881.

Sugawara Y, Zasadny K, Grossman H, Francis I, Clarke M, Wahl R. Germ cell tumor: differentiation of viable tumor, mature teratoma, and necrotic tissue with FDG PET and kinetic modeling. Radiology. 1999; 211(1):249-56. http://dx.doi.org/10.1148/radiology.211.1.r99ap16249. PMid:10189480.

Sung KK, Jang DP, Lee S, Kim M, Lee SY, Kim YB, Park CW, Cho ZH. Neural responses in rat brain during acute immobilization stress: a [18F]FDG micro PET imaging study. Neuroimage. 2009; 44(3):1074-80. PMid:18952183. doi: 10.1016/j.neuroimage.2008.09.032.

Swanson LW. Brain maps: structure of the rat brain. San Diego: Elsevier Academic Press; 2004.

Takikawa S, Dhawan V, Spetsieris P, Robeson W, Chaly T, Dahl R, Margouleff D, Eidelberg D. Noninvasive quantitative fluorodeoxyglucose PET studies with an estimated input function derived from a population-based arterial blood curve. Radiology. 1993; 188(1):131-6. http://dx.doi.org/10.1148/radiology.188.1.8511286. PMid:8511286.

Thie JA. Clarification of a fractional uptake concept. J Nucl Med. 1995; 36(4):711-2. PMid:7699475.

Toyama H, Ichise M, Liow JS, Vines D, Seneca N, Modell K, Seidel J, Green MV, Innis RB. Evaluation of anesthesia effects on [18F]FDG uptake in mouse brain and heart using small animal PET. Nucl Med Biol. 2004; 31(2):251-6. http://dx.doi.org/10.1016/S0969-8051(03)00124-0. PMid:15013491.

Tsukada H. Animal PET research with non-human primates for drug development in pre-clinical stage - The Hamamatsu experience. In: Elsinga PH, Waarde A van, Paans AMJ, Dierckx RAJO, editors. Trends on the role of PET in drug development. Singapore: Word Scientific; 2012. p. 241-60. http://dx.doi.org/10.1142/9789814317740_0010.

Tylski P, Stute S, Grotus N, Doyeux K, Hapdey S, Gardin I, Vanderlinden B, Buvat I. Comparative assessment of methods for estimating tumor volume and standardized uptake value in (18)F-FDG PET. J Nucl Med. 2010; 51(2):268-76. http://dx.doi.org/10.2967/jnumed.109.066241. PMid:20080896.

Vállez Garcia D, Casteels C, Schwarz A, Dierckx R, Koole M, Doorduin J. A standardized method for the construction of tracer specific PET and SPECT rat brain templates: validation and implementation of a toolbox. PLoS One. 2015; 10(3):e0122363. http://dx.doi.org/10.1371/journal.pone.0122363. PMid:25823005.

van den Hoff J. Kinetic modeling. In Kiessling F, Pichler BJ, editors. Small animal imaging: basics and practical guide. 2nd ed. Heidelberg: Springer; 2011. p. 559-80. http://dx.doi.org/10.1007/978-3-642-12945-2_27.

Vanhove C, Bankstahl J, Krämer S, Visser E, Belcari N, Vandenberghe S. Accurate molecular imaging of small animals taking into account animal models, handling, anaesthesia, quality control and imaging system performance. EJNMMI Phys. 2015; 2(1):31. http://dx.doi.org/10.1186/s40658-015-0135-y. PMid:26560138.

Vaska P, Woody CL, Schlyer DJ, Shokouhi S, Stoll SP, Pratte JF et al. RatCAP: miniaturized head-mounted PET for conscious rodent brain imaging. IEEE Trans Nucl Sci. 2004; 51(5 II):2718-22. doi:10.1109/NSSMIC.2003.1352223.

Veronese M, Rizzo G, Bertoldo A, Turkheimer FE. Spectral analysis of dynamic PET studies: a review of 20 years of method

developments and applications. Comput Math Methods Med. 2016; 2016:1-15. http://dx.doi.org/10.1155/2016/7187541. PMid:28050197.

Viglianti BL, Wong K, Wimer S, Parameswaran A, Nan B, Ky C, Townsend DM, Rubello D, Frey KA, Gross MD. Effect of hyperglycemia on brain and liver 18F-FDG standardized uptake value (FDG SUV) measured by quantitative positron emission tomography (PET) imaging. Biomed Pharmacother. 2017; 88:1038-45. http://dx.doi.org/10.1016/j.biopha.2017.01.166. PMid:28192877.

Wang G, Qi J. Direct estimation of kinetic parametric images for dynamic PET. Theranostics. 2013; 3(10):802-15. http://dx.doi.org/10.7150/thno.5130. PMid:24396500.

Weber B, Burger C, Biro P, Buck A. A femoral arteriovenous shunt facilitates arterial whole blood sampling in animals. Eur J Nucl Med Mol Imaging. 2002; 29(3):319-23. http://dx.doi.org/10.1007/s00259-001-0712-2. PMid:12002705.

Weber WA, Ziegler S, Thodtmann R, Hanauske AR, Schwaiger M. Reproducibility of metabolic measurements in malignant tumors using FDG PET. J Nucl Med. 1999; 40(11):1771-7. PMid:10565769.

Weisenberger AG, Gleason SS, Goddard J, Kross B, Majewski S, Meikle SR. A restraint-free small animal SPECT imaging system with motion tracking. IEEE Trans Nucl Sci. 2005; 52(3I):638-44. doi:10.1109/TNS.2005.851399.

Welch A, Mingarelli M, Riedel G, Platt B. Mapping changes in mouse brain metabolism with PET/CT. J Nucl Med. 2013; 54(11):1946-53. http://dx.doi.org/10.2967/jnumed.113.121509. PMid:24009277.

White DRR, Houston A, Sampson W, Wilkins G. Intra-and interoperator variations in region-of-interest drawing and their effect on the measurement of glomerular filtration rates. Clin Nucl Med. 1999; 24(3):177-81. http://dx.doi.org/10.1097/00003072-199903000-00008. PMid:10069728.

Yakushev I, Hammers A, Fellgiebel A, Schmidtmann I, Scheurich A, Buchholz H-G, Peters J, Bartenstein P, Lieb K, Schreckenberger M. SPM-based count normalization provides excellent discrimination of mild Alzheimer's disease and amnestic mild cognitive impairment from healthy aging. Neuroimage. 2009; 44(1):43-50. http://dx.doi.org/10.1016/j.neuroimage.2008.07.015. PMid:18691659.

Zanotti-Fregonara P, Chen K, Liow JS, Fujita M, Innis RB. Image derived input function for brain PET studies: many challenges and few opportunities. J Cereb Blood Flow Metab. 2011; 31(10):1986-98. http://dx.doi.org/10.1038/jcbfm.2011.107. PMid:21811289.

Zanotti-Fregonara P, Fadaili IM, Maroy R, Comtat C, Souloumiac A, Jan S, Ribeiro MJ, Gaura V, Bar-Hen A, Trébossen R. Comparison of eight methods for the estimation of the image-derived input function in dynamic [(18)F]-FDG PET human brain studies. J Cereb Blood Flow Metab. 2009; 29(11):1825-35. http://dx.doi.org/10.1038/jcbfm.2009.93. PMid:19584890.

Zanotti-Fregonara P, Hirvonen J, Lyoo CH, Zoghbi SS, Rallis-Frutos D, Huestis MA, Morse C, Pike VW, Innis RB. Population-based input function modeling for [18F]FMPEP-d2, an inverse agonist radioligand for cannabinoid CB1 receptors: validation in clinical studies. PLoS One. 2013; 8(4):e60231. http://dx.doi.org/10.1371/journal.pone.0060231. PMid:23577094.

Zanotti-Fregonara P, Liow JS, Comtat C, Zoghbi SS, Zhang Y, Pike VW, Fujita M, Innis RB. Image-derived input function in PET brain studies: blood-based methods are resistant to motion artifacts. Nucl Med Commun. 2012; 33(9):982-9. http://dx.doi.org/10.1097/MNM.0b013e328356185c. PMid:22760300.

6.3 Comparison of different quantification methods for 18F-flurodeoxyglucose-positron emission tomography studies in rats brains (Publicação 2).

CLINICS

ORIGINAL ARTICLE

Comparison of different quantification methods for ^{18}F-fluorodeoxyglucose-positron emission tomography studies in rat brains

Silvana Prando [I,*] Camila de Godoi Carneiro [I] Cecil Chow Robilotta [II] Marcelo Tatit Sapienza [I]

[I] Centro de Medicina Nuclear, Faculdade de Medicina FMUSP, Universidade de Sao Paulo, Sao Paulo, SP, BR. [II] Instituto de Fisica, Universidade de Sao Paulo, Sao Paulo, SP, BR.

Prando S, Carneiro CG, Robilotta CC, Sapienza MT. Comparison of different quantification methods for ^{18}F-fluorodeoxyglucose-positron emission tomography studies in rat brains. Clinics. 2019;74:e1273

*Corresponding author. E-mail: prando@usp.br

OBJECTIVES: This study aimed to evaluate several methods to estimate glucose consumption in the male Wister rat brain as measured by PET.

METHODS: Fourteen male Wistar normoglycemic rats were studied. The input function consisted of seventeen blood samples drawn manually from the femoral artery. Glucose uptake values were calculated using the input function resulting from the arterial blood samples and the tissue time-activity curve derived from the PET images. The estimated glucose consumption rate (K_i) based on the 2-tissue compartment model (2TCM) served as the standard for comparisons with the values calculated by the Patlak analysis and with the fractional uptake rate (FUR), standardized uptake value (SUV) and glucose corrected SUV (SUV_{glu}).

RESULTS: No significant difference between the standard K_i and the Patlak K_i was observed. The standard K_i was also found to have strong correlations and concordance with the K_i value estimated by the Patlak analysis. The FUR method presented an excellent correlation with the K_i value obtained by the 2TCM/Patlak analyses, in contrast to the SUV or SUV_{glu}.

CONCLUSIONS: From a methodological point of view, the present findings confirm the theoretical limitations of the cerebral SUV and SUV_{glu} as a substitute for K_i in the estimation of glucose consumption in the brain. Our data suggest that the FUR is the surrogate to K_i.

KEYWORDS: Quantification; [18F]FDG; SUV; FUR; K_i.

INTRODUCTION

Positron emission tomography (PET) combined with 18F-fluorodeoxyglucose ([18F]FDG) is a powerful tool for investigating brain metabolism *in vivo* (1-4). PET is a medical imaging technique that is based on the administration of labeled drugs with positron-emitting radioisotopes, where the chemical form of the radiopharmaceutical is designed to provide information on tissue biochemistry rather than anatomy. The images are formed by the detection of two opposing gamma rays that are produced in the annihilation process between the positron and the electron. Thus, PET provides a means to measure the local concentrations of positron emitters and to reconstruct the images of the radiopharmaceutical distribution in the brain. The images obtained from the brains of small animals through PET are often evaluated using several quantitative analysis approaches.

Copyright © 2019 **CLINICS** – This is an Open Access article distributed under the terms of the Creative Commons License (http://creativecommons.org/licenses/by/4.0/) which permits unrestricted use, distribution, and reproduction in any medium or format, provided the original work is properly cited.

No potential conflict of interest was reported.

Received for publication on March 22, 2019. **Accepted for publication on** July 4, 2019

DOI: 10.6061/clinics/2019/e1273

The gold standard in PET quantification is the compartment model. Well-established compartmental models in PET include those used for quantification of blood flow (5), the cerebral metabolic rate for glucose (6,7) and neuroreceptor binding (8).

However, these particular models require the acquisition of dynamic images and an arterial or plasma blood input function, with the number of tissue compartments dictated by the physiological, biochemical and physiological parameters that are properties of the system being studied.

A simplification of the compartmental methods is the Patlak graphical analysis (9,10). The main advantage of this approach is the possibility of acquiring PET images at a late stage, where the system is in the steady state, after the injection of the radiopharmaceutical. The Patlak standard linear graphical analysis is a robust modeling approach and allows a direct estimation, from the reconstructed PET images and the input function, of the influence of the tracer K_i and blood volume V (9).

However, the application of compartmental or Patlak models is technically challenging, somewhat complicated and not sufficiently practical for routine use, even in small animals (11). Simplified quantification approaches have been introduced to overcome these challenges.

The standardized uptake value (SUV) is the parameter frequently used to measure [18F]FDG uptake and to

distinguish between areas with altered metabolism concerning the normal brain (12,13). Its use is related to ease of implantation, without the need to acquire dynamic images or obtain the concentration of the radiopharmaceutical in the blood (the function of entrance). However, the SUV is strongly dependent on the time of injection and the current metabolic state of each animal. Its outcome can also be affected by factors including animal management and biological or technical considerations (13-17). Anesthesia is a factor that is present in the vast majority of preclinical studies, and it affects glucose metabolism, frequently causing hyperglycemia (18-20). In hyperglycemic animals, Woo et al. (21) suggest that the SUV can be corrected through a normalized serum baseline glycemia value for the population mean.

An alternative to SUV correction for basal glycemia is the use of the fractional uptake rate (FUR), which normalizes the plasma variability of the population through the acquisition of the concentration of the radiopharmaceutical in the blood between the time of injection and the end of the image acquisition (22,23). The FUR is considered an approximation of the slope (K_i) obtained by the Patlak linearization technique for a delay time after the injection (24).

In this study, we used the [18F]FDG radiopharmaceutical to evaluate the methods of quantification of glucose metabolism measured by PET in small animals. Net glucose consumption values (K_i) were obtained through the compartmental (2TCM) and Patlak method and were compared with the values obtained by the SUV, SUV_{glu}, and FUR methods.

MATERIALS AND METHODS

Animals

The procedures described in the present work are part of a small-animal PET experiment examining the effects of anesthetics on cerebral glucose metabolism (25). The current work addresses the issue of comparing different quantification methods. Only the animals with 17 samples of arterial blood were analyzed. We retrospectively analyzed fourteen male Wistar rats obtained from the Animal Facility Center of the Medical School at the University of São Paulo, Brazil. The animals were given at least 7 days to acclimate to the vivarium of the Laboratory of Medical Investigation - LIM 43 in a climate-controlled room with a 12-hour circadian cycle and free access to food and water. On the day of the experiment, the animals were subjected to surgery for implantation of a cannula into the femoral artery and to PET under anesthesia with isoflurane or ketamine-xylazine.

All procedures were in accordance with ethical principles adopted by the Brazilian College of Animal Experimentation and approved by the Ethical Committee for Animal Research of School of Medicine, University of São Paulo (protocol 026/14).

Anesthesia

Prior to the PET scan, a mixture of 5% isoflurane (FORANE, Baxter Healthcare Corporation) and medical air was used to anesthetize the animals, which were maintained under anesthesia at 1.5 – 2.0% isoflurane (n=5) or with an intraperitoneal injection of ketamine (n=9) (100 mg/kg) associated with xylazine alpha2-agonist (10 mg/kg) (DOPALEN, Sespo Indústria e Comércio Ltda; ANASEDAN, Sespo Indústria e Comércio Ltda).

Animals anesthetized with intraperitoneal ketamine injection associated with alpha2-xylazine agonist received a standardized dose by weight during induction and a second fractionated dose every 30 minutes. In total, each animal received two doses of the anesthetic.

A PE50 cannula (0.58 mm internal diameter and 0.96 mm outside diameter, Becton Dickinson) was inserted into the femoral artery to obtain arterial blood samples (26).

The mean time between the onset of induction and [18F]FDG injection was 30 minutes. The total experiment time was 90 minutes. The animals remained on a surface heated to 37°C for the experimental duration to avoid hypothermia. During induction, the baseline serum weights and glycemia levels of the animals were measured.

Positron emission tomography

After the general procedures, image acquisition and arterial blood collection were started synchronically with the injection of the radiopharmaceutical. A bolus injection of 48.9 ± 3.5 MBq of [18F]FDG was administered manually into the penile vein.

The dynamic images of one bed position were acquired in list mode with a LabPET 4 system (Gamma Medica-Ideas, Northridge, CA) (27) over 1 hour. The acquired data were divided into 20 images (six series with the following numbers and durations: 8/30 s, 2/60 s, 2/120 s, 2/150 s, 3/300 s, and 3/600 s). Reconstruction was performed using the OSEM-2D method (20 iterations, 4 subsets, FOV=60 mm, high resolution mode), which resulted in 0.500 x 0.500 x 0.597 mm voxels. The data were corrected for radionuclide decay and random coincidences.

Simultaneous with PET image acquisition, 17 arterial blood samples were collected from the femoral artery at the PET acquisition timepoints 0, 5, 10, 20, 30, 40, 50, 60, 90, 120, 180, 300, 450, 600, 900, 1800 and 3600 s. The count rate per minute for an aliquot of 50 µL of sampled blood was measured with a gamma scintillation counter (Wallac Wizard 3, Perkin-Elmer), and the counts obtained were corrected for radionuclide decay and converted to activity concentration (kBq/mL) based on the gamma scintillation counter calibration factor, which was previously determined on the day of the experiment. The activity levels of the samples were corrected for the accumulated [18F]FDG activity in red blood cells following the method formulated by Wu et al. (28). The time-activity curve (TAC) for blood was corrected to a delay between injections and the start of acquisition in PMOD software, version 3.4 (PMOD Technologies Ltd., Zurich, Switzerland). The result was used as an arterial input function.

Data analysis

Standardized uptake value. The set of dynamic images for each animal was automatically coregistered using the T2-MRI template available in PMOD software, version 3.4 (PMOD Technologies Ltd., Zurich, Switzerland), and the mean SUV was generated by projection volumes of interest (VOIs) on the dynamic images.

The mean SUV (29) was calculated using the following equation:

$$SUV = \frac{C_{PET}(t)}{A/W} \quad (1)$$

where $C_{PET}(t)$ is the mean [18F]FDG concentration in dynamic images; A is the [18F]FDG activity injected into

the animal corrected for radionuclide decay and residual remaining in the syringe; and W is the animal's body weight.

The whole brain, consisting of the thalamus, cerebellum, hypothalamus, hippocampus, caudate nucleus, putamen, and cortex as defined in Schiffer's brain atlas (30) available in the PMOD software, was designated the VOI, and the VOI was used to obtain the mean SUV.

To calculate the metabolism value, we considered the last 30 minutes of the study.

The SUV_{glu} was generated by multiplying the SUV by the basal serum glycemia level of each animal.

Fractional uptake ratio. The FUR was obtained according to equation 2 and represents the ratio of tissue activity at time t and the integral of plasma activity from time 0 to t (22-24):

$$FUR = \frac{C_{tissue}(t)}{\int_0^t C_{plasma}(t)dt} \quad (2)$$

For the FUR calculation, we used the concentration of the activity per voxel in 45 minutes, which corresponds to the mean time of the last 30 minutes of the study, and the input function from 0 to 45 minutes.

Kinetic analysis. Kinetic analysis was performed in PMOD software, version 3.4 (PMOD Technologies Ltd., Zurich, Switzerland) using the compartmental method of irreversible tissues (2TCM) (6) and Patlak (9,10).

Whole-brain TACs were obtained by applying the VOI described above.

Two-tissue compartment model (2TCM). In the 2TCM (6) (Figure 1), it is assumed that the [18F]FDG is exchanged between the compartments, where each compartment represents a homogeneous, physiological or biochemical entity, and the rates at which the [18F]FDG is transferred between the compartments are described by first-order differential equations, namely, equations 3 and 4. The 2TCM requires dynamic imaging from the time of injection and, in general, a TAC to measure the concentration of the radiopharmaceutical in the plasma as a function of the time of the study. The advantages of this method are its reliability and its independence of examination time or plasma clearance, in contrast to the SUV. Because 2TCM can estimate kinetic parameters, we can determine glucose transport and hexokinase activity for each region of interest in the image.

$$\frac{dC_p(t)}{dt} = K_1C_p(t) - (k_2 + k_3)C_T(t) + k_4C_m(t) \quad (3)$$

$$\frac{dC_m(t)}{dt} = k_3C_T(t) - k_4C_m(t) \quad (4)$$

The difficulty in solving the differential equations above is that the values for the transfer rates for glucose (K_1, k_2, and k_3) must be determined. Direct measurement of transfer rates to glucose is very complicated, so we used [18F]FDG-PET measurements to estimate these values from [18F]FDG.

Initially, the cerebral metabolic rate of glucose cMRglu is expressed in terms of [18F]FDG transfer constants (K_1*, k_2*, k_3* and k_4*) and can be expressed in the form of equation 5:

$$CMRglu = \frac{K_1^*k_3^*}{k_2^* + k_3^*}C_P/LC = K_i\frac{C_P}{LC} \quad (5)$$

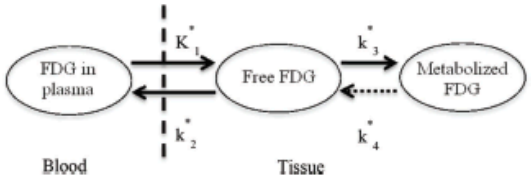

Figure 1 - Two-tissue compartment model describing [18F]FDG pharmacokinetics, including the blood-to-tissue [18F]FDG transport rate (K_1), tissue-to-blood [18F]FDG transport rate (k_2), phosphorylation to [18F]FDG-6-phosphate rate (k_3), and dephosphorylation rate (k_4).

The cMRglu equation is a simple equation involving the transfer rates of [18F]FDG (K_1*, k_2* and k_3*), the blood glucose concentration C_P during the equilibrium phase and the lumped constant, representing the difference between the metabolism of glucose and [18F]FDG. The LC value depends on the basal serum glucose level of the animal (31) and the region of the brain (32).

Since we used different anesthetics in this work and did not determine the appropriate lumped constant for each anesthetic protocol, we chose to use K_i as the metabolic rate for the whole brain.

The graphing methods allow appropriate estimations of certain combinations of micro parameters by transforming the estimation equations on which the compartmental models are based. There are two types of graphing methods, namely, the Patlak method and the Logan method, which can be applied to irreversible or reversible substances, respectively.

In the Patlak linearization method, one should presume that at least one compartment contains the radiopharmaceutical irreversibly and that the examination time is sufficient for the plasma and tissue compartments to reach steady state. In the case of [18F]FDG, the radiopharmaceutical is transformed into [18F]FDG-6-PO_4 and remains irreversibly retained within the neurons. In these circumstances, only the accumulation of the tracer in irreversible compartments affects the apparent volume of distribution.

After a certain time t *, which depends on the plotter, the subject and the ROI, the relationship of the TAC of the tissue C_T (t) and C_T of the plasma C_P (t) (y-axis) with the ratio of the integral to the instantaneous value of C_P (t) (x-axis) becomes linear, as expressed by equation 6:

$$\frac{C_{Tecido}(t)}{C_{Plasma}(t)} = K_i\frac{\int_0^t C_{Plasma}(u)du}{C_{Plasma}(t)} + V \quad (6)$$

where K_i, in equation 7, indicates the rate at which the tracer is irreversibly retained and can be calculated from the above equation using a simple linear estimation procedure.

$$K_i = \frac{K_1^*k_3^*}{k_2^* + k_3^*} \quad (7)$$

This method requires the acquisition of dynamic images beginning 15 to 30 minutes after the tracer injection and arterial blood samples. Due to the linearity of the above equation, the method is much faster and less sensitive to noise than the 2TCM and is therefore suitable for voxel applications. For [18F]FDG, we can calculate the cerebral

metabolic rate of glucose cMRglu (μmol/min/100 g) from K_i by equation 8:

$$CMRglu = K_i \cdot \frac{C_p}{LC} \quad (8)$$

For each animal, we obtained the rate of net glucose uptake (K_i).

Statistical analysis

The results of the study were analyzed by means of the SPSS 22.0 statistical package (SPSS Inc., Chicago, IL, USA). The Shapiro-Wilk test was used to verify the normality of variables.

Pearson's correlation coefficient was used to analyze the correlation between all the methods used in this study and classified as weak ($0.05 < p \leqslant 0.01$), strong ($0.01 < p \leqslant 0.05$) or strongest ($p < 0.01$).

The Bland-Altman method (33) and the Lin correlation coefficient (34) were used to analyze the agreement between K_i estimated by the 2TCM and Patlak models and the SUV and SUV_{glu} models.

RESULTS

All variables used in this study showed a normal distribution according to the Shapiro-Wilk test. Table 1 shows the mean, standard deviation and confidence interval for the baseline serum glycemia, weight and injected activity of the total sample studied.

Figure 2 shows the TACs for the whole brain (a) and input functions for animals anesthetized with ketamine/xylazine (b) or isoflurane (c).

Figure 3 shows a representative TAC and 2TCM fit for the whole brain and the input function for each anesthetic. The visual inspection revealed a satisfactory fit between the data and the 2TCM.

Table 1 - Mean, standard deviation and confidence interval of serum basal glycemia (mmol), weight (g) and injected activity (MBq).

	Mean	SD	95% CI
Glycemia (mmol)	7.11	1.07	6.59–7.78
Weight (g)	343.67	55.55	312.90–374.43
Injected activity (MBq)	49.15	3.41	47.26–51.04

SD = Standard Deviation, IC = Confidence Interval.

Their mean and respective error values are shown in Table 2.

The correlations between the methods used can be visualized in Figure 4 and in Table 3. There were significant positive correlations between K_i (Patlak) and K_i (2TCM) (r=0.9935, $p<0.001$); FUR and K_i (Patlak) (r=0.9472, $p<0.001$); FUR and K_i (2TCM) (r=0.9385, $p<0.001$); SUV_{glu} and SUV (r=0.7671, p=0.001); SUV and K_i (2TCM) (r=0.7336, p=0.002); SUV and K_i (Patlak) (r=0.7123, p=0.004); SUV

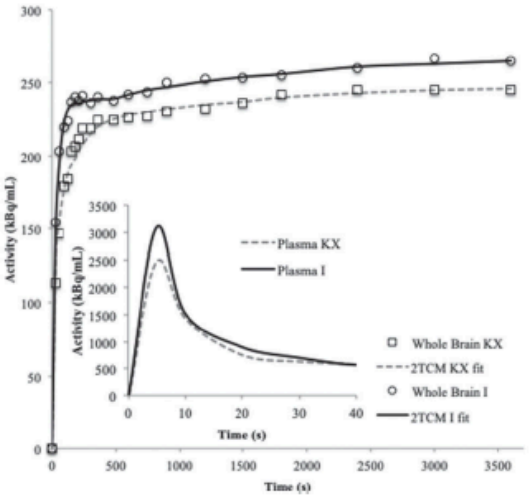

Figure 3 - Representative (n=1) time-activity curve and 2TCM fit for the whole brain and time-activity curve of the whole blood of an animal from the ketamine/xylazine or isoflurane group.

Table 2 - Mean, standard error mean and confidence interval of K_i (2TCM) (mL*(min*mL)$^{-1}$), K_i (Patlak) (mL*(min*mL)$^{-1}$), SUV, SUV_{glu} (mmol) and FUR (min^{-1}).

	Mean	SEM	95% CI
K_i (2TCM)	0.0207	0.0018	0.0169–0.0245
K_i (Patlak)	0.0202	0.0017	0.0165–0.0239
FUR	0.0011	0.0001	0.0009–0.0013
SUV_{glu}	2.03	0.12	1.76–2.29
SUV	1.57	0.09	1.38–1.76

SEM = Standard Error of the Mean, IC = Confidence Interval.

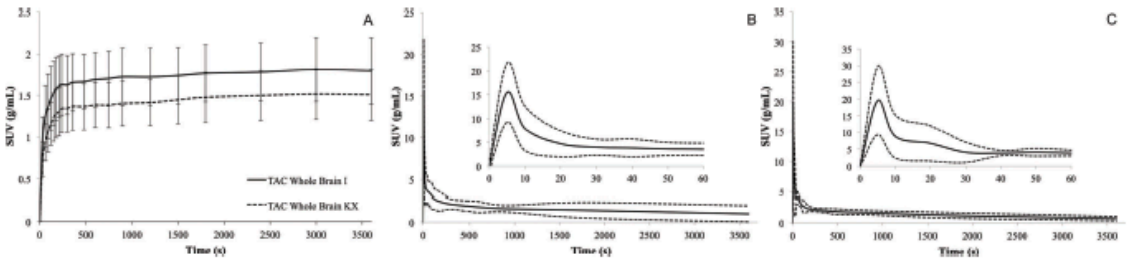

Figure 2 - Representative time-activity curves of brain and plasma input from the ketamine/xylazine or isoflurane group. A) Average [18F]FDG time-activity curves of the brain. Data are expressed as the standardized uptake value (mean ± SD). B) [18F]FDG time-activity curves for whole blood from the ketamine/xylazine group. The dashed line represents the confidence interval, and the solid line represents the mean. C) [18F]FDG time-activity curves for whole blood from the Isoflurane group. The dashed line represents the confidence interval, and the solid line represents the mean.

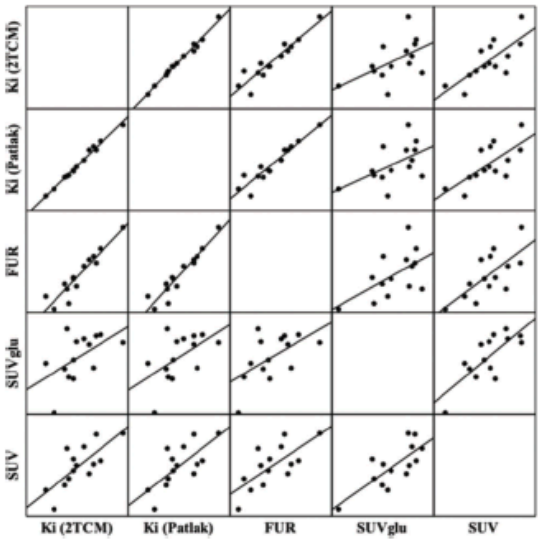

Figure 4 - Correlation graphs and linear regression matrix between the methods of quantification of the cerebral metabolism of glucose measured by PET-[18F]FDG. The solid lines represent the regression lines. K_i: net glucose consumption; 2TCM: two-tissue compartment model; FUR: fractional uptake value; SUV_{glu}: standardized uptake value corrected by glucose, SUV: standardized uptake value.

Table 3 - Pearson correlation coefficient.

	K_i (2TCM)	K_i (Patlak)	FUR	SUV_{glu}	SUV
Ki (2TCM)	1.0000				
K_i (Patlak)	0.9935 $p<0.001$	1.0000			
FUR	0.9385 $p<0.001$	0.9472 $p<0.001$	1.0000		
SUV_{glu}	0.5419 $p=0.045$	0.5456 $p=0.044$	0.5752 $p=0.031$	1.0000	
SUV	0.7336 $p=0.002$	0.7123 $p=0.004$	0.7095 $p=0.004$	0.7671 $p=0.001$	1.0000

SUV: standardized uptake value; FUR: fractional uptake value; K_i: net glucose consumption; 2TCM: two-tissue compartment model.

and FUR (r=0.7095, p=0.004); SUV_{glu} and FUR (r=0.5752, p=0.031); and SUV_{glu} and K_i (Patlak) (r=0.045, p=0.545) (r=0.045, p=0.545).

Figure 5 shows the Bland-Altman scatter plot used to determine the agreement between K_i obtained by the 2TCM and Patlak analyses. It was observed that the methods were concordant and with reduced cases of dispersion beyond the upper and lower limits of the standard deviations of the means.

In Table 4, Lin's correlation coefficients indicate that there is excellent agreement between K_i (2TCM) and K_i (Patlak).

DISCUSSION

In this article, we chose not to use the cerebral metabolic rate of glucose consumption (cMRglu) in the comparison of the methods. Methods using a tracer for the measurement of cMRglu require knowledge of the value of the lumped constant, which explains the difference in enzymatic kinetics

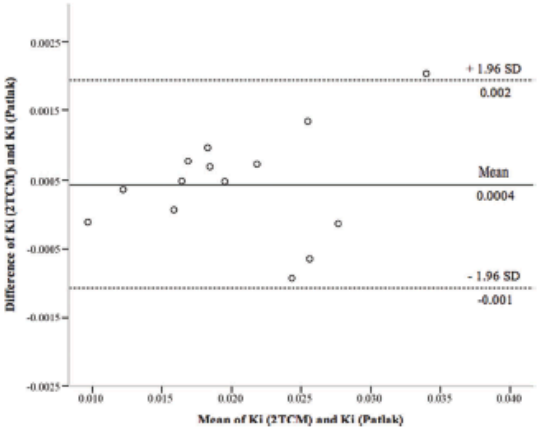

Figure 5 - Representative Bland-Altman plot of the agreement in the K_i estimation between the Patlak and reference values obtained from the 2TCM. The dashed line represents the confidence interval, and the solid line represents the bias. K_i: net glucose consumption; 2TCM: two-tissue compartment model; SD: standard deviation.

Table 4 - Results of the Lin (CC) correlation coefficient of the Bland-Altman analysis (mean differences and confidence intervals).

	CC	Mean Differences (SD)	95% CI
K_i (2TCM) *vs.* K_i (Patlak)	0.991	0.000 (0.001)	(-0.0019) - 0.002

CC = Correlation Coefficient; SD = Standard Deviation; CI = Confidence Interval.

of transport and phosphorylation between tracer and glucose. Although the relative activity of an enzyme for the tracer and natural substrate is generally constant and predictable, it has been reported previously that changes in basal glycemia levels alter the value of the lumped constant (31,35,36). As the anesthetics used in this study alter glycemia levels, we chose not to use cMRglu because we believed that we would be introducing a source of error that would impair the comparison of the methods.

In the absence of cMRglu, we chose to use K_i as the reference, which represents the glucose uptake rate and incorporates both internal net transport and tracer trapping in the tissue. K_i can be calculated by fitting the compartment model; in this case, 2TCM or the graphical approach of Patlak can be used to measure K_i without making assumptions about the metabolic compartments (9).

The compartmental model, namely, the 2TCM, is considered the gold standard in quantification because it contains a larger amount of acquired data and is subject to fewer assumptions. However, our results demonstrate that the 2TCM and Patlak graphical approach are strongly correlated (r=0.9935, $p<0.001$) and are concordant (CC=0.991) with each other. This result indicates that the K_i obtained by Patlak can be used in the quantification of the cerebral metabolism of small animals in place of the 2TCM. The primary advantage of adopting the Patlak method in the experimental routine lies in the fact that the method is less

sensitive to the noise of the initial part of the study and requires a simpler acquisition protocol that may eventually be translated into clinical practice (37).

As an alternative to compartmental methods, simplified methods have been proposed over the years to facilitate quantification by avoiding dynamic acquisitions and arterial blood collection. The best-known simplified method today is the standardized uptake value, namely, the SUV.

The SUV is an estimate of the glucose consumption rate (K_i) related to the concentration of radiopharmaceutical activity in a voxel, acquired by the equipment, and the concentration of activity in the animal. The accuracy of this estimate depends on several technical, physiological and methodological factors (16,37,38).

The acquisition and processing parameters affect the estimates of metabolism and must be standardized to ensure that the image reflects the behavior of the tracer, producing an accurate and reproducible result.

Factors including hyperglycemia, competition and metabolic differences between glucose and [18F]FDG affect all methods and should not be seen as a technical/methodological disadvantage because they are intrinsic to the animal. Although compartmental methods attempt to correct transport and metabolism variations through the lumped constant, to date, it has not been possible to eliminate the associated uncertainties (32,39-41). One of the ways found to approach the SUV of the cMRglu was to correct it by means of the basal serum glycemia level, thus generated the SUV_{glu} (21). Our data show that the SUV_{glu} has no advantage over the SUV, FUR or K_i, as seen in the correlation coefficient between them (r=0.7671; r=0.5752; r=0.5456). The correlation between the SUV_{glu} and K_i decreased with the coefficient obtained between the SUV and K_i (0.5456 *vs.* 0.7336). A plausible and already verified explanation with patients is related to the method of measurement of the basal serum glucose concentration. When methods known as bedside methods are used, as in this article, the reproducibility of the blood glucose measurement is 10 to 15%, in contrast to that of the hexokinase method, which is a more accurate measurement method. The use of these methods can lead to SUV variations of up to 30% (38). Therefore, SUV correction is not recommended unless an accurate method of measuring blood glucose is available (42).

In general, the main parameters related to glucose uptake and that may alter the result are the rate of glucose extraction by the organ of interest and other organs, perfusion, injected activity and volume of distribution (15,17). The main limitations of the SUV related to errors including extravasation, recording of the injected activity, the variation of the absorption due to other organs and differences between plasma and body volume are corrected in the K_i calculation by the inclusion of the input function.

In the images obtained by PET, the region of interest used for quantification contains information on the concentration of metabolized and nonmetabolized [18F]FDG present in the vascular and extravascular compartments. In addition to accounting for the amount of unmetabolized [18F]FDG, the SUV takes into account that metabolism is related to the body weight, lean mass or body surface area of the animal. The total weight is the most common normalization method for the calculation of the SUV. However, there are differences between the plasma and body volume ratio in laboratory animals. Obese, dehydrated animals that have lost a large amount of body mass or that are very hydrated exhibit an altered relationship between the plasma and body volumes that can influence the outcome of the SUV. If the normalization of the dose injected by weight is not proportional to the integral of the [18F]FDG concentration in the plasma, namely, the dose of bioavailable [18F]FDG provided by the input function during the study time, the accuracy will be impaired. Additionally, one should keep in mind that quantitatively measuring uptake is not the same as measuring a pathophysiological process quantitatively.

It is known that hyperglycemia decreases [18F]FDG arterial inflow due to faster blood clearance and that the same injected dose of [18F]FDG does not guarantee the same arterial inflow of [18F]FDG (22). To minimize this problem, one can calculate the level of glucose consumption through the FUR that represents normalized glucose uptake by [18F]FDG arterial inflow and may neglect the influence of uptake by other [18F]FDG organs and of the patient's body weight (23-25). Our results, shown in Table 3 and Figure 4, indicate that there is an excellent correlation between the FUR and K_i (Patlak) (r=0.9472, $p<0.001$) and FUR and K_i (2TCM) (r=0.9385, $p<0.001$). The FUR has a better correlation with the more complex models than the SUV, which allows us to affirm that the method is an adequate substitute for the K_i when the objective is to make comparisons between normal and pathological states or between animals. The major advantage of the FUR method over the 2TCM and Patlak analysis is the use of static images for quantification, which would make translation easier for clinical studies.

However, if the aim of the study is primarily to identify relative metabolic heterogeneities, the SUV can be used as long as the acquisition and processing protocol is rigidly established.

From the methodological point of view, the present findings confirm the theoretical limitations of the SUV and cerebral SUV_{glu} as a surrogate for K_i in the estimation of glucose consumption in the brain. Our data suggest that the FUR is the surrogate for K_i when dynamic acquisition is not possible.

ACKNOWLEDGMENTS

The Laboratory of Nuclear Medicine of the University of São Paulo (LIM-43) supported this work.

AUTHOR CONTRIBUTIONS

Prando S was responsible for the study concept and design. Prando S and Carneiro C contributed to the acquisition of the animal data. Prando S, Sapienza MT and Robilotta CC assisted with the data analysis and interpretation of the findings, drafted the manuscript and critically revised the manuscript for important intellectual content.

REFERENCES

1. Ouchi Y, Fukuyama H, Ogawa M, Yamauchi H, Kimura J, Magata Y, et al. Cholinergic projection from the basal forebrain and cerebral glucose metabolism in rats: a dynamic PET study. J Cereb Blood Flow Metab. 1996;16(1):34-41. https://doi.org/10.1097/00004647-199601000-00004
2. Katsumi Y, Hayashi T, Oyanagi C, Nagahama Y, Yamauchi H, Ono S, et al. Glucose metabolism in the rat frontal cortex recovered without the recovery of choline acetyltransferase activity after lesioning of the nucleus basalis magnocellularis. Neurosci Lett. 2000;280(1):9-12. https://doi.org/10.1016/S0304-3940(99)00993-3
3. Moore AH, Osteen CL, Chatziioannou AF, Hovda DA, Cherry SR. Quantitative assessment of longitudinal metabolic changes *in vivo* after traumatic brain injury in the adult rat using FDG-microPET. J Cereb Blood Flow Metab. 2000;20(10):1492-501. https://doi.org/10.1097/00004647-200010000-00011
4. Shimoji K, Ravasi L, Schmidt K, Soto-Montenegro ML, Esaki T, Seidel J, et al. Measurement of cerebral glucose metabolic rates in the anesthetized

rat by dynamic scanning with 18F-FDG, the ATLAS small animal PET scanner, and arterial blood sampling. J Nucl Med. 2004;45(4):665-72.
5. Kety SS, Schmidt CF. The effects of altered arterial tensions of carbon dioxide and oxygen on cerebral blood flow and cerebral oxygen consumption of normal young men. J Clin Invest. 1948;27(4):484-92. https://doi.org/10.1172/JCI101995
6. Sokoloff L, Reivich M, Kennedy C, Rosiers MH, Patlak CS, Pettigrew KD, et al. The [14C]deoxyglucose method for the measurement of local cerebral glucose utilization: theory, procedure, and normal values in the conscious and anesthetized albino rat. J Neurochem. 1977;28(5):897-916. https://doi.org/10.1111/j.1471-4159.1977.tb10649.x
7. Phelps ME, Huang SC, Hoffman EJ, Selin C, Sokoloff L, Kuhl DE. Tomographic measurement of local cerebral glucose metabolic rate in man with (F-18)2- fluoro-2-deoxy-D-glucose: validation of method. Ann Neurol. 1979;6(5):371-88. https://doi.org/10.1002/ana.410060502
8. Mintun MA, Raichle ME, Kilbourn MR, Wooten GF, Welch MJ. A quantitative model for the *in vivo* assessment of drug binding sites with positron emission tomography. Ann Neurol. 1984;15(3):217-27. https://doi.org/10.1002/ana.410150302
9. Patlak CS, Blasberg RG, Fenstermacher JD. Graphical evaluation of blood-to-brain transfer constants from multiple-time uptake data. J Cereb Blood Flow Metab. 1983;3(1);1-7. https://doi.org/10.1038/jcbfm.1983.1
10. Patlak CS, Blasberg RG. Graphical evaluation of blood-to-brain transfer constants from multiple-time uptake data. Generalizations. J Cereb Blood Flow Metab. 1985;5(4):584-90. https://doi.org/10.1038/jcbfm.1985.87
11. Lindholm P, Minn H, Leskinen-Kallio S, Bergman J, Ruotsalainen U, Joensuu H. Influence of the blood glucose concentration on FDG uptake in cancer - a PET study. J Nucl Med. 1993;34(1):1-6.
12. Hamberg LM, Hunter GJ, Alpert NM, Choi NC, Babich JW, Fischman AJ. The dose uptake ratio as an index of glucose metabolism: useful parameter or oversimplification? J Nucl Med. 1994;35(8):1308-12.
13. Huang SC. Anatomy of SUV. Standardized uptake value. Nucl Med Biol. 2000;27(7):643-6. https://doi.org/10.1016/S0969-8051(00)00155-4
14. Paquet N, Albert A, Foidart J, Hustinx R. Within-patient variability of (18)F-FDG: standardized uptake values in normal tissues. J Nucl Med. 2004;45(5):784-8.
15. Thie JA. Understanding the standardized uptake value, its methods, and implications for usage. J Nucl Med. 2004;45(9):1431-4.
16. Fueger BJ, Czernin J, Hildebrandt I, Tran C, Halpern BS, Stout D, et al. Impact of animal handling on the results of 18F-FDG PET studies in mice. J Nucl Med. 2006;47(6):999-1006.
17. Durand E, Besson FL. How is the standard uptake value (SUV) linked to the influx constant in Sokoloff's model for 18F-FDG? Médecine Nucléaire. 2015;39(1):11-7. https://doi.org/10.1016/j.mednuc.2015.01.002
18. Matsumura A, Mizokawa S, Tanaka M, Wada Y, Nozaki S, Nakamura F, et al. Assessment of microPET performance in analyzing the rat brain under different types of anesthesia: comparison between quantitative data obtained with microPET and *ex vivo* autoradiography. NeuroImage. 2003;20(4):2040-50. https://doi.org/10.1016/j.neuroimage.2003.08.020
19. Toyama H, Ichise M, Liow JS, Vines DC, Seneca NM, Modell KJ, et al. Evaluation of anesthesia effects on [18F]FDG uptake in mouse brain and heart using small animal PET. Nucl Med Biol. 2004;31(2):251-6. https://doi.org/10.1016/S0969-8051(03)00124-0
20. Toyama H, Ichise M, Liow JS, Modell KJ, Vines DC, Esaki T, et al. Absolute quantification of regional cerebral glucose utilization in mice by 18F-FDG small animal PET scanning and 2-14C-DG autoradiography. J Nucl Med. 2004;45(8):1398-405.
21. Woo SK, Lee TS, Kim KM, Kim JY, Jung JH, Kang JH, et al. Anesthesia condition for (18)F-FDG imaging of lung metastasis tumors using small animal PET. Nucl Med Biol. 2008;35(1):143-50. https://doi.org/10.1016/j.nucmedbio.2007.10.003
22. Ishizu K, Yonekura Y. Letter to the editor: Clarification of a fractional uptake concept - reply. J Nucl Med. 1995;36:711-2.
23. Rutland M, Que L, Hassan IM. "FUR" - one size suits all. Eur J Nucl Med. 2000;27(11):1708-13. https://doi.org/10.1007/s002590000337
24. Thie JA. Clarification of a fractional uptake value. J Nucl Med. 1995;36:711-712.
25. Prando S, Carneiro CG, Otsuki DA, Sapienza MT. Effects of ketamine/xylazine and isoflurane on rat brain glucose metabolism measured by ^{18}F-fluorodeoxyglucose-positron emission tomography. Eur J Neurosci. 2019;49(1):51-61. https://doi.org/10.1111/ejn.14252
26. Jespersen B, Knupp L, Northcott CA. Femoral arterial and venous catheterization for blood sampling, drug administration and conscious blood pressure and heart rate measurements. J Vis Exp. 2012;(59). pii: 3496. https://doi.org/10.3791/3496
27. Bergeron M, Cadorette J, Tetrault MA, Beaudoin JF, Leroux JD, Fontaine R, et al. Imaging performance of LabPET APD-based digital PET scanners for pre-clinical research. Phys Med Biol. 2014;59(3):661-78. https://doi.org/10.1088/0031-9155/59/3/661
28. Wu HM, Sui G, Lee CC, Prins ML, Ladno W, Lin HD, et al. *In vivo* quantitation of glucose metabolism in mice using small-animal PET and a microfluidic device. J Nucl Med. 2007;48(5):837-45. https://doi.org/10.2967/jnumed.106.038182
29. Strauss LG, Conti PS. The applications of PET in clinical oncology. J Nucl Med. 1991;32(4):623-48.
30. Schiffer WK, Mirrione MM, Biegon A, Alexoff DL, Patel V, Dewey SL. Serial microPET measures of the metabolic reaction to a microdialysis probe implant. J Neurosci Methods. 2006;155(2):272-84. https://doi.org/10.1016/j.jneumeth.2006.01.027
31. Orzi F, Lucignani G, Dow-Edwards D, Namba H, Nehlig A, Patlak CS, et al. Local cerebral glucose utilization in controlled graded levels of hyperglycemia in the conscious rat. J Cereb Blood Flow Metab. 1988;8(3):346-56. https://doi.org/10.1038/jcbfm.1988.70
32. Alf MF, Duarte JM, Lei H, Kramer SD, Mlynarik V, Schibli R, et al. MRS glucose mapping and PET joining forces: re-evaluation of the lumped constant in the rat brain under isoflurane anaesthesia. J Neurochem. 2014;129(4):672-82. https://doi.org/10.1111/jnc.12667
33. Bland JM, Altman DG. Measuring agreement in method comparison studies. Stat Methods Med Res. 1999;8(2):135-60. https://doi.org/10.1177/096228029900800204
34. Lin LI. A concordance correlation coefficient to evaluate reproducibility. Biometrics. 1989;45(1):255-68. https://doi.org/10.2307/2532051
35. Hawkins RA, Phelps ME, Huang SC, Kuhl DE. Effect of ischemia on quantitation of local cerebral glucose metabolic rate in man. J Cereb Blood Flow Metab. 1981;1(1):37-51. https://doi.org/10.1038/jcbfm.1981.5
36. Crane PD, Pardridge WM, Braun LD, Oldendorf WH. Kinetics of transport and phosphorylation of 2-fluoro-2-deoxy-D-glucose in rat brain. J Neurochem. 1983;40(1):160-7. https://doi.org/10.1111/j.1471-4159.1983.tb12666.x
37. Lammertsma AA, Boellaard R, Hoekstra OS. Quantitative Issues in Response Measurement by PET. PET Clin. 2008;3(1):5-11. https://doi.org/10.1016/j.cpet.2008.08.003
38. Kotasidis FA, Tsoumpas C, Rahmim A. Advanced kinetic modelling strategies: towards adoption in clinical PET imaging. Clin Transl Imaging. 2014;2(3):219-37. https://doi.org/10.1007/s40336-014-0069-8
39. Hasselbalch SG, Madsen PL, Knudsen GM, Holm S, Paulson OB. Calculation of the FDG lumped constant by simultaneous measurements of global glucose and FDG metabolism in humans. J Cereb Blood Flow Metab. 1998;18(2):154-60. https://doi.org/10.1097/00004647-199802000-00005
40. Bøtker HE, Goodwin GW, Holden JE, Doenst T, Gjedde A, Taegtmeyer H. Myocardial glucose uptake measured with fluorodeoxyglucose: a proposed method to account for variable lumped constants. J Nucl Med. 1999;40(7):1186-96.
41. Graham MM, Muzi M, Spence AM, O'Sullivan F, Lewellen TK, Link JM, et al. The FDG lumped constant in normal human brain. J Nucl Med. 2002;43(9):1157-66.
42. Young H, Baum R, Cremerius U, Herholz K, Hoekstra O, Lammertsma AA, et al. Measurement of clinical and subclinical tumour response using [18F]-fluorodeoxyglucose and positron emission tomography: review and 1999 EORTC recommendations. European Organization for Research and Treatment of Cancer (EORTC) PET Study Group. Eur J Cancer. 1999;35(13):1773-82. https://doi.org/10.1016/S0959-8049(99)00229-4

6.4 Effects of ketamine/xylazine and isoflurane on rat brain glucose metabolism measured by ^{18}F-fluorodeoxyglucose-positron emission tomography (Publicação 3)

Received: 7 March 2018 | Revised: 27 September 2018 | Accepted: 29 October 2018

DOI: 10.1111/ejn.14252

RESEARCH REPORT

WILEY EJN European Journal of Neuroscience FENS

Effects of ketamine/xylazine and isoflurane on rat brain glucose metabolism measured by ^{18}F-fluorodeoxyglucose-positron emission tomography

Silvana Prando[1] | Camila de Godoi Carneiro[1] | Denise Aya Otsuki[2] | Marcelo Tatit Sapienza[1]

[1]Laboratory of Nuclear Medicine (LIM43), Department of Radiology and Oncology, Hospital das Clinicas HCFMUSP, Faculdade de Medicina, Universidade de São Paulo, São Paulo, Brazil

[2]Laboratory of Medical Investigation (LIM 08), Hospital das Clinicas HCFMUSP, Faculdade de Medicina, Universidade de São Paulo, São Paulo, Brazil

Correspondence
Silvana Prando, University of São Paulo, Nuclear Medicine, Center, São Paulo, Brazil.
Email: prando@usp.br

Funding information
The Laboratory of Nuclear Medicine of the University of Sao Paulo

Abstract

The aim of the present study was to investigate changes in glucose metabolism in male Wistar rats induced by the anesthetics isoflurane and ketamine combined with xylazine via ^{18}F-fluorodeoxyglucose-positron emission tomography. We analyzed the differential effects of the anesthetics on ^{18}F-fluorodeoxyglucose uptake and pharmacokinetics in 33 rats using quantification methods: (a) the standardized uptake value, (b) voxel-based analyses, and (c) kinetic analysis. Both anesthetics reduced glucose uptake in the entire brain. The voxel-based analyses detected smaller uptake reductions in the bilateral primary somatosensory system cortex and part of the limbic system in the ketamine-xylazine (KX) group and in the vestibular nucleus in the isoflurane group. Through kinetic analysis, we found that the volume of distribution and the membrane transport rate K_1 were reduced in the KX group. Through various methods of ^{18}F-fluorodeoxyglucose-positron emission tomography quantification, the present study found that anesthesia with the ketamine-xylazine combination induced a global reduction of glucose metabolism compared with isoflurane; this reduction of metabolism was relatively lower in the primary somatosensory cortex and part of the limbic system. The volume of distribution of ^{18}F-fluorodeoxyglucose and its Glut1-mediated transport across the brain membranes (K_1) were decreased in the KX group.

KEYWORDS

anesthetics, brain energy metabolism, ^{18}F-Fluorodeoxyglucose, positron emission tomography, Wistar

Abbreviations: 2D, 2-dimensional; 2TCM, 2-tissue compartment model; A, activity; C*m, FDG-6-PO_4 concentration; C^*_p, plasma FDG concentration; C^*_T, tissue-free FDG concentration; Cm, glucose-6-PO_4 concentration; C_p, plasma glucose concentration; C_T, tissue-free glucose concentration; FDG, ^{18}F-Fluorodeoxyglucose; FDG-PET, ^{18}F-fluorodeoxyglucose-positron emission tomography; FOV, field of view; FWE, family-wise error; I, isoflurane; K_1, blood-to-tissue FDG transport rate; k_2, tissue-to-blood FDG transport rate; k_3, metabolized FDG rate; K_i, net FDG consumption; KX, ketamine-xylazine; NLR, nonlinear regression; NMDA, N-Methyl-D-Aspartate; OSEM, Ordered-subsets expectation maximization; *p*(unc)u, uncorrected *p* value for multiple comparisons; PET, Positron emission tomography; *p*FDR, corrected *p* value for multiple comparisons by means of the false discovery rate method; PFUS, Image fusion; *p*FWE, corrected *p* value for multiple comparisons by means of the family-wise error method; PKIN, General kinetic modeling; SAMIT, Small Animal Molecular Imaging Toolbox; SPM, Statistical Parametric Mapping; SUVr, standardized uptake value ratio; SUV, standardized uptake value; T2-MRI, T2-weighted magnetic resonance imaging; TACs, time-activity curves; VBA, voxel-based analyses; V_d, volume of distribution; VINCI, Volume Imaging in Neurological Research, Co-Registration and ROIs included; VOIs, volumes of interest; W, weight.

Edited by Paul Bolam. Reviewed by Johannes Klein.

All peer review communications can be found with the online version of the article.

 © 2018 Federation of European Neuroscience Societies and John Wiley & Sons Ltd

1 | INTRODUCTION

Positron emission tomography (PET) is a well-established imaging method for in vivo assessments of functional and metabolic parameters in preclinical studies. The use of positron-emitting radionuclide-labeled drugs enables noninvasive investigations of various metabolic processes and the brain receptor occupancy rate (Lancelot & Zimmer, 2010).

^{18}F-Fluorodeoxyglucose (FDG) is an 18-fluoro-labeled glucose analog radiopharmaceutical used to assess abnormalities of glycolytic metabolism. Increases or decreases in the regional brain metabolism are indicative of neuronal activity, which might be altered by diseases or through the use of drugs in animal models. However, for investigations of glycolytic metabolism abnormalities in small animals using ^{18}F-fluorodeoxyglucose-positron emission tomography (FDG-PET), the animals are usually anesthetized, and the anesthesia itself induces significant changes in central nervous system metabolism. The effects of anesthetics on drug kinetics or targeted disease are not always known and might confound the results of a study. In addition to their direct effects, the use of anesthetics might make comparisons of results and their reproduction in different laboratories impossible.

Previous studies have demonstrated changes in blood flow and brain glucose metabolism in association with different classes of anesthetics (Långsjö et al., 2005; Matsumura et al., 2003; Mizuma, Shukuri, Hayashi, Watanabe, & Onoe, 2010; Sokoloff et al., 1977; Toyama, Ichise, Liow, Modell, et al., 2004; Toyama, Ichise, Liow, Vines, et al., 2004). While the molecular mechanisms underlying the actions of anesthetics on the brain are not fully understood, the anesthetic state is believed to result from multiple molecular targets in the different brain and central nervous system regions. Anatomically, each anesthetic action occurs at different regions, resulting in distinct electroencephalogram signatures (Hemmings et al., 2005; Purdon, Sampson, Pavone, & Brown, 2015).

We hypothesized that various anesthetic regimens might also induce different glucose metabolic characteristics within the brain.

The aim of the present study was to use PET to identify changes in glucose metabolism caused by isoflurane and ketamine combined with xylazine, which are frequently used anesthetics in small rodents. Therefore, we analyzed the differential effects of these anesthetics on FDG uptake and pharmacokinetics through the following quantification methods: (a) the standardized uptake value (SUV), (b) voxel-based analyses (VBAs), and (c) kinetic analysis.

2 | MATERIALS AND METHODS

2.1 | Animals

Thirty-three male Wistar rats (350 ± 62 g), obtained from Animal Facility Center from Medical School at the University of Sao Paulo, Brazil, were given at least 7 days to acclimate to the vivarium of the Laboratory of Medical Investigation - LIM 43 in a climate-controlled room with a 12-hour circadian cycle and free access to food and water. On the day of the experiment, the animals were subjected to surgery for implantation of a cannula into the femoral artery and to PET under anesthesia with either isoflurane (I) or ketamine-xylazine (KX).

All procedures were in accordance with ethical principles adopted by the Brazilian College of Animal Experimentation and approved by the Ethical Committee for Animal Research of School of Medicine, University of Sao Paulo (protocol 026/14).

The procedures performed during the study are depicted in Figure 1. Each step of the experimental protocol is explained below.

2.2 | Anesthesia and general procedures

In all of the animals, anesthesia was induced with 5% isoflurane (FORANE, Baxter Healthcare Corporation) in 2 L/min O2 using a duly calibrated vaporizer (SUMMIT Anesthesia). Baseline serum glycemia was measured during the step of anesthesia induction; the values were 6.71 ± 1.03 mmol/L (I) and 7.00 ± 1.09 mmol/L (KX).

Following induction, the animals were divided into two groups per anesthetic selected for maintenance of anesthesia:

- I group ($n = 15$): maintenance via inhalation of isoflurane at concentrations of 2.0%–2.5%.
- KX group ($n = 18$): maintenance through intraperitoneal injection of racemic ketamine combined with the alpha-2 agonist xylazine (DOPALEN and ANASEDAN, Sespo Indústria e Comércio Ltda) in doses of 100 and 10 mg/kg, respectively. The first dose was administered during induction, and half of the standardized dose per animal was administered every 30 min to a total of 200 mg/kg of ketamine and 20 mg/kg of xylazine over the duration of the experiment (1.5 hr).

The animals remained on a surface heated to 37°C for the experimental duration to avoid hypothermia.

Before administration of the radiopharmaceutical, a cannula with an internal diameter of 0.58 mm and an external diameter of 0.96 mm (Becton Dickinson PE50) was inserted into the femoral artery for blood sample collection (Jespersen, Knupp, & Northcott, 2012).

The mean time between the onset of induction and FDG injection was 30 min. The total experiment time was 90 min.

2.3 | Positron emission tomography

After the general procedures, image acquisition and arterial blood collection were started synchronically with the

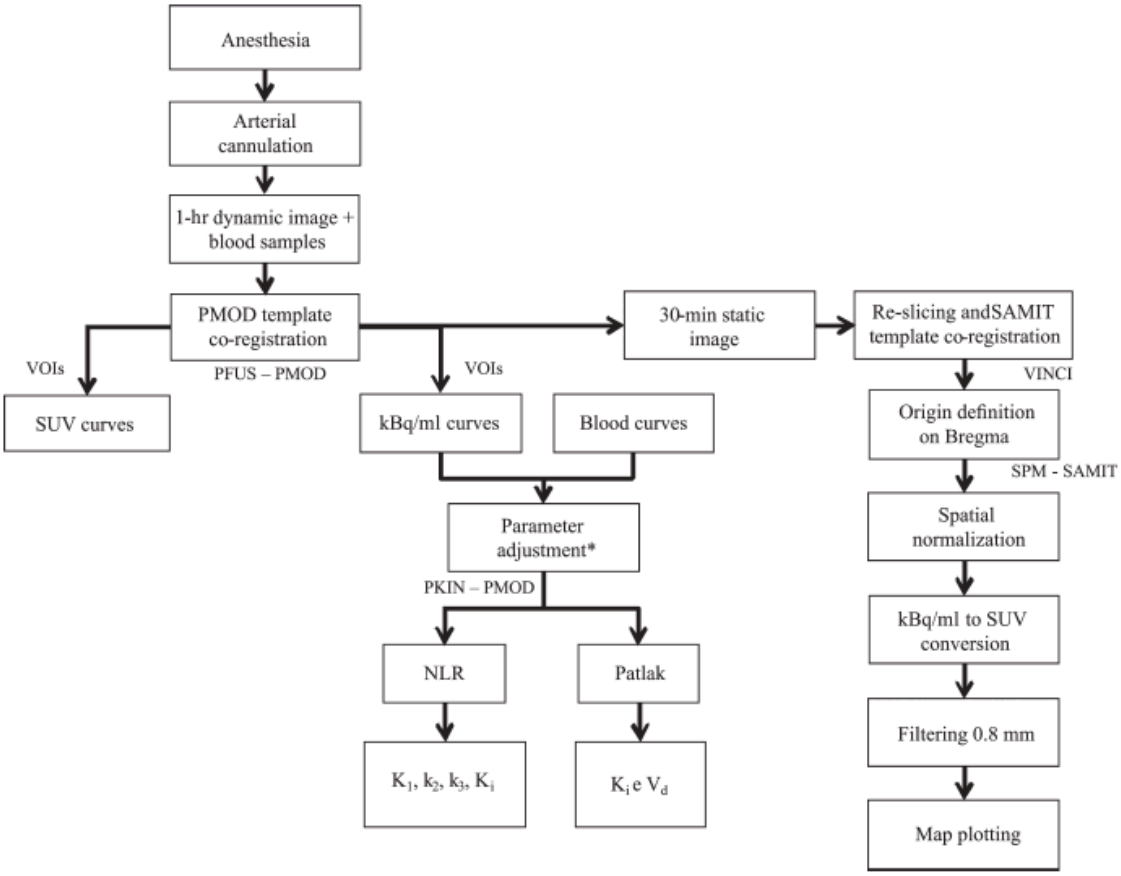

FIGURE 1 The flowchart is representing the data acquisition and processing protocol. Software used: PMOD (PFUS and PKIN tools), VINCI, SPM, and SAMIT. K_i: net glucose consumption; K_1: blood-to-tissue FDG transport rate; k_2: tissue-to-blood FDG transport rate; k_3: metabolized FDG rate; NLR: nonlinear regression; V_d: volume of distribution; VOIs: volumes of interest. * Adjusted parameters: *lumped constant*, glycemia, injection and acquisition synchrony

injection of the radiopharmaceutical. In each group, a bolus injection of either 46.2 ± 8.8 MBq (I) or 47.0 ± 6.0 MBq (KX) of FDG was administered into the penile vein.

The dynamic images were acquired in list mode with a LabPET 4 system (Gamma Medica-Ideas, Northridge, CA) (Bergeron et al., 2009, 2014) over 1 hr. The acquired data were divided into 20 images (six series with the following numbers and durations: 8/30, 2/60, 2/120, 2/150, 3/300, and 3/600 s). Reconstruction was performed using the OSEM-2D method (20 iterations, four subsets, FOV = 60 mm, high resolution mode), which resulted in 0.500 × 0.500 × 0.597 mm voxels. The data were corrected for radionuclide decay and random coincidences.

Simultaneous with PET image acquisition, 17 arterial blood samples were collected from the femoral artery at the PET acquisition time-points 0, 5, 10, 20, 30, 40, 50, 60, 90, 120, 180, 300, 450, 600, 900, 1,800, and 3,600 s. The count rate per minute for an aliquot of 50 µl of sampled blood was measured with a gamma scintillation counter (Wallac Wizard 3, Perkin-Elmer) and the counts obtained were corrected for radionuclide decay and converted to activity concentration (kBq/ml) based on the gamma scintillation counter calibration factor, which was previously determined on the day of the experiment. The activity levels of samples were corrected for the accumulated FDG activity in red blood cells following the method formulated by Wu et al. (2007). The result was used as arterial input function.

2.4 | Data analysis

2.4.1 | Standardized uptake value

The set of dynamic images for each animal was automatically co-registered using the T2-MRI template available in PMOD

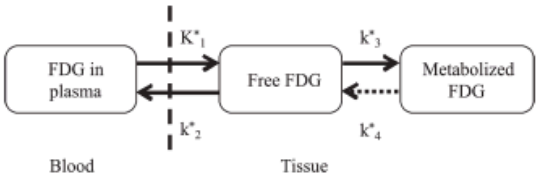

FIGURE 2 Two-tissue compartment model describing FDG pharmacokinetics, including blood-to-tissue FDG transport rate (K_1), tissue-to-blood FDG transport rate (k_2), phosphorylation to FDG-6-phosphate (k_3), and dephosphorylation (k_4)

software, version 3.4 (PMOD Technologies Ltd., Zurich, Switzerland) and the mean SUV was generated by projection VOIs on the dynamic images.

Mean SUV was calculated using the following equation (Strauss & Conti, 1991):

$$SUV = \frac{C_{PET}(t)}{(A/W)}$$

where $C_{PET}(t)$ is the mean FDG concentration in dynamic images; A is the FDG activity injected into the animal corrected for radionuclide decay and residual remaining in the syringe; W is the animal's body weight.

A volume of interest (VOI) designated the whole brain consisting of the thalamus, cerebellum, hypothalamus, hippocampus, caudate nucleus, putamen, and cortex as defined in Schiffer's brain atlas available in the PMOD software and used to obtain the mean SUV. The cortex/brain SUV ratio (SUVr) was calculated for all of the animals using the previously established VOIs.

To calculate the differences in metabolism between the groups, we considered the last 30 min of the study.

2.5 | Kinetic analysis

Kinetic analysis was performed with the PMOD Kinetic package using the irreversible 2-tissue compartment (2TCM) and Patlak methods. The groups were reduced for I: $n = 11$ and KX: $n = 15$.

In PMOD, the dynamic images were automatically co-registered with the T2-MRI template available in the software and the time-activity curves (TACs) for the whole brain were obtained through the application of the previously described VOIs. For both methods, the input function obtained from the arterial blood samples was adjusted using the tri-exponential function.

2.6 | Two-tissue compartment model

For the 2TCM (Figure 2), we assumed that FDG is exchanged between compartments as each compartment represents a homogeneous physiological or biological entity, and the rates of FDG transfer between compartments are described by first-order differential equations.

^{18}F-Fluorodeoxyglucose is transported from the plasma to the tissue as free FDG and is then metabolized to FDG-6-PO_4. Its concentrations in the compartments are represented by the plasma concentration, C^*_p; tissue-free FDG concentration, C^*_T; and metabolized FDG concentration, C^*_m. In addition to concentrations, the 2TCM also allows assessment of the rate of FDG transfer between compartments (K_1, k_2, k_3, and k_4) and the net FDG consumption (K_i):

$$K_i = \frac{K_1 k_3}{k_2 + k_3}$$

The brain represents an irreversible model of FDG metabolism because the dephosphorylation rate of FDG-6-phosphate in brain tissue is small enough that it can be ignored ($k_4 = 0$) (Sokoloff et al., 1977).

The net FDG uptake rate (K_i), transfer rates (K_1, k_2, and k_3) were calculated for all animals.

2.7 | Patlak

To employ Patlak's linearizing method (Patlak & Blasberg, 1985; Patlak, Blasberg, & Fenstermacher, 1983), one should assume that at least one of the compartments would irreversibly retain the radiopharmaceutical and that the duration of the test will suffice for the plasma and tissue compartments to attain the stationary phase. In the case of brain metabolism of FDG, $k_4 = 0$ and the irreversible model can be adopted.

The net FDG uptake rate (K_i) and the volume of distribution were obtained for all of the animals, represented by the slope and intersection of the fit with the *y*-axis.

2.8 | Voxel-based analyses

Voxel-based analyses were performed using *Statistical Parametric Mapping* (SPM8) and *Small Animal Molecular Imaging Toolbox* (SAMIT) software (Wellcome Department of Cognitive Neurology, University College London, UK) (Garcia et al., 2015).

The last three images acquired in the dynamic study were selected, and the mean concentration was calculated with PMOD software, resulting in one static image representing the last 30 min of the test. Each static image was manually aligned using the FDG Wistar template and was then cut and resampled to generate a 180 × 180 × 180 matrix using VINCI software (VINCI 4.45, Max Planck Institute for Metabolism Research, Cologne, Germany). The dimensions of the resulting voxel were 0.2 × 0.2 × 0.2 mm.

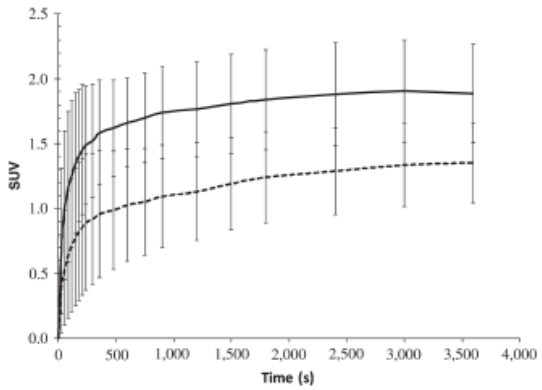

FIGURE 3 The whole brain mean SUV variation curves for the I group (solid line, $n = 15$) and the KX group (dotted line, $n = 18$)

The images thus generated were spatially normalized for the template using the affine registration algorithm and the activity concentration data (kBq/ml) extracted from the images were converted to SUV. Application of a mask removed extracerebral signals, and the final image was smoothed with a 0.8-mm isotropic Gaussian kernel.

The analysis was performed with and without global normalization (proportional scale) to verify the global and regional actions of the anesthetics on the cerebral metabolism of glucose. The supraliminal clustering coordinates were attributed to the brain areas using a rat brain atlas (Paxinos & Watson, 2007).

2.9 | Statistical analysis

The obtained values are described as the means and standard error of the mean (mean ± *SEM*). The biometric variables, SUV, and kinetic analysis were subjected to nonparametric, bivariate statistical tests; statistical analysis was performed with SPSS 22.0 (SPSS Inc., Chicago, IL, USA). The Mann–Whitney test was used to compare continuous measures between groups and p values below 0.05 were considered to be statistically significant. Moreover, the magnitude of the difference between groups was assessed using the Cohen's d effect size index.

In the analysis performed with SPM software, we used the unpaired t test to compare between groups (I vs. KX). Illustrative images of areas with relative increases or decreases in the metabolism in the KX group compared with the I group were generated with a cutoff point for visualization of $p < 0.05$, uncorrected. For the interpretation of the difference between groups, T maps with $p = 0.001$ (uncorrected) were plotted; only areas with a minimum extension of 200 voxels were considered and only clusters with $p < 0.001$ corrected for multiple comparisons (family-wise error - FWE) were considered significant.

TABLE 1 SUV (mean ± *SEM*) for the last 30 min of the study, p and effect size obtained for whole brain (WB), cortex (CTX), and CTX/WB

SUV	n	Mean ± *SEM*	p^a	d
WB				
I	15	1.879 ± 0.010	<0.001	1.60
KX	18	1.305 ± 0.077		
CTX				
I	15	1.777 ± 0.094	<0.001	1.38
KX	18	1.301 ± 0.076		
CTX/WB				
I	15	0.947 ± 0.007	<0.001	−2.69
KX	18	1.001 ± 0.003		

Note. SUV: standardized uptake value.
[a]Mann–Whitney test.

3 | RESULTS

3.1 | Standardized uptake value

The curves of the variation of the brain mean SUV per time-point of PET acquisition and type of anesthetic are depicted in Figure 3 and Table 1. As Figure 3 shows, the behaviors of the mean SUV time curves were similar. However, glucose uptake was higher in the I group from the start of the study onward.

The data relative for the whole brain (WB) and cortex (CTX) to the last 30 min of the test for I and KX group are depicted in Figures 4, 5, and Table 1. Figure 4 depicts the mean and corresponding standard deviation of the mean for the WB and CTX. Figure 5 depicts the relationship between the mean SUV for the cortex and the whole brain.

In Figure 4, one may notice that the mean SUV for the last 30 min of the study emphasizes the difference in FDG uptake between the groups. The mean SUV for WB was reduced in the KX group compared with that in the I group (KX [$n = 18$]: 1.305 ± 0.077 vs. I [$n = 15$]: 1.879 ± 0.010; $p < 0.001$; d: 1.60).

In Figure 5, the CTX/WB SUV for the last 30 min of the study denotes a smaller reduction in the glucose metabolism in the CTX of the KX group animals in relationship with WB when compared with the I group (KX [$n = 18$]: 1.001 ± 0.003 vs. I [$n = 15$]: 0.947 ± 0.007; $p < 0.001$).

3.2 | Voxel-based analyses

Comparisons conducted without global normalization indicate that the reduction in glucose consumption was significantly higher in the KX group than in the I group.

The VBA method with global normalization by the proportional scale showed differences in relative glucose metabolism levels between the groups subjected to the tested anesthetics (Figure 6).

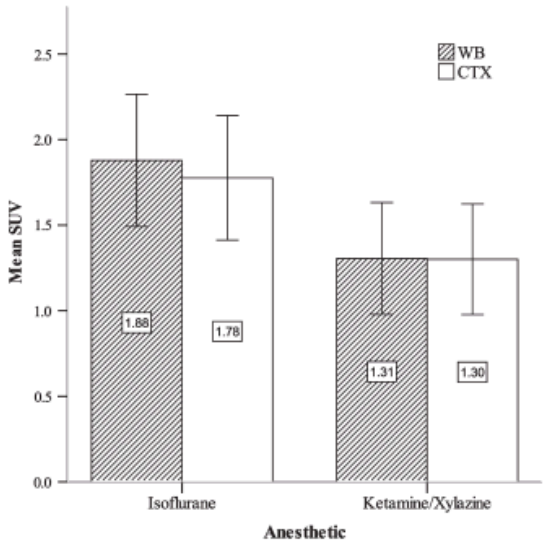

FIGURE 4 Difference in the mean SUVs for the last 30 min of the test for WB (I: 1.88 vs. KX: 1.31; $p < 0.001$) and CTX (I: 1.78 vs. KX: 1.30; $p < 0.001$)

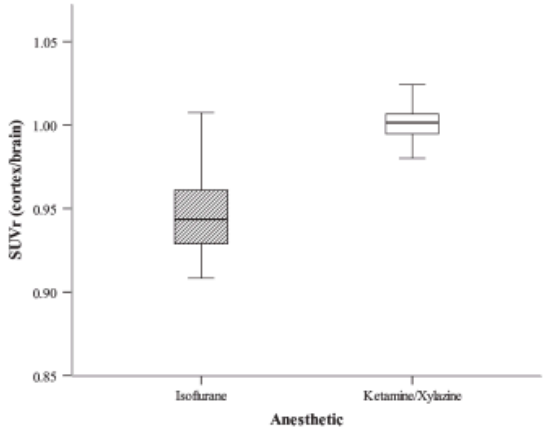

FIGURE 5 Cortex/brain SUVr for the last 30 min of the test for the I and KX groups (I: 0.95 vs. KX: 1.00; $p < 0.001$)

While the animals in the KX group showed a lower global metabolic activity compared with the I group, as shown by the mean SUV, metabolic reduction in the relationship with mean uptake followed different patterns of distribution in each group. The metabolic reduction induced by ketamine-xylazine was proportionally lower relative to the mean uptake in the cortical structures compared to that in the isoflurane group, resulting in an apparent pattern of "increased" activity in these areas. The subcortical structures/basal ganglia and the cerebellum showed opposite behavior, exhibiting

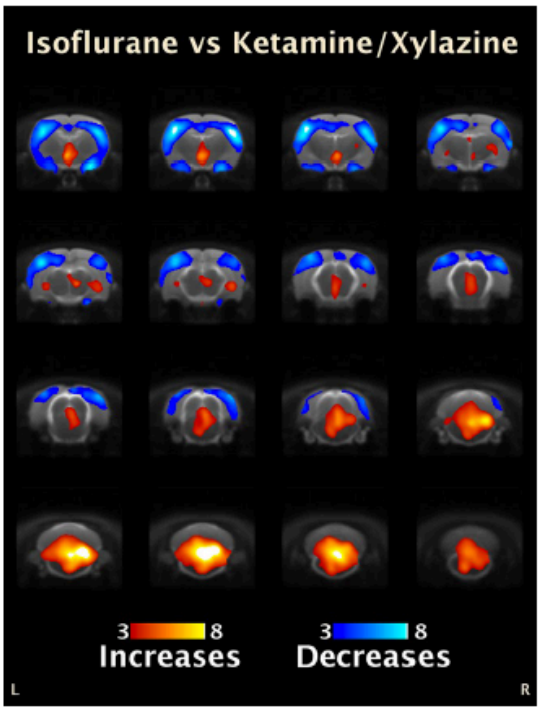

FIGURE 6 Representative SPM images of the SUVs between rats maintained under isoflurane or ketamine/xylazine anesthesia during the FDG uptake period. T-map data (visualization cutoff point: $p < 0.05$; uncorrected) are depicted using Mango as a multislice coronal MRI template overlay (Schwartz et al., 2006). The color bar was set to a minimum of three and a maximum of eight for both increases and decreases in glucose uptake relative to the mean uptake for the subjects anesthetized with isoflurane ($n = 15$) compared to the subjects anesthetized with ketamine/xylazine ($n = 18$). [Colour figure can be viewed at wileyonlinelibrary.com]

relatively reduced activity concerning average consumption, in the KX group. Table 2 describes the areas that showed the most significant differences in relative metabolism between the groups when a rigid threshold to the statistical maps ($p < 0.001$; minimum area 200 voxels) was applied. In the relationship with the average metabolism, ketamine-xylazine induced a smaller relative reduction of glucose metabolism in the primary somatosensory cortex bilaterally, the amygdaloid area and the endopiriform nucleus and a higher relative reduction of glucose metabolism in the medial vestibular nucleus.

3.3 | Kinetic analysis

Application of Patlak's method (Table 3) revealed a reduced volume of distribution of FDG under the influence of ketamine-xylazine. Despite the lower mean value and the higher effect size, the net FDG consumption (represented

TABLE 2 Areas exhibiting relative changes in glucose metabolism as measured via FDG-PET and determined by SPM processing, with global normalization, between the I and KX groups. The cutoff point for visualization, $p < 0.001$, and minimum significant area, 200 voxels

Comparisons[a]	Number of voxels in the area	*p*FWE	*p*FDR	*p*(unc)	Z *score*
Ketamine/Xylazine (increase)[b]					
Right primary somatosensory area	607	<0.001	0.013	<0.001	6.35
Left somatosensory area	1,068	<0.001	0.022	<0.001	6.14
Anterior amygdaloid area/Endopiriform nucleus	295	<0.001	0.038	<0.001	5.96
Ketamine/Xylazine (reduction)[c]					
Medial vestibular nucleus	3,344	<0.001	<0.001	<0.001	6.72

Notes. *p*FDR: corrected *p* value for multiple comparisons by means of the false discovery rate method; *p*FWE: corrected *p* value for multiple comparisons by means of the family-wise error method; *p*(unc): uncorrected *p* value for multiple comparisons.
[a]Comparison between the I and KX groups via SPM processing with global normalization. [b]Relative increase in FDG uptake in the KX group compared with that in the I group. [c]Relative decrease in FDG uptake in the KX group compared with that in the I group.

by K_i) did not significantly differ between the KX and I groups.

The 2TCM method (Table 3) showed a difference in the Glut1-mediated glucose transport into the cells. Transport was reduced under the influence of KX compared with the I group. None of the other analyzed transfer constants showed a statistically significant difference.

TABLE 3 Net FDG consumption, volume of distribution, and transfer constants (mean ± *SEM*) obtained with Patlak's and 2TCM methods for the whole brain

	n	Mean ± *SEM*	*p*[a]	*d*
Patlak				
K_i				
I	11	0.018 ± 0.002	0.052	0.88
KX	15	0.014 ± 0.001		
V_d				
I	11	0.760 ± 0.054	0.001	1.55
KX	15	0.505 ± 0.038		
2TCM				
K_1				
I	11	0.283 ± 0.022	0.001	1.47
KX	15	0.173 ± 0.019		
k_2				
I	11	0.353 ± 0.048	0.754	0.13
KX	15	0.331 ± 0.046		
k_3				
I	11	0.023 ± 0.002	0.205	−0.49
KX	15	0.030 ± 0.005		
K_i				
I	11	0.018 ± 0.001	0.056	0.80
KX	15	0.014 ± 0.001		

Notes. K_1 (μmol/min/100 g): blood-to-tissue FDG transport rate; k_2 (min^{-1}): tissue-to-blood FDG transport rate; k_3 (min^{-1}): phosphorylation to FDG-6-phosphate; K_i: net FDG consumption.
[a]Mann—Whitney test.

4 | DISCUSSION

After Sokoloff's article (1977), several studies analyzed the effects of anesthetics on brain glucose metabolism utilizing FDG-PET in various animal species. According to the reports in the literature, most general anesthetics, such as isoflurane, halothane, propofol, ketamine associated with xylazine reduce brain metabolism as shown by reductions in FDG absorption varying from 22% to 66% (Alstrup & Smith, 2013; Lee et al., 2010; Mizuma et al., 2010; Noda, Takamatsu, Minoshima, Tsukada, & Nishimura, 2003; Toyama, Ichise, Liow, Vines, et al., 2004). In contrast to the diffuse brain metabolic reduction induced by most anesthetics, previous studies have found that ketamine changes the metabolism heterogeneously (Freo & Ori, 2004; Matsumura et al., 2003; Toyama, Ichise, Liow, Modell, et al., 2004; Toyama, Ichise, Liow, Vines, et al., 2004).

In the present study, we investigated the effects of the anesthetics isoflurane and ketamine-xylazine on FDG uptake in the rat brain. We found differences in the global and relative glucose uptake levels between both anesthetics and their influence on the glucose pharmacokinetics.

4.1 | Global glucose uptake

The mean SUV value for the whole brain found in the present study showed a reduction of the global brain metabolism with combination ketamine-xylazine compared with isoflurane (KX [$n = 18$]: 1.305 ± 0.077 vs. I [$n = 15$]: 1.879 ± 0.010; $p < 0.001$; d: 1.60). Although K_i is not statistically significant

between groups, the effect size is >0.8 regardless of the method of calculating (Patlak: (KX [$n = 15$]: 0.018 ± 0.002 vs. I [$n = 11$]: 0.014 ± 0.001; $p = 0.052$; d: 0.88); 2TCM (KX [$n = 15$]: 0.018 ± 0.001 vs. I [$n = 11$]: 0.014 ± 0.001; $p = 0.056$; d: 0.80)). This finding agrees with the results of previous studies, which showed that both combination ketamine-xylazine and isoflurane alone induced accentuated reductions in glucose uptake in the brain (Matsumura et al., 2003; Mizuma et al., 2010; Toyama, Ichise, Liow, Modell, et al., 2004; Toyama, Ichise, Liow, Vines, et al., 2004).

According to the kinetic analysis performed following Patlak's method (Table 3), the volume of FDG distribution decreased in the KX group (KX [$n = 15$]: 0.505 ± 0.038 vs. I [$n = 11$]: 0.760 ± 0.054; $p < 0.001$; d: 1.55). Such a reduction might be accounted for by two mechanisms: (a) ketamine increases the levels of norepinephrine by reducing its uptake, resulting in peripheral vasoconstriction, which leads to increases in the systolic and diastolic arterial pressure, attended by a reflex decrease in the heart rate; in turn, isoflurane reduces the peripheral resistance, with a consequent decrease in the arterial pressure; and (b) ketamine acts on the sympathetic nervous system, promoting lipolysis in the adipose tissue, resulting in elevation of the plasma fatty acid concentration (Carruba, Bondiolotti, Picotti, Catteruccia, & Da Prada, 1987; Sano et al., 2016). As a consequence of the reduction in the intravascular volume and greater competition with fatty acids as extraneuronal metabolic substrates, the FDG concentration increased, and the volume of distribution decreased in the KX group. The data from 2TCM (Table 3) show that transfer constant K_1 was reduced in the KX group (KX [$n = 15$]: 0.173 ± 0.019 vs. I [$n = 11$]: 0.283 ± 0.022; $p < 0.001$; d: 1.47). Transfer constant K_1 represents Glut1-mediated glucose transport across brain membranes and in the context of an acute glycemia increase; the substrates glucose and FDG compete for transporters, resulting in reduced FDG uptake (Orzi et al., 1988; Viglianti et al., 2017). Increased glycemia during the use of anesthetics, including isoflurane, has been reported in several studies (Saha, Xia, Grondin, Engle, & Jakubowski, 2005; Sano et al., 2016). Sano et al. (2016) found that the combination ketamine-xylazine (50 and 10 mg/kg, respectively) and isoflurane (at a concentration of ~2.5%) caused equal-magnitude increases in glycemia among anesthetized animals. However, our result indicates a decrease in K_1 only in the KX group, which may be a result of a more marked increase in the glycemia of the individuals in the group or another aspect not yet known.

Therefore, future studies are needed to evaluate other factors that influence the pharmacokinetics of glucose in the brain of anesthetized animals.

The difference between the magnitude of the effect in SUV and K_i for the whole brain can be explained by the metabolic differences between the groups. The KX group presents a reduction of the intravascular volume, an increase of the concentration of FDG and consequent decrease of K_1. Compared with the KX group, the group I does not show these differences that are considered in K_i but not in SUV values. Therefore, the SUV value should not be more valued than the K_i.

In addition to SUV analyses and FDG kinetics, we compared 30-minute images of the whole brain using VBA. The result of the comparison without the use of global normalization (proportional scale) indicated that the cerebral metabolism of KX-anesthetized animals is decreased in comparison with animals anesthetized with isoflurane, which agree with our results of SUV and K_i.

4.2 | Relative differences

In addition to the difference in the global metabolism, relative differences are also relevant to the study of new drugs or the pathophysiology of brain diseases.

Upon discussing the relative variations in metabolism, we should first stress that the VBA method includes a step for normalization of brain metabolism before the analysis of regional variations between groups. Detection of "increased" activity in region "X" might mean that intervention caused: (a) an increase in region "X" activity compared with the mean metabolism of the brain or (b) a smaller reduction in region "X" activity compared with the mean metabolism of the brain. This caution in interpretation applies to all studies on brain metabolism that use techniques similar to VBA.

Considering that the global metabolism is more strongly reduced by ketamine-xylazine compared with isoflurane, the areas with "higher" activity in the KX group represent smaller metabolic reductions compared with mean metabolism of the brain, rather than a real increase in the metabolism by comparison to the I group, as can be seen in Figure 4 and 5. Therefore, in the present study, the VBA method indicated that the bilateral primary somatosensory cortex, amygdaloid area, and endopiriform nucleus presented lower reductions relative to the mean metabolism in KX-anesthetized rats compared to those in isoflurane-anesthetized rats (Table 2).

As is known, the effects of anesthetics on relative metabolism differ as a function of the drug used. The inhaled agents, like isoflurane, act at multiple targets in the brain and central nervous system, enhancing and blocking different receptors and channels (Purdon et al., 2015). Ketamine acts on the brain mainly through binding to NMDA receptors, blocking the excitatory glutamatergic input to inhibitory interneurons, thus causing excitatory activity on pyramidal neurons. Impaired control of the pyramidal neurons is the leading cause of the increase in brain metabolism. The higher activity of these neurons might account for clinically recognizable exacerbations of limbic system functions (Brown, Solt, Purdon, & Johnson-Akeju, 2015).

In our study, in addition to the primary somatosensory cortex, the amygdala and endopiriform nucleus showed relative increases in metabolism in the KX group compared with the I group. Similar to the amygdaloid area and the claustrum, the endopiriform nucleus is also a part of the cortical sublayer, namely, a transitional area below the cortical layer and above the intermediate area in the developing cortex. Recent studies have suggested that the cortical sublayer structures are part of an interhemispheric circuit that interconnects infralimbic cortical areas of both brain hemispheres. The laminar analysis of cortical neurons that project to the endopiriform nucleus performed by Watson, Smith, and Alloway (2017) showed that the cortico-endopiriform neurons originate in layers 2–5, which include the internal and external pyramidal layers (Watson et al., 2017). Thus, our findings suggest that, in addition to the amygdala, the endopiriform nucleus is also involved in the limbic release effect induced by ketamine.

By comparison to the KX group, the I group showed a relative metabolic increase only in the medial vestibular nucleus. Other studies have also reported relative metabolic increases in the vestibular nucleus of animals anesthetized with isoflurane (Shimoji et al., 2004; Spangler-Bickell, De Laat, Fulton, Bormans, & Nuyts, 2016).

In addition to the global reduction of the metabolism and regional variations in the glucose consumption resulting from the direct effects of the anesthetics on the brain, changes in biodistribution might also be studied as functions of alterations in the glucose transport and metabolism mechanisms.

The most critical limitations of the present study were (a) the failure to measure blood glucose at different times to compare if the increased blood glucose caused by xylazine and isoflurane could lead to a decrease in K_1 and (b) the lack of a nonanesthetized control group to compare the global and regional biodistributions of FDG and the SUV.

The measurement of the effects of anesthetics on the brain performed in the present study — which we consider to be one of the most representatives in this field for associating quantification methods and comparing different anesthetics — provides parameters likely to contribute to future studies on the effects of anesthetics and, more particularly, to identify potential confounding factors in the assessment of other drugs or experimental models targeting the central nervous systems of anesthetized animals.

Through various methods of FDG-PET quantification, the present study found that anesthesia with the combination ketamine-xylazine induced a global reduction in glucose metabolism compared to isoflurane. The VBA method revealed a difference in biodistribution of FDG induced by the anesthetics. The animals anesthetized with KX exhibited a more marked FDG uptake pattern in the cortex and part of the limbic system relative to the mean brain uptake, while the animals in the I group demonstrated a more significant reduction of uptake compared to the mean uptake in the same areas. The volume of distribution of FDG and its Glut1-mediated transport across the brain membranes (K_1) decreased in the KX group.

ACKNOWLEDGEMENTS

The authors would like to thank Dr. Fabio Luis de Souza Duran for technical assistance. This work was supported by the Laboratory of Nuclear Medicine of the University of Sao Paulo.

CONFLICT OF INTEREST

The authors have no conflicts of interest to declare.

DATA ACCESSIBILITY

All relevant data within the document will be made available on demand by email prando@usp.br.

AUTHOR CONTRIBUTIONS

SP was responsible for the study concept and design. SP and CG contributed to the acquisition of the animal data. SP, MTS, and DAO assisted with the data analysis and interpretation of the findings. SP, MTS, and DAO drafted the manuscript. SP, MTS, and DAO critically revised the manuscript for important intellectual content.

ORCID

Silvana Prando http://orcid.org/0000-0002-8038-271X

REFERENCES

Alstrup, A. K. O., & Smith, D. F. (2013). Anaesthesia for positron emission tomography scanning of animal brains. *Laboratory Animals*, *47*, 12–18. https://doi.org/10.1258/la.2012.011173

Bergeron, M., Cadorette, J., Beaudoin, J.-F., Lepage, M. D., Robert, G., Selivanov, V., … Lecomte, R. (2009). Performance evaluation of the LabPET APD-based digital PET scanner. *IEEE Transactions on Nuclear Science*, *56*, 10–16. https://doi.org/10.1109/TNS.2008.2010257

Bergeron, M., Cadorette, J., Tétrault, M.-A., Beaudoin, J.-F., Leroux, J.-D., Fontaine, R., & Lecomte, R. (2014). Imaging performance of LabPET APD-based digital PET scanners for pre-clinical research. *Physics in Medicine & Biology*, *59*, 661–678. https://doi.org/10.1088/0031-9155/59/3/661

Brown, E. N., Solt, K., Purdon, P., & Johnson-Akeju, O. (2015). Monitoring brain state during general anesthesia and sedation. In R. D. Miller, L. I. Eriksson, L. A. Fleisher, J. P. Wiener-Kronish, N. H. Cohen, & W. L. Young (Eds.), *Miller's anesthesia E-book* (pp. 1524–1540). Philadelphia: Elsevier.

Carruba, M. O., Bondiolotti, G., Picotti, G. B., Catteruccia, N., & Da Prada, M. (1987). Effects of diethyl ether,

halothane, ketamine and urethane on sympathetic activity in the rat. *European Journal of Pharmacology*, *134*, 15–24. https://doi.org/10.1016/0014-2999(87)90126-9

Freo, U., & Ori, C. (2004). Effects of anesthesia and recovery from Ketamine racemate and Enantiomers on regional cerebral glucose metabolism in rats. *Anesthesiology*, *100*, 1172–1178. https://doi.org/10.1097/00000542-200405000-00020

Garcia, D. V., Casteels, C., Schwarz, A. J., Dierckx, R. A. J. O., Koole, M., & Doorduin, J. (2015). Correction: A standardized method for the construction of tracer specific PET and SPECT rat brain templates: Validation and implementation of a toolbox. *PLoS ONE*, *10*, e0143900. https://doi.org/10.1371/journal.pone.0143900

Hemmings, H. C., Akabas, M. H., Goldstein, P. A., Trudell, J. R., Orser, B. A., & Harrison, N. L. (2005). Emerging molecular mechanisms of general anesthetic action. *Trends in Pharmacological Sciences*, *26*, 503–510. https://doi.org/10.1016/j.tips.2005.08.006

Jespersen, B., Knupp, L., & Northcott, C. A. (2012). Femoral arterial and venous catheterization for blood sampling, drug administration and conscious blood pressure and heart rate measurements. *Journal of Visualized Experiments*, *59*, e3496. https://doi.org/10.3791/3496

Lancelot, S., & Zimmer, L. (2010). Small-animal positron emission tomography as a tool for neuropharmacology. *Trends in Pharmacological Sciences*, *31*, 411–417. https://doi.org/10.1016/j.tips.2010.06.002

Långsjö, J. W., Maksimow, A., Salmi, E., Kaisti, K., Aalto, S., Oikonen, V., … Scheinin, H. (2005). S-Ketamine anesthesia increases cerebral blood flow in excess of the metabolic needs in humans. *Anesthesiology*, *103*, 258–268. https://doi.org/10.1097/00000542-200508000-00008

Lee, M. S., Ko, J., Lee, A. R., Lee, I. H., Jung, M. A., Austin, B., … Eom, K. (2010). Effects of anesthetic protocol on normal canine brain uptake of18F-FDG assessed by PET/CT. *Veterinary Radiology & Ultrasound*, *51*, 130–135.

Matsumura, A., Mizokawa, S., Tanaka, M., Wada, Y., Nozaki, S., Nakamura, F., … Watanabe, Y. (2003). Assessment of microPET performance in analyzing the rat brain under different types of anesthesia: Comparison between quantitative data obtained with microPET and Ex vivo autoradiography. *NeuroImage*, *20*, 2040–2050. https://doi.org/10.1016/j.neuroimage.2003.08.020

Mizuma, H., Shukuri, M., Hayashi, T., Watanabe, Y., & Onoe, H. (2010). Establishment of In vivo brain imaging method in conscious mice. *Journal of Nuclear Medicine*, *51*, 1068–1075. https://doi.org/10.2967/jnumed.110.075184

Noda, A., Takamatsu, H., Minoshima, S., Tsukada, H., & Nishimura, S. (2003). Determination of kinetic rate constants for 2-[18F]fluoro-2-deoxy-d-glucose and partition coefficient of water in conscious macaques and alterations in aging or anesthesia examined on parametric images with an anatomic standardization technique. *Journal of Cerebral Blood Flow and Metabolism*, *23*, 1441–1447. https://doi.org/10.1097/01.WCB.0000090623.86921.47

Orzi, F., Lucignani, G., Dow-Edwards, D., Namba, H., Nehlig, A., Patlak, C. S., … Sokoloff, L. (1988). Local cerebral glucose utilization in controlled graded levels of Hyperglycemia in the conscious rat. *Journal of Cerebral Blood Flow and Metabolism*, *8*, 346–356. https://doi.org/10.1038/jcbfm.1988.70

Patlak, C. S., & Blasberg, R. G. (1985). Graphical evaluation of blood-to-brain transfer constants from multiple-time uptake data. generalizations. *Journal of Cerebral Blood Flow and Metabolism*, *5*, 584–590. https://doi.org/10.1038/jcbfm.1985.87

Patlak, C. S., Blasberg, R. G., & Fenstermacher, J. D. (1983). Graphical evaluation of blood-to-brain transfer constants from multiple-time uptake data. *Journal of Cerebral Blood Flow and Metabolism*, *3*, 1–7. https://doi.org/10.1038/jcbfm.1983.1

Paxinos, G., & Watson, C. (2007). *The rat brain in stereotaxic coordinates: Hard cover*. Nova Iorque, Brazil: Academic Press.

Purdon, P. L., Sampson, A., Pavone, K. J., & Brown, E. N. (2015). Clinical electroencephalography for anesthesiologists. *Anesthesiology*, *123*, 937–960. https://doi.org/10.1097/ALN.0000000000000841

Saha, J. K., Xia, J., Grondin, J. M., Engle, S. K., & Jakubowski, J. A. (2005). Acute hyperglycemia induced by ketamine/xylazine anesthesia in rats: Mechanisms and implications for preclinical models. *Experimental Biology and Medicine*, *230*, 777–784. https://doi.org/10.1177/153537020523001012

Sano, Y., Ito, S., Yoneda, M., Nagasawa, K., Matsuura, N., Yamada, Y., … Nagata, K. (2016). Effects of various types of anesthesia on hemodynamics, cardiac function, and glucose and lipid metabolism in rats. *American Journal of Physiology. Heart and Circulatory Physiology*, *311*, H1360–H1366. https://doi.org/10.1152/ajpheart.00181.2016

Schwarz, A. J., Danckaert, A., Reese, T., Gozzi, A., Paxinos, G., Watson, C., … Bifone, A. (2006). A stereotaxic MRI template set for rat brain with tissue class distribution maps and co-registered anatomical atlas: Application to pharmacological MRI. *NeuroImage*, *32*, 538–550. https://doi.org/10.1016/j.neuroimage.2006.04.214

Shimoji, K., Ravasi, L., Schmidt, K., Soto-Montenegro, M. L., Esaki, T., Seidel, J., … Eckelman, W. C. (2004). Measurement of cerebral glucose metabolic rates in the anesthetized rat by dynamic scanning with 18F-FDG, the ATLAS small animal PET scanner, and arterial blood sampling. *Journal of Nuclear Medicine*, *45*, 665–672.

Sokoloff, L., Reivich, M., Kennedy, C., Rosiers, M. H. D., Patlak, C. S., Pettigrew, K. D., … Shinohara, M. (1977). The [14c]Deoxyglucose method for the measurement of local cerebral glucose utilization: Theory, procedure, and normal values in the conscious and anesthetized albino rat. *Journal of Neurochemistry*, *28*, 897–916. https://doi.org/10.1111/j.1471-4159.1977.tb10649.x

Spangler-Bickell, M. G., De Laat, B., Fulton, R., Bormans, G., & Nuyts, J. (2016). The effect of isoflurane on 18F-FDG uptake in the rat brain: A fully conscious dynamic PET study using motion compensation. *EJNMMI Research*, *6*, 86. https://doi.org/10.1186/s13550-016-0242-3

Strauss, L. G., & Conti, P. S. (1991). The applications of PET in clinical oncology. *Journal of Nuclear Medicine*, *32*, 623–648.

Toyama, H., Ichise, M., Liow, J. S., Modell, K. J., Vines, D. C., Esaki, T., … Innis, R. B. (2004). Absolute quantification of regional cerebral glucose utilization in mice by 18F-FDG small animal PET scanning and 2-14C-DG autoradiography. *Journal of Nuclear Medicine*, *45*, 1398–1405.

Toyama, H., Ichise, M., Liow, J.-S., Vines, D. C., Seneca, N. M., Modell, K. J., … Innis, R. B. (2004). Evaluation of anesthesia effects on [18F]FDG uptake in mouse brain and heart using small animal PET. *Nuclear Medicine and Biology*, *31*, 251–256. https://doi.org/10.1016/S0969-8051(03)00124-0

Viglianti, B. L., Wong, K. K., Wimer, S. M., Parameswaran, A., Nan, B., Ky, C., … Gross, M. D. (2017). Effect of hyperglycemia on brain

and liver 18 F-FDG standardized uptake value (FDG SUV) measured by quantitative positron emission tomography (PET) imaging. *Biomedicine & Pharmacotherapy*, *88*, 1038–1045. https://doi.org/10.1016/j.biopha.2017.01.166

Watson, G. D. R., Smith, J. B., & Alloway, K. D. (2017). Interhemispheric connections between the infralimbic and entorhinal cortices: The endopiriform nucleus has limbic connections that parallel the sensory and motor connections of the claustrum. *Journal of Comparative Neurology*, *525*, 1363–1380. https://doi.org/10.1002/cne.23981

Wu, H. M., Sui, G., Lee, C. C., Prins, M. L., Ladno, W., Lin, H. D., … Huang, S. C. (2007). In vivo quantitation of glucose metabolism in mice using small-animal PET and a microfluidic device. *Journal of Nuclear Medicine*, *48*, 837–845. https://doi.org/10.2967/jnumed.106.038182

How to cite this article: Prando S, Carneiro CDG, Otsuki DA, Sapienza MT. Effects of ketamine/xylazine and isoflurane on rat brain glucose metabolism measured by ^{18}F-fluorodeoxyglucose-positron emission tomography. *Eur J Neurosci*. 2019;49:51–61. https://doi.org/10.1111/ejn.14252

7. REFERÊNCIAS BIBLIOGRÁFICAS

Adams MC, Turkington TG, Wilson JM, Wong TZ. A systematic review of the factors affecting accuracy of measurements. *AJR Am J Roentgenol*. 2010; 195(2):310-20.

Alf M et al. High-resolution spacial mapping of changes in the neurochemical profile after focal ischemia in mice. *NMR Biomed*. 2012;25:247-54.

Alf M et al. MRS glucose mapping and PET joining forces: re-evaluation of the lumped constant in the rat brain under isoflurane anaesthesia. *J Neurochem*. 2014;129:672-82.

Alstrup A, Smith D. Anaesthesia for positron emission tomography scanning of animals brains. *Lab Anim.* 2013;47:12-8.

Amaral I, Nogueira MI, Ferreira FRM. Entre neurônios e sinapses: as contribuições de Cajal e Athias para a medicina ibérica entre os séculos XIX e XX. *Hist. cienc. saude-Manguinhos*. 2017;24(1):187-99.

Backes H et al. Whiskers area as extracerebral reference tissue for quantification of rat brain metabolism using 18F-FDG PET: application to focal cerebral ischemia. *J Nucl Med*. 2011;52:1252-60.

Blandini F, Armentero MT. Animal models of Parkinson's disease. *FEBS J.* 2012;279:1156–66.

Boellaard R et al. Effects of noise, image resolution, and ROI definition on the accuracy of standard uptake value: a simulation study. J Nucl Med. 2004; 45(9):1519-27.

Boellaard R et al. FDG PET/CT: EANM procedure guidelines for tumour imaging: version 2.0. *Eur J Nucl Med Mol Imaging*. 2015;42:328–54.

Brown EN, Solt K, Purdon P, Johnson-Akeju O. Monitoring brain state during general anesthesia and sedation. In RD Miller, LI Eriksson, LA Fleisher, JP Wiener-Kronish, NH Cohen, & WL Young (Eds.), *Miller's anesthesia*. Philadelphia: Elsevier; 2015. p.1524–1540.

Buvat I. Quantification in emission tomography: challenges, solution, and performance. *Nucl Instr Meth Phys*. 2007;571:10-13.

Byrnes K et al. FDG-PET imaging in mild traumatic brain injury: a critical review. *Frontiers in Neuroenergetics*. 2014;5:1-24.

Catafau A. Brain SPECT in Clinical Practice. Part I: Perfusion. *J Nucl Med*. 2001;42:259-71.

Cherry SR, Sorenson JA, Phelps ME. *Physics in nuclear medicine.* 4th. ed. Philadelphia: Elsevier, 2012.

Duelli R, Kuschinsky W. Brain Glucose Transporters: Relationship to Local Energy Demand. *News Physiol. Sci.* 2001;16:71-6.

ElMotal S, Sharp G. Inhibition of glucose-induced insulin releaase by xylazine. *Endocrinology.* 1985;116:2337-40.

Elsinga PH et al. *Trends on the role of pet in drug development*. Singapore: World Scientific, 2012.

Frey E, Humm J, Ljungberg M. Accuracy and precision of radioactivity quantification in nuclear medicine images. *Semin Nucl Med.* 2012;42(3):208-18.

Friston KJ et al. *Statistical Parametric Mapping: the Analysis of Functional Brain Images.* London:Elsevier/Academic Press; 2007.

Fueger B et al. Impact of Anmal Handling on the Results of 18F-FDG PET Studies in Mice. *J Nucl Med.* 2006:47:999-1006.

Hall JE. *Tratado de fisiologia médica.* 13th. ed. Rio de Janeiro: Elsevier, 2017.

Haller J, Alicki M. Current animal models of anxiety, anxiety disorders, and anxiolytic drugs. *Curr Opin Psychiatry.* 2012;25:59–64.

Hansen T et al. The role of cerebral metabolism in determining the local cerebral blood flow effects of volatile anesthetics: Evidence for persistent flow-metabolism coupling. *J Cereb Blood Flow Metab.* 1989;9(3):323-28.

Ido T et al. Labeled 2-deoxy-D-glucose analogs. 18F-labeled 2-deoxy-2-fluoro-D-glucose, 2-deoxy-2-fluoro-D-mannose and 14C-2-deoxy-2-fluoro-D-glucose. *J Label Compounds Radiopharm.* 1978;14:175-83.

Ingvar D. Mental-Illness and Regional Brain Metabolism. *Trends Neurosci.* 1982;5:199-203.

Kreissl M; Stout D; Wong K. Influence of dietary state and insulin on myocardial, skeletal muscle and brain [18F]-fluorodeoxyglucose kinetics in mice. *EJNMMI Res.* 2011;1:8.

Lancelot S, Zimmer L. Small-animal positron emission tomography as a tool for neuropharmacology. *Trends Pharmacol Sci.* 2010;31:411-17.

Långsjö MD et al. Effects of Subanesthetic Ketamine on Regional Cerebral Glucose Metabolism in Humans. *Anesthesiology*. 2004;100:1065-71.

Lenz C et al. Local Coupling of Cerebral Blood Flow to Cerebral Glucose Metabolism during Inhalational Anesthesia in Rats. Desflurane versus Isoflurane. *Anesthesiology.* 1999;91:1720-23.

Leybaert L et al. Neurobarrier coupling in the brain: Adjusting glucose entry with demand. *J Neurosci Res.* 2007;85:3213-20.

Matsumura A et al. Assessment of microPET performance in analyzing the rat brain under different types of anesthesia: comparison between quantitative data obtained with microPET and ex vivo autoradiography. *NeuroImage.* 2003;20:2040-50.

Mergenthaler P et al. Sugar for the brain: the role of glucose in physiological and pathological brain function. *Trends Neurosci.* 2013;36(10):587-97.

Mizuma H et al. Establishment of In Vivo Brain Imaging Method in Counscious Mice. *J Nucl Med.* 2010;51(7):1068-75.

Moore A et al. Quantitative Assessment of Longitudinal Metabolic Changes In Vivo After Traumatic Brain Injury in the Adult Rat Using FDG-MicroPET. *J Cereb Blood Flow Metab.* 2000;20(10):1492-1501.

Nehlig A. Cerebral energy metabolism, glucose transport and blood flow: changes with maturation and adaptation to hypoglycaemia. *Diabetes Metab.* 1997;23:,18-29.

Orzi F et al. Local Cerebral Glucose Utilization in Controlled Graded Levels of Hyperglycemia in the Conscious Rat. *J Cereb Blood Flow Metab*. 1988;8:346-56.

Patlak CS, Blasberg RG, Fenstermacher JD. Graphical evaluation of blood-to-brain transfer constants from multiple-time uptake data. *J Cereb Blood Flow Metab.* 1983;3:1-7.

Patlak CS, Blasberg RG. Graphical evaluation of blood-to-brain transfer constants from multiple-time uptake data. Generalizations. *J Cereb Blood Flow Metab.* 1985;5:584-90.

Phelps ME, Mazziota JC, Schelbert HR. *Positron emission tomography and autoradiography:* principles and applications for the brain and heart. New York: Raven Press Books Ltd., 1986.

Phelps M et al. Tomographic measurement of local cerebral glucose metabolic rate in man with (18F) fluorodeoxyglucose: Validation of method. *Am Neurol.* 1979;6:371-88.

Polidori A et al. The eye of nuclear medicine. *Clin Transl Imaging.* 2019;7:233-5.

Prieto E et al. Statistical parametric maps of 18F-FDG PET and 3-D autoradiography in the rat brain: a cross-validation study. *Eur J Nucl Med Mol Imaging.* 2011;38(12):2228-37.

Roy C, Sherrington C. On the Regulation of the Blood-supply of the Brain. *The Journal of Physiology.* 1890;11:85-158.

Schiffer W, Mirrione M, Dewey S. Optimizing Experimental Protocols for Quantitative Behavioral Imaging with 18F-FDG in Rodents. *J Nucl Med.* 2007;48(2):277-87.

Shah K, De Silva S, Abbruscato T. The Role of Glucose Transporters in Brain Disease: Diabetes and Alheimer's Disease. *Int. J. Mol. Sci.* 2012;13:12629-55.

Shimoji K et al. Measurement of cerebral glucose metabolic rates in the anesthetized rat by dynamic scanning with 18F-FDG, the ATLAS small animal PET scanner, and arterial blood sampling. *J Nucl Med.* 2004;45:665-72.

Sokoloff L. Localization of functional activity in the central nervous system by measurement of glucose utilization with radioactive deoxyglucose. *J Cereb Blood Flow Metab.* 1981;1(1):7-36.

Sokoloff L. The deoxyglucose method: theory and practice*. Eur Neurol*. 1981;20:137-45.

Sokoloff L et al. The [14C]Deoxyglucose method for the measurement of local cerebral glucose utilization: Theory, procedure and normal values in the conscious and anesthetized albino rat. *J Neurochem.* 1977;28(5):897-916.

Sossi V, Ruth T. MicroPET imaging: in vivo biochemistry in small animals. *J Neural Transm.* 2005;112:319-30.

Toyama H et al. Evaluation of anesthesia effects on [18F]FDG uptake in mouse brain and heart using small animal PET. *Nucl Med Biol.* 2004a;31:251-56.

Toyama H et al. Absolute Quantification of Regional Cerebral Glucose Utilization in Mice by 18F-FDG Small Animal PET Scanning and 2-14C-DG Autoradiography. *J Nucl Med.* 2004b;45(8):1398-1405.

Vanhove C et al. Accurate molecular imaging of small animals taking into account animal models, handling, anaesthesia, quality control and imaging system performance. *EJNMMI Phys.* 2015;2:31.

Varrone A et al. EANM procedure guidelines for PET brain imaging using [18F]FDG, version 2. *Eur J Nucl Med Mol Imaging*. 2009;36(12):2103-10.

Woo SK et al. Anesthesia condition for 18F-FDG imaging of lung metastasis tumors using small animal PET. *Nucl Med Biol.* 2008;35:143–50.

Yamaji S et al. Evaluation of Standardized Uptake Value to Assess Cerebral Glucose Metabolism. *Clin Nucl Med.* 2000;25(1):11-6.

Yu A et al. Quantification of Cerebral Glucose Metabolic Rate in Mice Using 18F-FDG and Small-Animal PET. *J Nucl Med.* 2009;50:966-73.

Zaidi H, Alavi A. Trends in PET quantification: opportunities and challenges. *Clin Transl Imaging.* 2014;2(3):183-5.